Bottom-up Surface Engineering of DNA Macro-assemblies for Nanoelectronics and Optical Biosensors

by

Tony Jefferson Gnanaprakasa

A thesis submitted to the Graduate Faculty of
Auburn University
in partial fulfillment of the
requirements for the Degree of
Master of Science

Auburn, Alabama
May 09, 2011

Keywords: Optical DNA biosensors, SECM,
charge transfer kinetics, nanoelectronics

Approved by

Aleksandr L. Simonian, Chair, Professor of Materials Engineering
Dong-Joo Kim, Associate Professor of Materials Engineering
ZhongYang Cheng, Associate Professor of Materials Engineering

Abstract

Nanotechnology has promised an out of the ordinary impact on mankind. From the most mundane of consumables to the indispensible advancements in health care and medicine that it has potential in; make it an exciting revolution in science and engineering. Design and implementation of nanomaterials for the applications mentioned afore is the next big challenge. Despite the prodigious efforts carried out in unraveling the complications encountered, it is still problematical to engineer nanomaterials because of their physiochemical properties that make them complex systems to manifest, yet enthralling to work with. Standing out from this category of fascinating materials, single-walled carbon nanotubes (SWNTs) have been of great interest for their outstanding physical and chemical properties and their potential in the future of nanoelectronics and nanomedicine. In recent years, three dimensional nanoarchitectures have been found to be the apt candidates for the development of nanoelectronic devices and novel sonde diagnostic platforms. But lack of the proper chemical functionalities and biocompatibility has impeded their impact on nanomedicine and clinical diagnostics. Deoxyribonucleic acid (DNA) is a bio-nanomaterial from nature's tool box and forms the central icon of modern medicine and has been greatly admired for its versatility and complex design.

As a result, DNA was used as a template to design a layer-by-layer assembled SWNT based macromolecular surfaces for nanoelectronics with great control. These 3D nanoarchitectures provide a promising step in developing novel biomimetic antimicrobial thin

films. The electron transfer properties and conductivity of these materials was then studied using scanning electrochemical microscopy (SECM) as a non-destructive method. It was verified that the charge injection through the multilayers were solely due to electron hoping across the DNA-SWNT adducts, as a result of an increase in feedback response from the SECM.

Subsequently, portable and sensitive optical biosensors were designed for the detection of the virulent disease causing gene in foodborne pathogens. In this case, the virulent *hipO* gene from *Campylobacter jejuni* was detected using a DNA self-assembled monolayer developed over gold surface on a surface plasmon resonance (SPREETA) platform and avidinated polystyrene surface on the diffraction optics technology (DOT) platform in real-time with high specificity. Hence the research presented here elaborates the use of DNA as a molecular tool to develop novel biomimetic nanoelectronic and medical diagnostic sensor platforms.

Acknowledgements

In the first place, I would like to express my deepest and sincere gratitude to my mentor Dr. Aleksandr L. Simonian for providing me with his diligent support and guidance. His enduring motivation has fostered in me, a never-ending opportunity to excel during the course of this research and will be a pillar of support throughout my professional career.

I am grateful to my committee members, Dr. Dong-Joo Kim and Dr. ZhongYang Cheng for providing their time and invaluable review of this manuscript. My sincere thanks to Dr. Virginia A. Davis for her collaboration and insightful discussions during this research. I am also thankful to Dr. Omar A. Oyarzabal and Dr. Eric V. Olsen for their critical and intuitive reviews and their collaboration. This work wouldn't have been possible without the financial support from NSF, AUDFS, USAF and NATO. I extend my sincere gratitude to Dr. Minseo Park for the collaborative research. I am always thankful to Mr. Roy Howard, Ms. Alison Mitchell and Mr. Steven Moore for all their help. My professors at the Central Electrochemical Research Institute (CECRI, India), Dr. N. G. Renganathan, Dr. K. R. Murali and Dr. S. Mohan have been responsible for setting up the foundation for my research career.

I wouldn't have initiated and enjoyed my research career without the constant support from my colleague and friend Shankar. Furthermore, I would like to extend my thanks to my colleagues Valber, Saroja, Shawn, Rigved, Sheetal, Madhumati, Siddharth, Nitil and Jeff for all their help and making the research lab a fun place to work.

I would like to pay tribute to all my friends at Auburn, who have been more than a friendly ear or an encouraging word. Though I am not able to accommodate everyone here, my special gratitude to Anand, Karthik, Anty, Borat, Nono, Cheechu, Rahul, Shyam, Kausar, Jola, Sonal, Kristen, Bala and Raja for making my three and a half year lodge at Auburn a long lasting memory. I would also like to thank all my friends back at home for staying in touch and for being there when I needed them.

Finally, I would like to thank my parents Grace Mary and Paul Arasu, and loving sister Steffi for being extra supportive and determined towards my education since I was a child. They have been the source of encouragement and unconditional love and I dedicate my work to their indomitable spirit. In the end, I would like to thank the immaculate mother of god for guiding me all the way through. Thank you guys!!!

The following peer-reviewed publication and conference presentations were a product of this thesis:

Peer-reviewed publication:

- Valber A. Pedrosa#, *Tony Gnanaprakasa#*, Shankar Balasubramanian, Eric V. Olsen, Virginia A. Davis, Aleksandr L. Simonian, "Electrochemical properties of interface formed by interlaced layers of DNA- and Lysozyme-coated single-walled carbon nanotubes", *Electrochemistry Communications*, 2009, 11, 1401-1404 (# Authors contributed equally in this work)

- *Tony J. Gnanaprakasa#*, Omar A. Oyarzabal#, Eric V. Olsen, Valber A. Pedrosa, Aleksandr L. Simonian, "Tethered DNA scaffolds on optical sensor platforms for detection of *hipO* gene from *Campylobacter jejuni*", *Sensors and Actuators B: Chemical*, (Submitted) (# Authors contributed equally in this work)

- Siddharth Alur, *Tony J. Gnanaprakasa*, Yaqi Wang, Yogesh Sharma, Jing Dai, Jong W. Hong, Aleksandr L. Simonian, Michael Bozack, Claude Ahyi, Minseo Park, "AlGaN/GaN HEMT Based Biosensor", *ECS Transactions*, 2010, 28, 61-64

Conference Presentations:

- *Gnanaprakasa, T.J.*; Simonian, A.L.; "Electrochemical DNA nano-biosensors based on MWCNT-AuNP nanocomposites", 218th meeting of The Electrochemical Society, October 10-15, 2010, Las Vegas, NV

- *Gnanaprakasa, T.J.*; Davis, V.A., Simonian, A.L.; "Development of MWCNT/AuNP Nanostructures for Label-Free Localized SPR Based Biosensing", AIChE Annual Meeting, November 7-12, 2010, Salt lake City, UT

- *Gnanaprakasa, T.J.*; Pedrosa, V.A.; Olsen, E.V.; Oyarzabal, O.A.; Chin, B.A.; Simonian, A.L.; "DNA biosensors for the detection of the hippuricase gene of Campylobacter jejuni based on SPREETA™ and dotLab™ platforms", Biosensors 2010, 20th Anniversary World Congress on Biosensors, May 26-28, 2010, Glasgow, United Kingdom

- *Gnanaprakasa, T.J.*; Pedrosa, V.A.; Olsen, E.V.; Oyarzabal, O.A.; Simonian, A.L.; "Electrochemical Impedance Spectroscopy Studies of hippuricase Gene Hybridization for Campylobacter jejuni Specific Detection", 217th meeting of The Electrochemical Society, April 25-30, 2010, Vancouver, Canada

- *Gnanaprakasa, T.J.*; Pedrosa, V.A.; Olsen, E.V.; Oyarzabal, O.A.; Simonian, A.L.; "DNA biosensors for the detection of Campylobacter jejuni nucleic acids based on SPR and laser diffraction platforms", AIChE Annual Meeting, November 8-13, 2009, Nashville, TN

- Pedrosa, V.A.; *Gnanaprakasa, T.J.*; Olsen, E.V.; Davis, V.A.; Simonian, A.L.; "Electrochemical properties of interface formed by interlaced layers of DNA and lysozyme-coated single-walled carbon nanotubes", 216th meeting of The Electrochemical Society, October 4-9,2009, Vienna, Austria

- *Gnanaprakasa, T.J.*; Pedrosa, V.A.; Olsen, E.V.; Davis, V.A.; Simonian, A.L.; "Probing conductivity and lateral charge transfer across LSZ-SWNT/DNA-SWNT nanocomposites using scanning electrochemical microscopy", 215th meeting of The Electrochemical Society, May 24-29, 2009, San Francisco, CA

- Alur, S.; *Gnanaprakasa, T.J.*; Xu, H.; Wang, Y.; Simonian, A.L.; Oyarzabal, O.A.; Park, M.; "A Biosensor Based on GaN Field Effect Transistor", International Conference on Compound Semiconductor Technology, May 18-21, 2009, Miami, FL

- Pedrosa, V.A.; *Gnanaprakasa, T.J.*, Davis, V.A.; Simonian, A.L.; "Lateral conductivity of single-walled carbon nanotube reinforced with biopolymers by scanning electrochemical microscopy", Mini Symposium, ECS Local Section and Atlanta Student Chapter at the Georgia Institute of Technology, February 18, 2009, Atlanta, GA (invited)

- Balasubramanian, S.; Nepal, D.; *Gnanaprakasa, T.J.*; Davis, V.A.; Simonian, A.L.; "Electrochemical characteristics of SWNT-biopolymer nanocomposites", 213th meeting of The Electrochemical Society, May 18-23, 2008, Phoenix, AZ

Table of Contents

List of Figures

List of Tables

List of Abbreviations, Acronyms and Symbols

2. Literature Review

θ	Fraction of the surface covered by the adsorbent
p_{a}	Pressure of the adsorbent
k_a	Rate constant for adsorption
k_d	Rate constant for desorption
K	k_a/k_d
ε_0	Permittivity of free space
ε	Dielectric constant of the electrolyte
A	Area of the SWNT layer
d_{OHP}	Distance to the outer Helmholtz plane
C_{dl}	Double layer capacitance of SWNT

3. Scanning Electrochemical Microscopy – Principle & Experimental Setup

O	Oxidation species
R	Reduction species
$i_{T,\infty}$	Steady state diffusion controlled current
n	Number of electrons transferred per redox event
F	Faraday

D	Diffusion coefficient of species O
a	Radius of the conductive disk (tip)
c_i	Concentration of species i (O, R)
R_G	Dimension sheath radius
r_g	Radius of insulating sheath
i_T	Current flowing through tip
d	Distance between tip and substrate
e^-	electron
c_O°	Bulk concentration of O
t	time
r, z	Coordinates in the directions radial and normal to the electrode surface
D_i	Diffusion coefficient of species i
c^o	Bulk concentration of electroactive species
E	Electrode potential
$E^{o\prime}$	Formal potential
f	Parameter equal to F/RT, R is the gas constant and T the temperature
$I_T(L)$	Diffusion-limiting tip current
L	Normalized tip/substrate separation
$I_S(T)$	Dimensionless substrate current
J_T, J_S	Dimensionless variables equal to $ja/(Dc^o)$
j	Diffusion flux density
k^o	Standard rate constant

$k_{f/b}$	Heterogeneous rate constants for oxidation and reduction
$K_{f/b,s}$	Dimensionless rate constant equal to $k_{f/b,s}\, a/D$
T	Dimensionless variable equal to tD/a^2
α	Transfer coefficient
D_{surf}	Surface diffusion coefficient
D_{soln}	Solution diffusion coefficient
Δz	Thickness of the film
μ	Electrochemical potential of electrons in the nano-film monolayer
μ^0	Standard electrochemical potential
e	Elementary charge
$\phi(r)$	Local electrostatic potential in the film
μ_{eq}	Equilibrium electrochemical potential
i	Current density
σ	Conductivity
N_A	Avogadro's number
r_e	Microelectrode radius
$\tilde{\mu}_{eq}$	Equilibrium electrochemical potential of the film with respect to the standard chemical potential of the redox couple

1. Introduction

Interdisciplinary research in engineering, with unclouded insight and advanced instrumentation has brought the field of surface science into common parlance, with its inception from the Nobel Prize winning work by Langmuir for his studies on surface adsorption. The field of surface science has undergone an enormous expansion, driven by the combination of different techniques for the preparation of macroscopic surfaces and ultra-high vacuum environments. Yet many uncertainties pervade this field, ranging from self-assembly of advanced materials structures to the practical viabilities to invest in knowledge, on nano-molecular recognition processes to large-scale mesoscopic formation phenomena. Both controlled placement and orientation of these molecules is required for their anisotropic properties to be fully manifested in the macro-scale. Hence the development of new surface chemistries and nano-scale materials paves way for a new paradigm in developing revolutionary technologies.

Extensive studies have been conducted on materials from microstructures to the macro scale. However, the challenge prevails in understanding the fundamental properties of materials at the nano scale. Nanomaterials exhibit significantly modified physical, chemical and biological properties owing to their quantum confinement. Thanks to the tremendous growth of nanotechnology over the past few decades, recent developments in nanoscience have been applied to a number of innovations in medicine and healthcare, agriculture, chemical and biological technologies, environmental and energy storage and materials manufacturing. Conventional fabrication of devices start from patterning a silicon wafer and then obtaining the

desired features on the nano scale using reliable but expensive nanofabrication methods – simply called "top-down" approach. The need for precision and reliability in the fabricated devices, escalate the costs of top-down routes. Preferably, nanostructures are conceived from atoms and molecules which are reacted chemically and ordered physically to obtain the desired features, which is the "bottom-up" approach. Based upon self-organization processes and in particular self-assembly, bottom-up approach is the coordinated action of independent entities under local control of driving forces in order to achieve a group effect for macrostructures [1].

The key to nanomaterials organization is not only controlled by the presence of physical impulses such as temperature, photonic input, electrical modulation or pH; but also changes in chemical impulses such as the presence of molecules which enhance stimuli between these materials. Apropos, nature's tool box provides an array of nanoscale fabrication methods, including assembly of superstructures like lipids, organelles and microtubules. Likewise, nucleic acids are found to have a high affinity and specificity towards a wide range of molecules, and regulate the *in vivo* and *in vitro* functionalities of any biological system. Hence nucleic acids such as DNA can be used as templating agents for nanomaterials because their structure can be easily regulated by physical and chemical means, because of their rich chemical functionality. Recently, Belcher *et al* [2] reported the development of an M13 virus based scaffold for the development of semiconductor nano-wires; which pioneered the concept of 'bottom-up' nanofabrication using biological templates. Although nanofabrication using biological templates appears to be a long term goal, several processes such as biomineralization and nucleic acid mediated self-assembly appear to be a promising strategy. As a result, the extensible ruggedness and high functionality of DNA makes it an attractive alternative for nanofabrication and self-

assembly, in developing nanoelectronic devices and functional surfaces for a wide range of applications.

DNA consists of chemical functionalities called ‘chemical handles’ that allow it to interact with a myriad of inorganic nanomaterials. The three main chemical functionalities are: the negatively charged phosphate backbone, metal-chelating base groups and the aromatic rings that form the hydrophobic core. Furthermore, Seeman *et al* [3] showed that DNA based molecular networks with four-arm junction connectivity can be used to design closed self-assembled lattices. Therefore, DNA can be used as a versatile biological tool in developing mediated and template assemblies of nanomaterials.

More recently, single-walled carbon nanotubes (SWNTs) have been a promising candidate for great impact on mankind with its exceptional physical and chemical properties. Yet, their existence in a bundled state and the absence of chemical functionalities to minimize their attractive energies between each tube has hampered the development of novel building blocks using individually dispersed SWNTs. Nepal *et al* [4] reported a novel solid-state mechano-chemical reaction to individually disperse SWNTs using DNA as a template. These DNA dispersed SWNTs were then used as building blocks to develop large scale biomimetic antibacterial nanocomposites, which formed as a stepping stone to develop 3D nanostructures and devices.

In order for DNA to be manifested in to nanomaterials, there are several aspects that have to be established including its chemical and electrical properties. Much of work has been done on instituting the physiochemical properties of DNA-templated nanomaterials. The electrical properties of these hybrid materials form an inordinate factor in developing building blocks for nanoscale devices. Poor electrical performance of DNA based nanomaterials and the presence of

crystalline defects in these templates causes the material to suffer high resistive heating. Hence new schemes have to be developed in increasing their electrical properties and developing self-assembled 3D nanostructures based on DNA templates. There are a multitude of applications that can be projected using DNA-templated nanofabrication. When successful, it would allow the large integration these materials for macromolecular electronics, medical diagnostics and gene therapy.

Away from being used as a template in nanotechnology, DNA can also be used as a scaffold in developing medical diagnostic platforms. Mirkin *et al* [5, 6] reported a gold nanoparticle-DNA complex for the detection of proteins and DNA sequencing. They also reported a novel nano-patterning technique to develop self-assembled monolayers for fast, responsive DNA sensing used for diagnostics and biosensing. Shionoya *et al* [7] were successful in attaching metal nano-particles to the DNA helix, which has widespread applications in photo-electronics and biosensing. With DNA nanotechnology in the upsurge and medical science leaning towards developing novel diagnostics for diseases; there has been an erratic progress in health reforms across countries. Transmission of diseases and infections are elevated by the ubiquitous urbanization and globalization, thereby accelerating spread of chronic disorders and multiple illnesses [8]. As a result of this globalization, there is a rapid change in health systems which are currently not insulated from one another. Attenuated curative care, delivery of short term results where service is fragmented and laissez-fair approaches to health systems are a few of the lagging trends that need to be looked upon to reform increasing health concerns. Redressing these health reforms helps the commercialization of health reforms and to flourish with a clearer sense of purpose and direction [9].

Consequently, there is an obvious need for the development of bioanalytical devices to detect these foodborne pathogens for the safety and prevention of outbreaks. There is always a constant demand to sense these bio-threat agents mainly for collecting genomic data, diagnosis of diseases and controlling of production processes. The most common bio agents range from bacteria to viruses [10]. Biosensing requires short sensing time, low equipment and operating costs, compact system size and low power consumption. Most of the modern chemical and biosensors have changed the way by which these foodborne pathogens are detected [11].

A broad host range of human pathogens are an emerging threat for pathogenic diseases and coexist in several animal hosts and environmental reservoirs. Apparently, evidence-based disease control is adopted in order to identify transmission routes and sources. Isolating microbial samples and attributing them with different food sources has helped track microbial sources. Additionally, specific phage subtypes and serotypes should be found in the same host. This is because, the specific hosts have well adapted specific clones and secondly, a combination of both sero-typing and phage type provides a reliable indicator for that clone.

This has been unsuccessful for another branch of bacterial zoonosis, most commonly - *Campylobacter jejuni (C. jejuni)*, which is one of the main causes of human bacterial gastroenteritis. It shows marked seasonality as a result of infection in poultry products, livestock and most of all humans and a possibility of environmental triggering [12]. In 2010, the USDA reported that *C. jejuni* is responsible for 2.4 million illnesses and 124 deaths in the United States alone. A recent outbreak in the U.S. in 2009 led to 35 *C. jejuni* related outbreaks, because of consuming unpasteurized milk. Diarrheal illnesses were frequently caused by *C. jejuni* than *Salmonella* species, *Shigella* species, or *Escherichia coli* O157:H7. The annual cost associated with *C. jejuni* infections is estimated to be 2.4 billion dollars in the U.S. in 2000 and

approximately 136 million pounds in the United Kingdom in 1999. Besides, the emergence of antimicrobial-resistant *Campylobacter* strains has led to an increase proper clinical diagnostics and development of technologies for effective management of diseases [13].

Campylobacteriosis can occur in outbreaks, single and sporadic cases. It is associated with handling raw poultry, eating undercooked meat, cross-contamination from other foods, unpasteurized milk or contaminated water and contact with animals infected with *C. jejuni*, that show no signs of infection. The pathogenesis of *C. jejuni* has been proposed in four different ways. These include:

1. Motility, which is the penetration of intestinal mucosa and colonization of the intestine leading to the production of effector molecules
2. Chemotaxis, being the ability to sense chemical gradients that enables the organism to move across these gradients
3. Adhesion and invasion
4. Toxin production
5. Other mechanisms including iron acquisition, oxidative stress and heat shock response

Besides there are other factors that cause the anti-microbial resistance in *C. jejuni*. Administration of anti-microbials to farm animals either as a growth promoter or as a therapeutic agent enables the growth of anti-microbial resistant *C. jejuni* strains. Fluoroquinolone resistant *C. jejuni* strains occur in poultry animals, which renders the fluoroquinolone-susceptible *C. jejuni* drug-resistant [14]. Although, the FDA has withdrawn the use of fluoroquinolones in poultry animals, these organisms continue to circulate and transfer. Additionally, international travel is also associated with fluoroquinolone resistant *C. jejuni*. Millions of people travel across and develop fluoroquinolone-resistant *Campylobacter* enteric infection abroad, also known as

traveler's diarrhea. The continuous selection pressure from the widespread use of fluoroquinolones has led to its outbreak [15, 16].

Surface plasmon resonance (SPR) and Diffraction optics technology (DOT) are based on an optical transduction scheme and they offer, 'label-free' and 'near real-time' detection of the samples. Accordingly, the main objective of this work is to develop DNA-templated functional surfaces for sensing the virulent gene from pathogenic bacteria and to analyze charge transfer through self-assembled nanomaterials for nano-electronic applications. In the latter section, we have verified the electron transport and conductivity of DNA dispersed single-walled carbon nanotubes using scanning electrochemical microscopy (SECM). Hence, this research presents the application of DNA as a molecular scaffold in biosensing and its significance in the development of nanoelectronic materials. Chapter 2 describes the necessary literature work followed by the experimental setup for scanning electrochemical microscopy (SECM) in Chapter 3. Chapter 4 describes the experimental setup for the DOT system. The application of self-assembled monolayer to develop DNA based optical sensing platforms have been discussed in Chapter 5. Here various challenges related to DNA assembly increasing the sensitivity have been discussed. The electrochemical characteristics and charge transfer kinetics of self-assembled single-walled carbon nanotubes and DNA based bio-nanocomposites have been discussed in Chapter 6.

1.1. References

1. Dragoman, M. and D. Dragoman, *Nanoelectronics Principles and Devices*. 2006, Norwood: Artech House, Inc.
2. Mao, C., et al., *Virus-Based Toolkit for the Directed Synthesis of Magnetic and Semiconducting Nanowires.* Science, 2004. 303(5655): p. 213-217

3. Seeman, N.C., *Nucleic acid junctions and lattices.* J. Theo. Biol., 1982. 99(2): p. 237-247.

4. Nepal, D., et al., *Supramolecular Conjugates of Carbon Nanotubes and DNA by a Solid-State Reaction.* Biomacromolecules, 2005. 6(6): p. 2919-2922.

5. Cao, C.Y., R. Jin, and C.A. Mirkin, *Nanoparticles with Raman Spectroscopic Fingerprints for DNA and RNA Detection.* Science, 2002. 297(5586): p. 1536-1540

6. Jin, R., et al., *What Controls the Melting Properties of DNA-Linked Gold Nanoparticle Assemblies?* J. Am. Chem. Soc., 2003. 125(6): p. 1643-1654.

7. Tanaka, K., et al., *A Discrete Self-Assembled Metal Array in Artificial DNA.* Science, 2003. 299(5610): p. 1212-1213.

8. Van Lerberghe, W., et al., *The world health report 2008 - primary health care now more than ever*. 2008, World Health Organization.

9. Altekruse, S.F., et al., *Campylobacter jejuni—An Emerging Foodborne Pathogen* Emerg Infect Dis, 1999. 5(1).

10. Ding, C., H. Zhong, and S. Zhang, *Ultrasensitive flow injection chemiluminescence detection of DNA hybridization using nanoCuS tags.* Biosens. Bioelectron., 2008. 23(8): p. 1314-1318.

11. Passamano, M. and M. Pighini, *QCM DNA-sensor for GMOs detection.* Sens. Actuators B, 2006. 118(1-2): p. 177-181.

12. Galanis, E., *Campylobacter and bacterial gastroenteritis.* CMAJ, 2007. 177(6): p. 570-571.

13. Stewart-Tull, D.E.S., et al., *Virulence spectra of typed strains of Campylobacter jejuni from different sources: a blinded in vivo study.* J. Med. Microbiol., 2009. 58: p. 546-553.

14. Bradbury, W.C., et al., *Investigation of a Campylobacter jejuni Outbreak by Serotyping and Chromosomal Restriction Endonuclease Analysis.* J. Clin. Microbiol., 1984. 19(3): p. 342-346.

15. Engberg, J., et al., *Quinolone and Macrolide Resistance in Campylobacter jejuni and C. coli: Resistance Mechanisms and Trends in Human Isolates.* Emerg. Infect. Dis, 2001. 7(1): p. 24-34.

16. Pickett, C.L., et al., *Prevalence of cytolethal distending toxin production in Campylobacter jejuni and relatedness of Campylobacter sp. cdtB gene.* Infect. Immun., 1996. 64(6): p. 2070-2078.

2. Literature Review

2.1. Agenda

Surface chemistry combined with nanotechnology and the right placement of quantum confined materials is a promising field which has immense applications in the field of nanoelectronics and clinical diagnostics. In his avant-garde speech at Caltech, Richard Feynman put forth "… the problem of manipulating and controlling things at the nanoscale" [1]. This marked the beginning of the manifestation of materials for the next generation of nanoelectronics. Today, keeping those words as the stepping stone, self-assembly of nanomaterials has a great impact in every possible façade of science and engineering. Various fabrication techniques have been used as an archetype in order to arrange these materials with precision and harness their properties to the fullest. Although, 'top-down' approaches have been successful in order to develop nanofabrication techniques, and to develop smaller machines; equipment costs and the difficulty that arises when manipulating nanomaterials have limited the use of this approach. Instead, precise building of materials from the molecular level known as 'bottom-up' approach has attracted scientists from all junctures of science exemplifying the basic rules of self-assembly.

On the contrary, naturally occurring self-assembly tools in living systems demonstrate the ability to produce complex molecular machines using advanced molecular engineering methods. Bio-nanotechnology provides a beachhead from which novel self-assembly techniques can be perceived and can provide a variety of tools which could lead to computational advances in manipulating nanomaterials. Out of these naturally occurring biomaterials, DNA has been

considered in the far side of the barrier that is facing conventional microelectronics. It is a celebrated molecule in modern biology, especially known for its protein folding capabilities and chemical functionalities that make it the right successor to conventional compounds. Hence, DNA can be used alongside with a number of nanomaterials, presumably as a manipulator in advanced molecular electronics or as a powerful tool to build novel molecular detection technologies [2].

2.2. DNA as dispersant for SWNTs

Single-walled carbon nanotubes (SWNTs) have been expected to become a potential source of functional materials, because of their unique combination of optical, mechanical, thermal and electrical properties. However, because of their strong cohesive nature, they exist in aggregated bundles. This is due to strong tube-tube van der Waals interactions and their axial geometry. Additionally, the absence of flexible group functionalities to interact with the surrounding medium, they are also poorly soluble in common solvents. Apparently, individual dispersion of SWNTs is the million dollar question. This opens opportunities for a wide range of applications, including nanoscale devices and novel nanostructures. Introduction of solubilization groups either at the ends or the side walls of SWNTs and converting them to amphiphilic compounds is the strategy. The SWNTs should also undergo minimum damage with its inherent properties intact and easily characterizable. Particularly, the method should be benign and should not involve harsh processing steps and functional groups. In recent years, a wide range of surfactants, synthetic polymers and biopolymers have been studied in order to obtain highly dispersed nanotubes.

Consequently, it has been realized that DNA can also be an apt candidate for aqueous solubilization and dispersion of SWNTs for potential applications in developing biochemical and biomedical devices. Yet challenges prevail in developing effective techniques for the large-scale

production of this mono-disperse solutions containing SWNTs using DNA, with reliable control over the interfacial chemistry. The unique double helix structure of DNA enables us to harness remarkable biological and non-biological applications. Other applications include decorating carbon nanotubes with metal nanoparticles, DNA-assisted chiral separation of SWNTs and sonication assisted dispersion of SWNTs in DNA. Hence, a solid-state mechano-chemical reaction (MCR) is adopted, in order to prepare DNA-SWNT adducts. SWNTs interact with the DNA as a result of the highly reactive centers generated by the mechanical energy during the solid phase. This resulted in a high aqueous solubility of the products with a stability of more than 6 months. Moreover, single-walled products were found to be 250 nm to 1 μm in length, while multi-walled products were 500 nm to 3 μm in length. This non-covalent method appears to be shorter in length and fully wrapped around the SWNTs and hence has been adopted for developing advanced 2D and 3D supramolecular nanostructures [3].

2.3. Layer-by-Layer assembly (LbL)

Materials science has grown in to an interdisciplinary field encompassing organic, polymeric and even biological nanostructures in addition to the classic metals and inorganics. Hence it is of great important that materials and devices of this kind have control of molecular orientation and organization at the nanoscale. Consecutively, deposition of single and multi layered nanomaterials can also be done in a controlled fashion on 2D solid substrates. Consequently, a fixed relation has to be established between the nano-scopic order and its macroscopic orientation. Harnessing every possible application from any nanostructure requires knowledge of the location and orientation of every molecule with respect to each other and to the macroscopic coordinate (e.g. liquid crystals). The most successful method followed in molecularly controlled fabrication of nanostructured films is the Langmuir-Blodgett (LB) technique, and has dominated the field of surface science for the last 60 years, where a

monolayer is formed on a water surface and then transferred to a 2D support. Kuhn *et al* [4] were the first to demonstrate the development of hetero-scale nanostructures using LB technique. Their work gave an insight in to nano-manipulation and mechanical handling of individual layers with nanometer sized precision. Although the LB technique had widespread use in nanomolecular design, it required special apparatus and several limitations oversaw its superior molecular architectures and applications in thin film development.

Electrostatic attraction between oppositely charged nanomaterials is a good candidate in developing 3D nano-architectures and acts as a good driving force for multilayer buildup, because of the less stearic demand of all chemical bonds. A charged surface and an oppositely charged molecule in solution undergo strong electrostatic attraction, which has been well known in the field of surface adsorption. As the molecules that form an assembly have more than one equal charge on their surface, it regulates the adsorption of charged molecules to a single layer and facilitates the adsorption of one molecule over another. Cyclic repetition of both the adsorption steps helps developing novel 3D superstructures. An added advantage is that it reduced phase segregation and makes the composite highly homogeneous, so that the nanostructures are well dispersed and interpenetrated [5]. Kotov *et al* [6] reported a nanostructured analog of abalone seashells using nanometer sized sheets of Na+-Montmorillonite clay and poly(diallyldimethylammonium chloride) (PDDA), using LbL technique. The nanocomposites had a tensile strength comparable with natural nacre and lamellar bones, (~100 ± 10 MPa) and a young's modulus of 11 ± 2 GPa. LbL assembly is a highly versatile method in merging various functionalities in to a single composite with application-tailored mechanical responses. Similarly, using a 'mix and match' approach highly tunable films can be obtained on geometric surfaces. For instance, LbL technique has found applications in developing super-

hydrophobic surfaces, semi-permeable membranes, drug delivery, optically active and responsive films, fuel cells and photovoltaic materials, biomimetic and bio-responsive coatings, semiconductors, catalysts and magnetic devices [7-12]. Olek *et al* reported a nano-composite using multi-walled carbon nanotubes (MWNTs) and branched polyethyleneimine (PEI) – a polyelectrolyte.

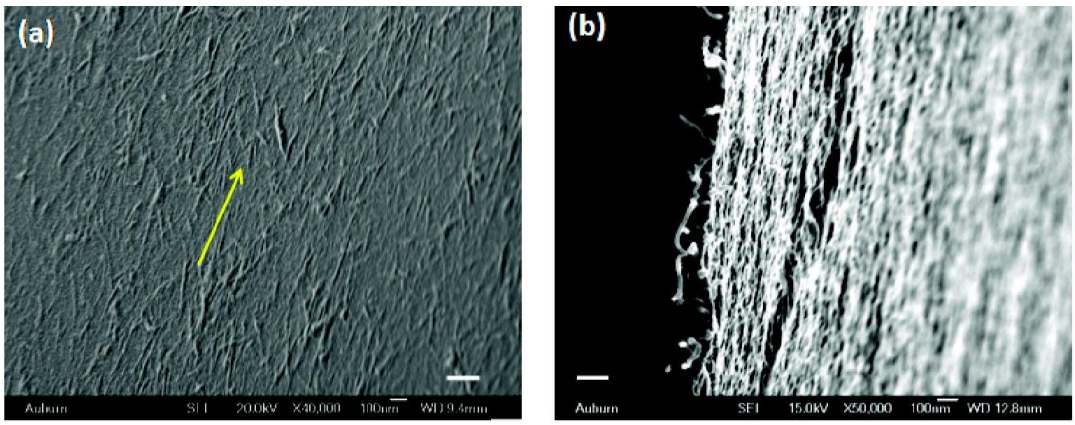

Figure 2-1 SEM Image SWNT based LbL assembly, (a) 8 layers (b) 68 layers.

Recently, LbL assembly of carbon nanotubes alternated with polyelectrolytes, have proven to show superior electrochemical properties and have widespread applications in conventional electrodes for sensor applications and energy storage devices [13, 14]. Subramanian *et al* reported a novel anti-microbial nanocomposites using positively charged DNA-SWNT and negatively charged Lysozyme-SWNT. Precise control of both thickness and SWNT alignment was achieved, and the coatings robust mechanical properties [15]. Therefore, the use of LbL technique is used extensively to develop large scale biomimetic nanocomposites for widespread applications.

2.4. Charge transfer across DNA based carbon nanotube hybrid materials

Although integration of nanotubes in electronics files beyond the next twenty years, they have emerged as an outstanding class of electronics materials due to their ballistic electronic conduction and insensitivity to electromigration. Charge transfer and the electrical properties of carbon nanotubes depend on their diameter and helicity, parameterized by its roll-up vector (*n, m*). Based on this prediction, SWNTs are classified in to three types: zigzag (*0, m*) or (*n, 0*); Armchair (*n, m*), where $n=m$; and chiral (*n, m*) where $n \neq m$. Besides, SWNTs possess electrical characteristics comparable to the best electronic material available, which has motivated many researchers to develop SWNT based field-effect transistors (FETs) and interconnects [16]. Charge transfer across carbon nanotubes can also be analyzed using electrochemical techniques. A charge transfer can also occur that does not result in a chemical change, but rather in a change of the electrical properties of the electrical double layer at the interface. The charge distribution of both parts of the double layer can be altered by charge transport through the material, which is termed 'non-faradaic' current. On the contrary, if the electronic state of the material is changed which results in a new chemical entity being formed, then it is termed 'faradaic' current [17].

The electrochemical behavior of SWNTs is similar to that of graphite, except for the additional effects of the specific electronic structure of rolled grapheme. The density of electronics states in SWNTs exhibit singularities typical to a 1D structure. These so called van Hove singularities (vHSs) originate from the size-dependent quantization of the electronic wave function around the circumference of the SWNTs. Additionally, the energy spacing between corresponding vHSs is controlled by the diameter of each SWNT. SWNTs can be applied in electrochemical techniques as a working electrode, free-standing bucky paper or even an individual SWNT in contact with the electrolytic solution as a working electrode. In an electrochemical cell, if a potential *U* is applied to the electrode, then a net charge is built up

across the electrode, which depends on the electrical double layer formed at the electrochemical interface. Additionally, an *iR* drop is formed across the double layer because of the resistance value of the SWNT. As a result, the potential across the cell is defined from the SWNT/electrolyte interface and this system behaves like a parallel-plate capacitor. Then the double-layer capacitance is given by:

$$C_{dl} \cong \frac{\varepsilon_0 \varepsilon A}{d_{OHP}}$$

Where, ε_0 and ε are the permittivity of free space and dielectric constant of the electrolyte solution, A is the area of the SWNT layer and d_{OHP} is the distance to the outer Helmholtz plane, which is about 0.5 nm for SWNTs. Considering all these parameters, the double-layer capacitance C_{dl} of SWNT is found to be 10 fF/μm of the tube length [18]. This is extremely difficult to evaluate if the SWNT is present as bundles as the double-layer is solely formed at the outer layer of the surface. Hence, it is necessary to individually disperse SWNTs in order to harness their electrical and charge transfer properties. Furthermore, the current flowing thorough a SWNT splits in to an electrostatic part over the double-layer capacitance C_{dl} and a chemical part over the quantum capacitance,C_q which is estimated to be of the order to 1 fF/μm of the tube length. A qualitative difference exists between a classical metal electrode and SWNT electrode. In the case of metal electrode, the applied potential moves the bands by eU_{dl} without changing the relative position of the Fermi level against the band edges ($C_q \gg C_{dl}$). On the other hand, the reaction through a SWNT is quantum-capacitance dominated. Hence, the Fermi level moves eU_{ch} but the bands remain intact. Besides, $C_q \gg C_{dl}$ and hence the potential dependencies vary according to a particular band structure of the SWNT.

The electrolyte is the limiting component in terms of the overall stability of the electrochemical system. Because the unmodified SWNTs are almost insoluble in all usual

solvents, electrochemical stability is the only deciding factor for any electrolyte. While ionic liquids are sufficiently conductive, addition of a supporting electrolyte increases the conductivity of the solution. As a result, the electrochemical doping of SWNTs become easier, this does not perturb the so called 'potential window', and hence finds its way in a wide range of applications. SWNTs can be used in a different configuration of FETs, in which SWNTs is surrounded by an electrolyte and the system undergoes electrochemical gating, which is mainly used in analytical chemistry and sensors. The electrochemistry of nanotubes also finds practical applications in energy storage, batteries, supercapacitors, sensors and actuators and nanoelectronics. Carbon nanotubes can be modified using a wide range of functional groups and hence specific molecules can be detected via electron-transfer reactions and amperometric sensors. Most commonly used electrochemical sensors are called ChemFETs or chemisresistors, for the detection of glucose, cholesterol, dopamine and other biomolecules.

2.5. DNA templated diagnostic platforms

Foodborne diseases have emerged to be one of the major causes of illnesses and deaths throughout the world. Ingestion of contaminated and intoxicated foods and beverages are few of the most common sources of infections. Efficient strategies were developed for the prevention of foodborne diseases and most often depend on the use of molecular and cellular biological techniques. The Center for Disease Control and Prevention (CDC) identifies and categorizes the most significant causes that contribute to foodborne illnesses including; food from unsafe sources, inadequate cooking and improper holding temperatures of raw food, contaminated equipment and poor personal hygiene. Foodborne outbreaks were identified and reported to the CDC, including infections, hospitalizations and deaths associated with each outbreak. In 2007, a total of 698 outbreaks (497 confirmed and 201 suspected) were reported, resulting in 15,477 illnesses with their etiological agents either confirmed or unidentified. Identifying the food

vehicle is one of the major steps in identifying any etiology. Unidentified etiological agents arise due to 1) irregular reporting of diseases to the health department, 2) different types of food consumed which makes it difficult to identify it as a single contaminated food vehicle and 3) human and food test results were unavailable due to improper documentation. Sudden population based-outbreaks were reported electronically which helps guide the surveillance system design a toolkit for investigation. Pathogenic bacteria associated with food products are a major concern for both the food industry and the governing bodies. Bacterial foodborne outbreaks caused in 2007 were almost similar to the number of outbreaks in the 2002-2006 average.

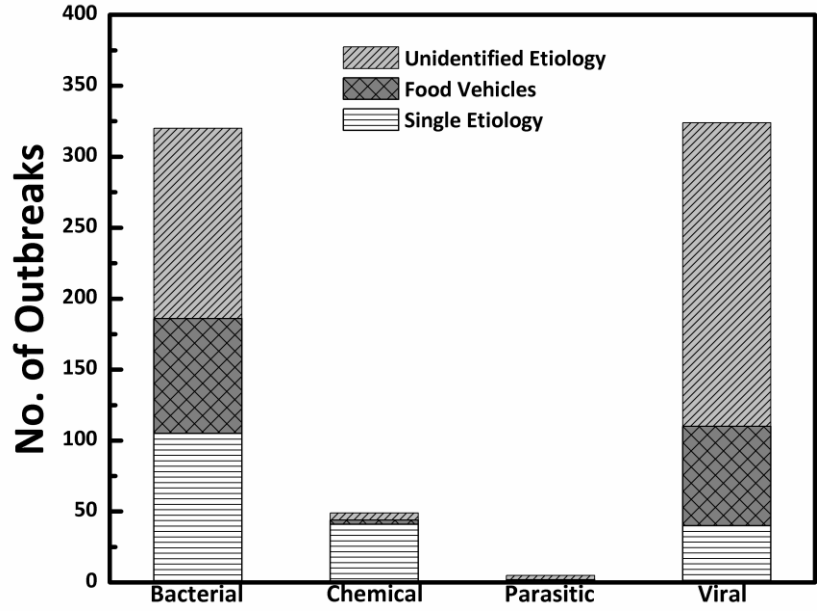

Figure 2-2 Number of food-borne related outbreaks and cases reported from 2002 to 2007

Reported data shows that *Campylobacter* is one of the most common causes of acute bacterial enteritis globally. Among 12,767 illnesses due to outbreaks, bacteria with a single etiological agent caused 259 (52%) outbreaks with 6,441 (50%) illnesses. Additionally in 2007, *Campylobacter* was responsible for 372 outbreak related illness out of 7115 due to a bacterial outbreaks.

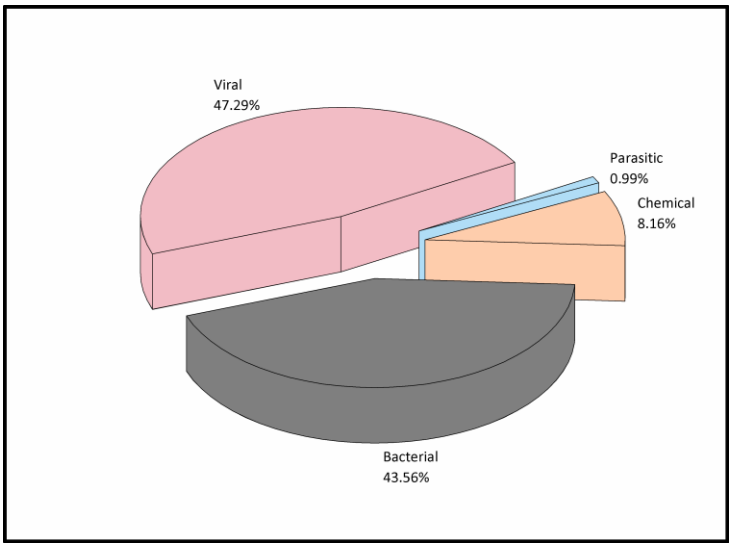

Figure 2-3 Breakdown of foodborne outbreaks by source from 2002 to 2007

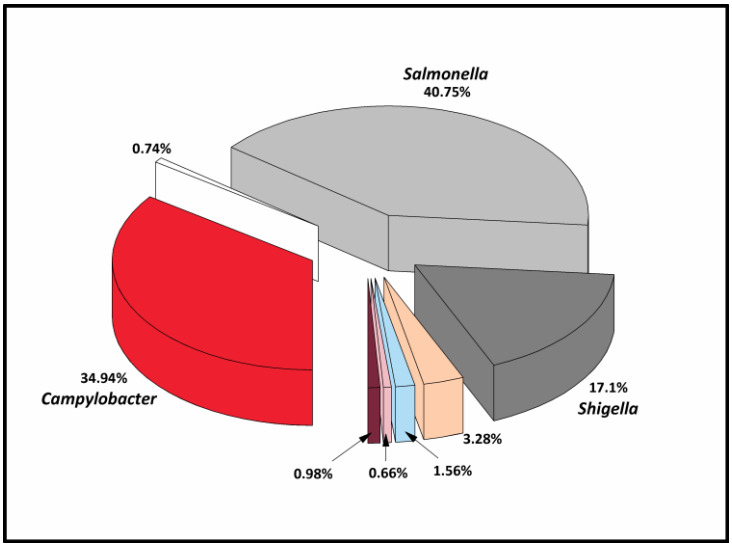

Figure 2-4 Foodborne pathogens responsible for transmitted diseases in 2007

2.6. *Campylobacter jejuni* (*C. jejuni*)

Although campylobacters were first recognized about 100 years ago, their widespread association with diseases in humans was observed in recent times [19]. *C. jejuni* is by far the most important human enteropathogen among *Campylobacters*. It is a micro-aerophilic, gram-negative, flagellated spiral bacterium that are mostly slender, curved and motile rods, 0.2 μ to 0.8

μm wide and 0.5 to 5 μm long. Cells of some species are predominantly straight rods while old cultures may form coccoid bodies that are a degenerative form in the bacterial cycle, than a dormant stage of the organism. Owing to its aerophilic nature, it requires 3 – 5% oxygen and 2 – 10 % carbon dioxide for optimal growth. Also known as a antecedent of Guillain-Barré syndrome. Two sub species are recognized within *C. jejuni*: *C. jejuni* subsp. *jejuni and C. jejuni* subsp. *doylei*. Both the strains differ from each other by the absence of a nitrate reduction, cephalothin susceptibility and often catalase activity. These species are respiratory and chemoorganotropic types that grow under microaerophilic conditions, typically between 30 and 37 °C. Hence, they are able to flourish across a wide range of dairy and poultry products [20].

2.7. Pathogenesis of *C. jejuni* diseases

C. jejuni is a type of proteobacteria and belongs to the *Campylobacteriales* order, and is a member of the *Spirillaceae* family because of its physiological and anatomical similarities [21]. They have small genomes (1.6 – 2.0 megabases) and can establish long-term associations and pathogenic consequences with their hosts. In today's world waterborne infections are less likely to infect any host, and animals turn out to be the prime source of human infection and diseases. Acquired from the ingestion of contaminated poultry products, the human response to *C. jejuni* is more symptomatic than that of poultry animals. There have also been reports of *C. jejuni* infections leading to septicemia, skin and soft tissue infection and meningitis. Additionally, many other outcomes of *C. jejuni* infection in humans are not well understood, due to the lack of suitable models that emulate the symptoms and diseases.

Humans are always at a risk of acquiring acute gastroenteritis even from very low concentrations of *C. jejuni*, which is accompanied by inflammation, abdominal pain and diarrhea and in most cases leads to Guillain-Barré syndrome. Symptoms caused due to *Campylobacter* infection can be manifested in two ways; self-limiting inflammatory bloody diarrhea containing

leukocytes and non-inflammatory, watery diarrhea, predominantly among children. This virulence has been characterized by four major properties if *C. jejuni* namely: motility, adherence, invasion and toxin production. The motility and corkscrew morphology of *C. jejuni* facilitates moving towards the attaching sites of the epithelium. Following this, *C. jejuni* attacks the intestinal cells, by adhering to the cell wall and colonization. This is in turn characterized by the induction of proinflammatory cell-signaling proteins; an indication of *Campylobacteriosis*. Although adhesins and fimbrial structures are significant in colonization of bacteria, intracellular killing and growth occurs in vitro due to the secretion of proteinaceous toxins from the bacteria. These toxins can be classified in to two types based on their activity: enterotoxins and cytotoxins. Enterotoxins are secreted proteins that bind to the cellular receptor. They contain an enzymatic part A, and a receptor binding pentamer B. Deregulation of the cellular regulatory system occurs after receptor A binds to the target cell causing an uneven increase in intracellular cyclic AMP levels, leading to a change in ion flux, which secretes excess fluid from the body resulting in watery diarrhea.

As compared to the above effects, cytotoxins are proteins that kill target cells. They are classified in to two types based on their level of toxicity. The first type which is called verotoxins contains two subunits; an enzymatic subunit A and a receptor binding subunit B. On attaching to the cell, subunit A proteolytically cleaves and induces depurinating activity by inhibiting protein synthesis and resulting in cell death. Contrarily, the second type of toxin called hemolysins, have the capacity to form pores in nucleated cells. In the course of infection, profound effects like lysis of erythrocytes and cytoskeleton dysfunction causes damage to leukocytes and granulocytes, which eventually reduces the immune system of the host [22]. One of the widely studied mechanisms during *C. jejuni* infection is its Cytolethal Distending Toxin (CDT) activity.

Although produced in several pathogens such as *Escherichia coli*, *Shigella dysenteriae* and *Helicobacter* spp., not all of them are implicated to enteric diseases. CDT activity is expressed as a result of the formation of a tripartite holotoxin complex encoded from three tandem genes; *cdtA*, *cdtB* and *cdtC*. The active component of the toxin is bound to the host cell using *cdtA* and *cdtC*, while *cdtB* encodes the active component of the toxin. A high percentage of retailed poultry products are contaminated with *C. jejuni* which is a major factor in human exposure to this pathogen. Introducing antibiotics in poultry feed reduces the levels of *C. jejuni* contamination. The most commonly prescribed antibiotics for *Campylobacter* infections are macrolides and fluoroquinolones. Quinolones were introduced in the 1960's for treating *Campylobacteriosis* and *C. jejuni* infections. The FDA approved the use of two fluoroquinolones - sarafloxacin and enrofloxacin. However, by the 1980's it was confirmed that these pathogens developed resistance to fluoroquinolones within a span of two decades [23-25]. Additionally, resistance to erythromycin and tetracyclines in human and animal *Campylobacter* isolates have also been well documented [26]. Although resistance to macrolides has remained at a very low level, a recent outbreak of macrolide-resistant *C. jejuni* in Finland has raised serious concerns. It has also been indicated that very few alternatives exist for treatment of *Campylobacteriosis* caused by this multi-drug resistant *Campylobacter* strain. Also studies have shown that patients infected with quinolone and erythromycin resistant *Campylobacter* strain have adverse effects than compared to antimicrobial susceptible drugs bacterial strains [27, 28]. The epidemiology of *C. jejuni* is unclear and it is believed that poultry and farm animals are the carriers of this organism, in most cases without showing any symptoms of the disease. It is also believed that the number of *Campylobacter* infections may exceed those caused by *Salmonella* spp., *Shigella* spp. and *Vibrio cholera* [29].

Anti-microbial agent	MIC (µg/ml) breakpoint of resistant isolates	% Resistant
Erythromycin	*16*	*10*
Azithromycin	*4*	*11*
Clindamycin	*8*	*11*
Nalidixic acid	*32*	*91*
Ciprofloxacin	*4*	*92*
Norfloxacin	*16*	*90*
Ofloxacin	*8*	*90*
Levofloxacin	*8*	*76*
Ampicilin	*32*	*40*
Co-amoxiclav	*32*	*42*
Chloramphenicol	*32*	*1*
Imipenem	*16*	*0*
Meropenem	*16*	*0*
Gentamicin	*16*	*2*
Tetracycline	*16*	*61*
Tigecycline	*0.5*	*0*

Table 2-1 Susceptibilities of clinical isolates of *C. jejuni* for different anti-microbial agents

Since, the discovery of the hippurate hydrolysis in 1980 [30, 31] to distinguish between *C. jejuni* (*hippurate* positive) and other *Campylobacters* (*hippurate* negative), triggered the research in to the taxonomical aspects of this thermophilic bacteria. The hippurate hydrolysis involves cleaving of *N*-Benzoylglycine to glycine and benzoic acids which are then, detected using a ninhydrin-based reagent system and precipitation with ferric chloride reagent. On the contrary, an occurrence of *hippuricase*-negative variants and size dependence of the phenotypic expression of enzymes led to the failure of assays in detecting low-level producers of *hippuricase*. Hence, the *hippuricase* activity was characterized and sequenced using deletion subclones and insertional inactivation permitting the development of a genetic probe specific only to *C. jejuni* and a practical approach to investigate the role of *hipO* gene in the activity [32, 33].

2.8. Biosensors

Chemical sensors which utilize a biochemical mechanism in recognizing the analyte are termed biosensors, with only a bioreceptor, at a direct spatial contact with the transducer. Being the key component of any sensor platform, a recognition element imparts selectivity acquiring a dose response from any given group of analytes. Thévenot *et al*. [34] classified biosensors in to catalytic and non-catalytic (affinity based) sensors, while some of the newly devised sensor platforms use microorganisms as receptors. Classic examples of catalytic platforms are glucose biosensors, biosensors involved in detection and decontamination of pesticides and chemical warfare agents. Since then, significant advance has been made in biosensor technologies including nucleotides, aptamers and peptides as biorecognition elements. Nucleotide or nucleic acid sensors belong to the class of chemical sensors which transforms a biochemical stimulus in to a readable signal (induced by change in chemical structure or analyte concentration). Venture in to developing small sensing devices for biomedical applications is rapidly flourishing, with an enormous potential in decentralizing point-of-care and critical-care. Breakthroughs in the field of nanotechnology and biosensors have paved way for rapid, sensitive and 'on-the-spot' clinical diagnostics including miniaturized devices, rapid monitoring of dynamic events and induction of advanced sensing materials. Potential applications include; patient health care, brewing industry, pharmaceutical synthesis, food manufacture, waste water treatment and energy production.

2.9. Biorecognition elements

2.9.1. Enzymatic Biosensors

In general, enzymes are employed as biocatalysts in reactions where the mode of action involves oxidation and reduction. They contain a prosthetic group that can bind itself to the substrate, and in most of the cases the detection is done electrochemically. Although, a very wide range of enzymes are available commercially with well defined assay characteristics, they are

expensive and the cost of extracting, isolating and purifying them is excessive. Also, they tend to lose activity and degrade after a relatively short period of time. Alternatively, plant and animal tissues were also used with minimal preparation. Presence of multiple enzymes makes them less selective than purified enzymes, but they undergo minimum degradation, which enables them to have a longer shelf-life. However, they have a very slow response and induce several interfering processes which are not desirable for any biosensor development.

2.9.2. Antibody-Based Biosensors

Being one of the most versatile biological selective agents, antibodies have been developed against a wide range of analytes. Although, they donot possess the catalytic activity as those of enzymes, antibodies have been long used as immunoassays, exhibiting higher binding power than enzymes have to their substrates, making them ultrasensitive recognition elements. This is due to the specificity of antigen-antibody interaction. Since the physiochemical change induced by antigen-antibody interaction does not produce any electrochemically detectable signal, the antibody or antigen is labeled with fluorescent compounds and electrochemically active species. Antibodies used are selective to the epitope on the antigen. A detectable signal is produced even if the epitope is present in live or a dead host. This is undesirable because a positive result from even a nonviable foodborne pathogen may raise a false alarm. Also, when adsorbed or covalently immobilized on the surface, they attach with a random orientation. Another pitfall in antibody based biosensors is the non-specific binding of proteins, instability and leakage of antibodies from the surface [35].

2.9.3. Aptasensors

Originating from in vitro selection across random sequence libraries nucleic acid aptamers are single-stranded oligonucleotides optimized for high affinity sensing. It is coined from the Latin '*aptus*', which means 'to fit' and involves the three-dimensional folding of a

peptidic bioreceptor with its target. This 3D folding falls under the category of stacking, shape complimentarity, electrostatic and hydrogen bonding. ‘Aptasensors’ are a novel class of receptors that bind to the target in picomolar and nanomolar concentrations which exceed the properties of antibody based biosensors. Aptamers are commonly used in therapeutic applications and one of the most commonly used model is Pegaptanib which is an aptamer directed against vascular endothelial growth factor (VEGF). The VEGF is a condition that causes blood-retina barrier breakdown and results in a reduction in fluid and electrolytes within the extracellular space. An anti-VEGF aptamer (PEGylated, short 2‘-F- and 2‘-methoxy-modified RNA oligonucleotide) is used as the nuclease resistant target [36].

Other common applications are the use of aptamers in common diagnostic assays including blot assays, immunoprecipitation and flow-cytometry. Various types of proteins were detected using different configurations of aptamers as target molecules [37-41]. The main advantages of using aptamers as bio-receptors are: does not require biological raw materials, cost effectiveness, high thermal stability, wide range of surface chemistries and higher affinity. Although, aptamers are used to detect a wide spectrum of proteins and disease biomarkers, there are factors which limit it to the laboratory setting, including longer incubation time due to slow diffusion of the analyte through an unstirred recognition layer.

2.9.4. Tethered DNA structures on 2D substrates

DNA serves as a very intriguing structure and forms the central icon of modern biology. Sensors using tethered DNA involve the selective interaction between immobilized receptors and its partner molecule and they are called affinity biosensors. Several types of biosensors have been developed, including electrochemical DNA sensors that use well defined plasmid nucleic acids. Synthetically prepared oligodeoxyribonucleotides (ODNs) are used as DNA probes in hybridization based sensing platforms. The end groups are labeled with thiols, amines or biotin

to be immobilized on to transducer surfaces. The probe sequence is generally designed complimentary to the target to be detected. As in the case of antibiotics, specific base-pairing between two strands of nucleic acids gives rise to a genetic code, which determines the replicating characteristics of the cell and thereby inherited properties of every living cell, proteins and enzymes. DNA receptors called “Probes” can be used either in the ‘short’ synthetic form or in the ‘long’ cloned form. They can be used to detect cancers, viral infections and genetic diseases. DNA can also be used to improve sensor development by increasing enzyme yield by effectively duplicating the gene that codes an enzyme. Virtually any biological agent can be identified using hybridization based systems (genotyping). Any hybridization based system is characterized by its ability to form stable hybrid complexes with complementary DNA strands. The mechanism with which a complementary strand anneals to its probe adheres to the general Watson-Crick rules of base pairing.

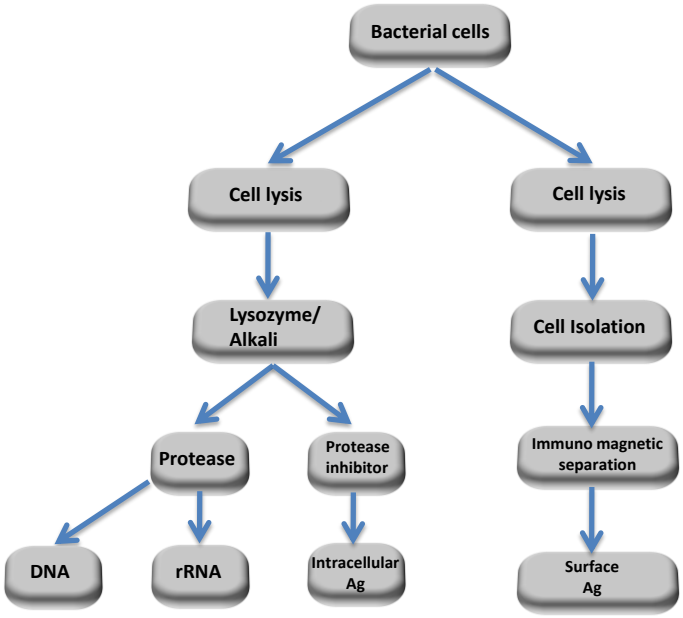

Figure 2-5 Sample preparation procedures for different types of DNA biosensors

Dissociation of the hybrid is directly related to the melting temperature (T_m) of the hybrid and directly corresponds to the stability of the DNA hybrid. As a general rule, the T_m is equivalent to the sum of 2°C for each A–T base pair and 4°C for each G–C base pair. Besides, melting temperature can also be affected by change in ionic concentration, pH, length of the complementary sequence and mismatches between the strands.

2.10. DNA as an alternate probe for biosensors

DNA sequencing technologies have turned out to be a laborious procedure involving electrophoretic size separation of labeled DNA fragments. Sequencing can also be achieved by hybridization of a specific target DNA with strands which have been attached to a surface [42]. In a typical DNA-based sensor array, single-stranded DNA (ssDNA) of different sequences called 'probe molecules' are attached to the surface. The array is then exposed to fluorescently or radioactively labeled ssDNA called 'target molecules' that hybridize with the probe molecules. Hence, DNA-based technologies hold great promise for diagnosis of genetic diseases and accurate sequence determination.

Almost all self-replicating eukaryotes and prokaryotes can be discriminated on their nucleic acid sequence unique to that biological organism. The most challenging aspect of this issue is to develop a multi-assay sensing platform that recognizes all the potential biological variants. Based on this consideration, DNA arrays can be developed using two strategies: target amplification and direct target probing with signal amplification. The number of target molecules in vitro can be increased by incorporating amplification processes that greatly improve hybridization based systems. Ideally, nuclei-acid based assays should generate a gazillion of target copies starting with one, and detect a single 'probe molecule' organism. The sensitivity of nucleic-acid based assays is limited to 10^5–10^6 targets, which is very low considering the number of target molecules. In general rRNA-based detection systems have a low limit of detection

considering the number of cells available for growth. Saiki *et al* [43] proposed a novel amplification method called polymerase chain reaction (PCR), which has wide spread applications in clinical analysis, environmental microbiology and forensics.

Recently, there have been reports of DNA assays developed for the detection of virulence gene in disease causing bacteria [44]. It involves a direct approach of coding genes that specify the virulence factor in biological threat agents. For instance, virulent strains in *Bacillus anthracis* such as 'Ames' and 'Vollum' are detected by targeting the corresponding genes *lef, cya and pag* that are present on its *pXO1* plasmid. For *Campylobacter jejuni* the *hippuricase* gene encodes the specific enzyme activity, which contains a single open reading frame of 1149 bp, which is absent in other species [45]. The sequence of both strands of *hipO* were determined from similar clones, by the di-deoxy chain termination method using nested deletions obtained using an exonuclease III and a S1 nuclease. Besides, PCR-RFLP studies also indicate that the virulent gene (*hipO*) conserved among *C. jejuni* strains alone and thus detection of *hipO* gene using PCR based amplification methods can be a reliable method to detect *C. jejuni* [46].

2.11. DNA Immobilization

2.11.1. Physisorption

Dense nucleic acid (NA) layers obtained by immersing the substrate in the NA solution are the key in developing electrochemical DNA sensors on carbon electrodes. The negative phosphate backbone of nucleic acid binds to the carbon paste electrode or on highly oriented pyrolytic graphite, thereby having a strong effect on the adsorption of oligonucleotides, and is strong enough to conduct experiments in solution. Besides, a positive potential applied on the electrode during immobilization at a pH of 5.3 forms more condensed and a compact DNA lattice [47]. Physisorption can lead to inaccessibility of the immobilized DNA by a target molecule as the backbone is attached to the electrode, which results in poor hybridization

efficiency. Entrapment within cationic and conducting polymers enables stable immobilization, better accessibility and conductivity. However, immobilization in polymeric materials can lead to conformational passivity and high loading of the probe molecules.

2.11.2. Covalent Immobilization

In order to maintain the primary recognition ability of a DNA molecule, the sensing platform can be prepared by immobilization via one end, which in turn increases reusability and longer shelf-life. Millan *et al.* [48] reported a novel DNA biosensor which involves the covalent immobilization of amine functionalized DNA probes using 1-(3-dimethylaminopropyl)-3-ethylcarbodiimide to glassy carbon electrodes (GCE). Henke *et al.* [49] designed a nucleic acid sensor using a amine terminal moiety extended from silanization of an optical fiber and covalently immobilizing DNA probes on the surface. DNA probes were also attached covalently attached using a self-assembled monolayer of a succinimidyl ester [50]. Recently, it was shown that nucleotides can be covalently immobilized on to aldehyde activated silanized alumina membranes, and detected using electrochemical impedance spectroscopy [51]. However, the reaction of these nucleotides with the corresponding amino groups has not been entirely documented.

2.11.3. Affinity binding

Highly specific interactions between avidin-biotin are used frequently to immobilize DNA probes biotinylated at the 5’ end to avidinated surfaces. DNA sensors on 3D surfaces were designed using biotin-avidin-biotin bridge that can be photo-activated. Highly specific affinity DNA biosensor with better regeneration efficiency was designed using an intercalation of avidin on a copolymer electro-synthesized from polypyrrole-biotin and then immobilizing biotinylated DNA on to this surface. Giakoumaki *et al* [52] reported a novel DNA biosensor using surface plasmon resonance, where biotinylated DNA was immobilized on to a avidinated dextran

modified surface. Besides, an avidinated surface can act as a barrier that inhibits redox mediators and hence increases sensitivity in electrochemical detection. However, incorporating avidin-biotin chemistry accompanies the problem of non-specific binding that produces a drift in most optical biosensors and is capable of producing a false positive result in most cases.

2.11.4. Chemisorption

Adsorption can be classified in to two types based on the type of bonding to the surface of interest: physisorption and chemisorption. It involves the attachment of biomolecules through hydrophobic or electrostatic interactions, weak charge transfer forces or formation of van der waals forces and hydrogen bonds. Proteins can be adsorbed on a number of surfaces like, alumina, charcoal, clay, cellulose, kaolin, silica gel, glass and collagen. A classic example is attaching wild type proteins to a biochemical analysis surface such as polystyrene, polyvinylidene fluoride (PVDF), nitrocellulose membrane or a poly-Lys-coated glass plate traditionally used for immunoblot and phage display [53-55]. Mathematically, this phenomenon can be represented by *Langmuir adsorption isotherm*, where the fraction of the surface covered by the adsorbent is related to various kinetic parameters as given:

$$\text{rate of adsorption} = k_a p_a \, N(1-\theta) \tag{2.1}$$

$$\text{rate of desorption} = k_a N\theta \tag{2.2}$$

At equilibrium, both the rates are equal, and hence:

$$\theta = \frac{Kp_a}{1+Kp_a} \tag{2.3}$$

Nuzzo *et al* [56] reported the first spontaneous self-assembly of alkanethiols on gold. Since then, SAMs have grown to be a widely used research tool for various surface chemistries with molecular organization and defined stoichiometry over large surface areas.

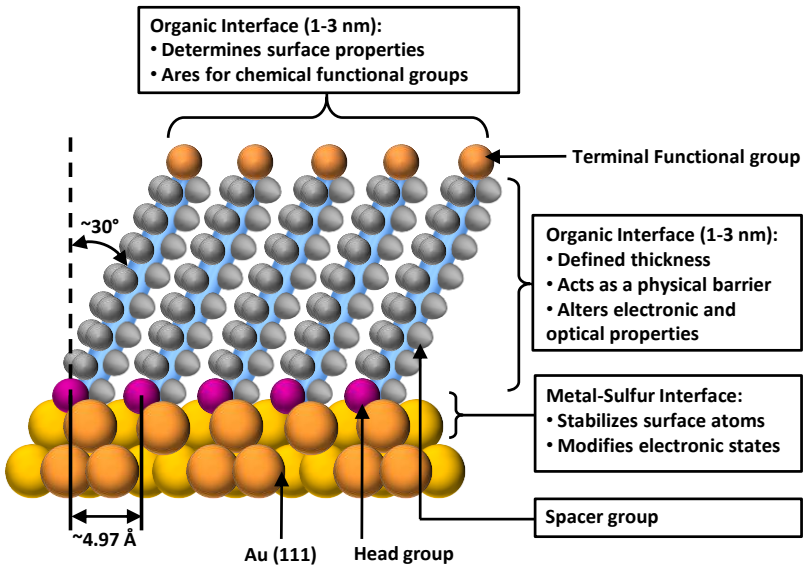

Figure 2-6 Schematic of an ideal Self-assembled monolayer formed on a gold (111) surface

SAMs are self-assembled nanostructures typically 1-3 nm in thickness and the most elementary form of any nano-meter sized thin-film material. In general, self-assembly involves the spontaneous organization of molecules in to reproducible arrangements in a drive to minimize interaction energy between molecules. Interfacial properties of metals and semiconductors can be tailored using this convenient system called self-assembled monolayers (SAM). These organic molecules assemble by the adsorption of molecular constituents from a solution or gas phase on to a solid platform in a regular array; or a spontaneous or epitaxial organization in to crystalline or semi-crystalline structures [57]. Additionally, the organic molecule acts as an electrostatic barrier against aggregation to minimize the interaction between surface atoms and behaves as an electrically insulation film. More specifically, proteins and single-stranded DNA align themselves and form a platform to sense its complement and hence to form a double-stranded helix. Hence a relatively strong and simple point self-assembled monolayer can be developed using chemisorption for effective DNA biosensors [58].

High purity should be maintained during the surface preparation, as SAM formation is an exchange process such that, the thiol molecule needs to displace any adventitious material adsorbed on the surface to form a spontaneous assembly. The rate of desorption of these foreign materials should aid the attachment of the thiols to the surface. Degassing the solvent before SAM development also reduces oxidation thiols to oxygenated species. Chemical activation is required for the S-H bond to form a thiolated on the surface.

Nuzzo *et al* [59] pioneered the studies behind the thermodynamics of SAM formation. Adsorption of a thiol is a fully reversible reaction, and the physisorption enthalpy was calculated to be ~33 kJ/mol [60, 61]. Also, the structural organization of thiols on Au (111) has been well documented, and is generally based on a $(\sqrt{3}\times\sqrt{3})$ R30° hexagonal closed packed structure, where R indicates rotated. Likewise the spacing between each alkane chain was found to be ~4.97 Å, which is three times the van der Waals diameter of a sulfur atom (~1.85 Å).

2.12. Structure-Property of biological ligands as SAMs

Although *n*-alkanethiols form ordered arrays of self-assembled molecules in a spontaneous or epitaxial fashion, the molecules used in biology and biochemistry differ substantially from these SAMs. More specifically, the factors that are not taken in to consideration are: size and shape of the ligands that form a SAM on gold, functional groups that counteract protein adsorption on to Au surface and interaction of the SAM with the aqueous media required for the biochemical reaction. Because of their large surface area ($\geq$ 0.25 nm^2) ligands and biomolecules are unable to form SAMs with the same organization as *n*-alkanethiolates. Stearic hindrances from the bulk of the ligands induce disorders across the SAM. Paradoxically, if the ligands are able to form an ordered domain, the structural formation differs completely from that of alkanethiolates and creates pinholes and defects in the assembly. These defects can be overcome by using a monolayer comprised of a mixture of molecules known as

'mixed-SAMs'. It involves the incorporation of a molecular species whose length and size would commence the formation if a well-ordered assembly. Herne *et al* [62] reported the first 'mixed-SAM' based platform for DNA hybridization. 6-Mercapto-1-hexanol (MCH) was used as the second thiol in order to prelude the formation of a well-ordered array of thiolated ssDNA on Au surface [57].

2.13. Commercial *C. jejuni* testing kits

The latex agglutination tests using a limited amount of bacteria and the corresponding neutralizing agent and a reactive latex has been the 'gold standard' for *Campylobacter* detection apart from the conventional culturing and staining methods [63]. However, the presence of antibiotics for suppressing bacterial growth and varying susceptibility of agar growth reduces the reliability of these tests. As a result, several commercial latex agglutination tests were conceived, including those incorporating polyclonal antibodies. In 1993, the Food and Drug Administration had approved 'Meritec-Campy', which are able to detect antigenic outer membrane proteins or antigenic epitopes from flagella, for samples isolated from clinical and food samples. Other latex agglutination tests include PanBio-Campy, the Dryspot *Campylobacter* and the Microgen M46 *Campylobacter*. These test kits showed reactivity to thermotolerant *Campylobacter* species, while the Dryspot *Campylobacter* showed difference by large clumps formation to other bacteria [64]. In order to avoid cross-reactivity and to detect as many *campylobacter* species, the appropriate test kit must be selected. However, these kits were not able to identify all of the *campylobacter* isolates, and had pooled serogroups. The change in antibody is not reliable enough to verify and confirm the diagnosis of a disease [65].

2.14. *C. jejuni* biosensors

Biosensing platforms for direct detection of *C. jejuni* are obsolete compared to traditional microbiological methods such as multiplex polymerase chain reaction (mPCR), which initially

focuses on amplification of the gene of interest and then identifying the host cell. However, there has been seldom a report on direct detection of *C. jejuni* using a well defined sensor platform. For instance, Kuijf *et al* reported a sialylation based sensing platform using TLR-4 in order to detect *C. jejuni*, having a limit of detection of 35 pg/ml [66]. Dong *et al* [67] reported a surface plasmon resonance based detection of *C. jejuni* cells by biotinylated anti-*C. jejuni* antibody immobilized on an avidinated gold surface and a sensitivity of 10^7 cfu/ml was obtained. A commercial *C. jejuni* detection platform was also designed based on PCR-ELISA, where a chemically tagged nucleotide was incorporated in to a PCR amplicon and the product of the this PCR was detected with an antibody-enzyme conjugate [68]. Recently, a new enzyme immunoassay (EIA) called 'ProSpecT *Campylobacter* Microplate Assay' was developed for the detection of *C. jejuni*, which involves the detection of the uncharacterized *Campylobacter*–specific antigen [69], which had a limit of detection varying from 3×10^4 cfu/ml to 3×10^5 cfu/ml. Although, these methods prove to be sensitive they invariably require complicated anti-*C. jejuni* antibody-enzyme interaction for specific detection on the surface.

2.15. Transducers – Why optical transducers?

Photon driven devices have mainly been based on photometric transducers, as in the case of spectroscopic methods. Research in optical transducers kicked off from the development of fiber optics, thus enabling greater flexibility and miniaturization. The most common optical transducer based techniques are absorption spectroscopy, fluorescence spectroscopy, luminescence spectroscopy, internal reflection spectroscopy, surface plasmon resonance and scattering of light. Transducers can be subdivided in to four main subdivisions as given. The main advantage of using optical transducers is because they can be used for different types of spectroscopy, with different spectro-chemical properties recorded, including amplitude, energy, polarization and decay time.

Transducer	Techniques
Optical	*Absorption, fluorescence, phosphorescence, Raman, SERS, refraction, dispersion spectrometry, Surface Plasmon Resonance spectroscopy, Luminescence*
Electrochemical	*Amperometric, Potentiometric, Voltammetric, Impedimetric and FET based sensors*
Mass	*Surface acoustic wave, love wave sensor, flexural plate wave, shear-horizontal acoustic wave (SH-APW)*
Thermal	*Catalytic gas sensors, thermistors, thermal conductivity devices*

Table 2-2 Different types of transducers employed in sensor development

Amplitude is the most commonly measured parameter, as it is directly related to the concentration of the analyte. Intramolecular atomic vibrations and conformational changes in the local environment can be monitored with change in energy (i.e. Raman or FT-IR Spectroscopy). Besides this, the interaction of a free molecule with any surface can be studied using polarization measurements. This is because the polarization of emitted light due to a molecule remaining fixed to a surface is constant. Time decay emissions can be used to obtain information about molecular interactions as the decay time and length are very much dependent on the excited state of the molecules. Additionally, the phase of any emitted radiation changes the refractive index of the medium during a biomolecular event. This phase change on the impinging radiation is due to the change in medium when the molecule binds to the surface. There were several reports of novel optical transducers in the past. Vo-Dinh *et al* [70, 71] reported a novel phase-resolved fiber optic fluoroimmunosensor (PR-FIS), which can differentiate a metabolite and the corresponding carcinogen based on fluorescence lifetimes. Plowman *et al* [72] reported an etched thin-film waveguide fluoroimmunosensor that was able to detect analyte molecules in the femto-molar concentrations. Besides, Balasubramanian *et al* [73] reported a novel immunosensor based

surface plasmon resonance spectroscopy for the detection of bacterial cells using lytic phage as a recognition element.

Surface plasmon resonance (SPR) biosensors are based on optical transduction and offer 'label-free' and 'near real-time' detection of the analyte of interest. The principle of this method has been discussed extensively in literature [74-76]. Total internal reflection (TIR) occurs at the interface between two completely different media. An evanescent wave infiltrates through the interface which is modified with a 50 nm gold film, and couples with the surface plasmons. As a result, the reflectivity and resonance angle changes, which is directly correlated to the change in refractive index (RI) of the medium. The change in RI which is continuously monitored as a function of time is due to the change in surface concentration of the interacting ligands. Typically, a response of 1000 RIU or 0.1° change in angle corresponds to a change in surface protein concentration of 1 ng/mm^2. SPR, coupled with the right surface chemistry, has proven to be a highly sensitive technique for the analysis of biological systems as labeling of ligands or receptor molecules are not required and can be used to determine kinetic parameters of the interacting molecules.

Diffraction Optics Technology (DOT) biosensing is similar to SPR based sensors, except that it is a grating-based light diffraction method. Probe molecules are immobilized on an optimized grating that produces a strong diffraction pattern when a coherent light strikes an array of molecules immobilized on the surface. Diffraction efficiency is improved when biomolecules bind to a patterned surface, which in turn increases the signal intensity and hence a measurable change in signal is produced. Being a self-referencing method, it is considered a robust sensor platform for analysis. In simplistic terms, the diffraction efficiency depends on the relative height difference between the patterned and non-patterned areas, thus non-specific binding to both the

patterned and non-patterned regions will not affect the signal significantly. This attribute provides a considerable advantage over other optical biosensor systems in which any surface binding event will cause a spurious increase in signal [77].

2.16. Thesis organization

Pathogenic bacteria should be eliminated from poultry and dairy products in order to avoid any potential health hazards and combat disease transmission. Although, there are several methods to detect bacteria, most of them are labor intensive when large samples have to be prepared. All microorganisms can be identified and differentiated based on a virulent gene that causes diseases. Biosensor platforms using immobilized ssDNA have the potential for quickly sequencing and detecting DNA samples by selective hybridization. Additionally DNA diagnostics find applications from sequencing the entire human genome (The Human Genome Project), detecting disease-causing food-contaminating microbes and forensic and environmental applications. However, applications of ssDNA in SPR and DOT based platforms for direct detection of virulent ssDNA is minimal. Hence a proof of concept was developed to show that ssDNA directly tethered to a substrate without complex surface chemistries can be used to capture the *hipO* gene of *C. jejuni* without losing the sensitivity after several trials and with the same hybridization efficiency after several trials of regenerating the sensor surface, by denaturation of the double-helix structure formed during detection. Finally, a novel non-destructive technique was developed to analyze the electron transfer and charge injection through SWNT based nanomaterials, where dsDNA has been used as a dispersant for SWNTs; using scanning electrochemical microscopy. These nanomaterials were developed using a 'bottom-up' approach with critical control for anti-bacterial applications.

Thus, the main objectives of the present study were:

I. Investigation of the prospects of DNA immobilized on a SPR and DOT sensor platform for the label-free detection of the hippuricase (*hipO*) gene in *Campylobacter jejuni*. Here we use ssDNA as a nanoscale scaffolds for 'real-time' detection of pathogenic bacteria. The detection was additionally verified with the immobilization chemistry using electrochemical impedance spectroscopy (EIS). DNA scaffolds were also developed using a long and a short probe to verify the prospects of using long chained ligands directly immobilized on the sensing surfaces.

II. The preparation of supramolecular adducts using DNA as a dispersing agent in order to prepare an aqueous phase of SWNTs with uniform length. Accordingly, DNA can also be used as a precursor and a building block for macromolecular electronics. An advanced analytical technique - scanning electrochemical microscopy (SECM), is used as a novel approach to measure the lateral (in-plane) and cross-film electron transport in nano-composite films developed using DNA and SWNT adducts. Energetics of the entire charge injection process can be quantified using SECM, with sensitivity across every single nanotube layer.

2.17. References

1. Feynman, R., *Miniaturization*, ed. H.D. Gilbert. 1961, New York: Reinhold. 282-296.
2. Drexler, K.E., *Molecular engineering: An approach to the development of general capabilities for molecular manipulation.* Proc. Natl. Acad. Sci. USA 1981. **78**(9): p. 5275-5278.
3. Nepal, D., et al., *Supramolecular Conjugates of Carbon Nanotubes and DNA by a Solid-State Reaction.* Biomacromolecules, 2005. **6**(6): p. 2919-2922.

4. Kuhn, H. and D. Möbius, *Systems of Monomolecular Layers—Assembling and Physico-Chemical Behavior.* Angew. Chem. internat. Edit., 1971. **10**(9): p. 620-637.

5. Decher, G., *Fuzzy Nanoassemblies: Toward Layered Polymeric Multicomposites.* Science, 1997. **277**: p. 1232-1237.

6. Podsiadlo, P., et al., *Fusion of Seashell Nacre and Marine Bioadhesive Analogs: High-Strength Nanocomposite by Layer-by-Layer Assembly of Clay and L-3,4-Dihydroxyphenylalanine Polymer.* Adv. Mater., 2007. **19**(7): p. 949-955.

7. Zhai, L., et al., *Patterned Superhydrophobic Surfaces: Toward a Synthetic Mimic of the Namib Desert Beetle.* Nano Lett., 2006. **6**(6): p. 1213-1217.

8. Ellis, D.L., et al., *Conductive Polymer Films as Ultrasensitive Chemical Sensors for Hydrazine and Monomethylhydrazine Vapor.* Anal. Chem., 1996. **68**(5): p. 817-822.

9. Farhat, T.R. and J.B. Schlenoff, *Ion Transport and Equilibria in Polyelectrolyte Multilayers.* Langmuir, 2001. **17**(4): p. 1184-1192.

10. Constantine, C.A., et al., *Layer-by-Layer Self-Assembled Chitosan/Poly(thiophene-3-acetic acid) and Organophosphorus Hydrolase Multilayers.* J. Am. Chem. Soc., 2003. **125**(7): p. 1805-1809.

11. Kleinfeld, E.R. and G.S. Ferguson, *Rapid, Reversible Sorption of Water from the Vapor by a Multilayered Composite Film: A Nanostructured Humidity Sensor.* Chem. Mater., 1995. **7**(12): p. 2327-2331.

12. Wood, K.C., et al., *Controlling interlayer diffusion to achieve sustained, multiagent delivery from layer-by-layer thin films.* Proc. Natl. Acad. Sci. USA, 2006. **103**: p. 10207-10212

13. Olek, M.J., et al., *Layer-by-Layer Assembled Composites from Multiwall Carbon Nanotubes with Different Morphologies.* Nano Lett., 2004. **4**(10): p. 1889-1895.

14. Lee, S.W., et al., *Layer-by-Layer Assembly of All Carbon Nanotube Ultrathin Films for Electrochemical Applications.* J. Am. Chem. Soc., 2009. **131**(2): p. 671-679.

15. Nepal, D., et al., *Strong Antimicrobial Coatings: Single-Walled Carbon Nanotubes Armored with Biopolymers.* Nano Lett., 2008. **8**(7): p. 1896-1901.

16. Wei, B.Q., R. Vajtai, and P.M. Ajayan, *Reliability and current carrying capacity of carbon nanotubes.* Appl. Phys. Lett., 2001. **79**: p. 1172.

17. Lie, L.H., et al., *Electrochemical detection of lateral charge transport in metal complex-DNA monolayers synthesized on Si(1 1 1) electrodes* J. Electroanal. Chem., 2007. **603**(1): p. 67-80.

18. Heller, I., et al., *Electrochemistry at Single-Walled Carbon Nanotubes: The Role of Band Structure and Quantum Capacitance.* J. Am. Chem. Soc., 2006. **128**(22): p. 7353-7359.

19. Butzler, J., ed. *Campylobacter Infection in Man and Animals*. 1984, CRC Press: Boca Raton.

20. Nachamkin, I., C.M. Szymanski, and M.J. Blaser, *Campylobacter*. Third ed. 2008, Washington DC: ASM Press.

21. Stern, N.J. and S.U. Kazmi, *Foodborne Bacterial Pathogens*, ed. M.P. Doyle. 1989, New York: Marcel Dekker, Inc.

22. Wassenaar, T.M., *Toxin Production by Campylobacter spp.* Clin. Microbiol. Rev., 1997. **10**(3): p. 466-476.

23. Engberg, J., F. , et al., *Quinolone and macrolide resistance in Campylobacter jejuni and C. coli: resistance mechanisms and trends in human isolates.* Emerg. Infect. Dis., 2001. **7**: p. 24-34.

24. Hoge, C.W., et al., *Trends in antibiotic resistance among diarrheal pathogens isolated in Thailand over 15 years.* Clin. Infect. Dis., 1998. **26**: p. 341-345.

25. Hakanen, A., et al., *Fluoroquinolone resistance in Campylobacter jejuni isolates in travelers returning to Finland: association of ciprofloxacin resistance to travel destination.* Emerg. Infect. Dis., 2003.

26. Michel, J., M. Rogol, and D. Dickman, *Susceptibility of Clinical Isolates of Campylobacter jejuni to Sixteen Antimicrobial Agents.* Antimicrob. Agents Chemother., 1983. **23**(5): p. 796-797.

27. Lehtopolku, M., et al., *Antimicrobial Susceptibilities of Multidrug-Resistant Campylobacter jejuni and C. coli Strains: In Vitro Activities of 20 Antimicrobial Agents.* Antimicrob. Agents Chemother., 2010. **54**(3): p. 1232-1236.

28. Young, K.T., L.M. Davis, and V.J. DiRita, *Campylobacter jejuni: molecular biology and pathogenesis.* Nat. Rev. Microbiol., 2007. **5**: p. 665.

29. Blaser, M.J. and L.B. Reller, N. Engl. J. Med. **305**: p. 1444-1452.

30. Harvey, S.M., *Hippurate hydrolysis by Campylobacter fetus.* J. Clin. Microbiol., 1980. **11**: p. 435-437.

31. Penner, J.L., *The Genus Campylobacter: a Decade of Progress.* Clin. Microbiol. Rev., 1988. **1**(2): p. 157-172.

32. Hofreuter, D., et al., *Unique Features of a Highly Pathogenic Campylobacter jejuni Strain.* Infect. Imm., 2006. **74**(8): p. 4694–4707.

33. Bacon, D.J., et al., *A phase-variable capsule is involved in virulence of Campylobacter jejuni 81-176.* Mol. Microbiol., 2001. **40**(3): p. 769-777.

34. Thévenot, D.R., et al., *Electrochemical biosensors: recommended definitions and classification.* Biosens. Bioelectron., 2001. **16**: p. 121-131.

35. Saerens, D., et al., *Antibody Fragments as Probe in Biosensor Development.* Sensors, 2008. **8**: p. 4669-4686.

36. Ruckman, J., et al., *2'-Fluoropyrimidine RNA-based Aptamers to the 165-Amino Acid Form of Vascular Endothelial Growth Factor (VEGF165)* J. Biol. Chem., 1998. **273**: p. 20556.

37. Liss, M., et al., *An Aptamer-Based Quartz Crystal Protein Biosensor*. Anal. Chem., 2002. **74**(17): p. 4488–4495.

38. Mucha, P., et al., *S tructural requirements for conserved Arg residue for interaction of the human immunodeficiency virus type 1 trans-activation responsive element with trans-activator of transcription protein (49–57) Capillary electrophoresis mobility shift assay.* J. Chromatogr. A, 2002. **968**: p. 211–220.

39. Lee, M. and D.R. Walt, *A Fiber-Optic Microarray Biosensor Using Aptamers as Receptors.* Anal. Biochem., 2000. **282**: p. 142-146.

40. Kirby, R., et al., *Aptamer-Based Sensor Arrays for the Detection and Quantitation of Proteins.* Anal. Chem., 2004. **76**(14): p. 4066–4075.

41. Savran, C.A., et al., *Micromechanical Detection of Proteins Using Aptamer-Based Receptor Molecules.* Anal. Chem., 2004. **76**(11): p. 3194–3198.

42. Pease, A.C., et al., *Light-generated oligonucleotide arrays for rapid DNA sequence analysis.* Proc. Natl. Acad. Sci. USA, 1994. **91**: p. 5022-5026.

43. Saiki, R.K., et al., *Enzymatic amplification of beta-globin genomic sequences and restriction site analysis for diagnosis of sickle cell anemia.* Science, 1985. **230**(4732): p. 1350-1354.

44. Iqbal, S.S., et al., *Detection of Yersinia pestis by pesticin fluorogenic probe-coupled PCR.* Mol. Cell. Probes, 1999. **14**: p. 109-114.

45. Hani, E.K. and V.L. Chan, *Expression and Characterization of Campylobacter jejuni Benzoylglycine Amidohydrolase (Hippuricase) Gene in Escherichia coli.* J. Bacteriol., 1995. **177**: p. 2396-2402.

46. Slater, E.R. and R.J. Owen, *Restriction fragment length polymorphism analysis shows that the hippuricase gene of Campylobacter jejuni is highly conserved.* Lett. Appl. Microbiol., 1997. **25**: p. 274-278.

47. Brett, A.M.O. and A. Chiorce, *Effect of pH and applied potential on the adsorption of DNA on highly oriented pyrolytic graphite electrodes. Atomic force microscopy surface characterisation* Electrochem. Commun., 2003. **5**(2): p. 178-183.

48. Millan, K.M., A.J. Spurmanis, and S.R. Mikkelsen, *Covalent immobilization of DNA onto glassy carbon electrodes.* Electroanalysis, 1992. **4**(10): p. 929-932.

49. Henke, L., et al., *Covalent immobilization of single-stranded DNA onto optical fibers using various linkers.* Anal. Chim. Acta, 1997. **344**(3): p. 201-213.

50. Loaiza, Ó.A., et al., *DNA sensor based on an Escherichia coli lac Z gene probe immobilization at self-assembled monolayers-modified gold electrodes* Talanta, 2007. **73**(5): p. 838-844.

51. Wang, X. and S. Smirnov, *Label-Free DNA Sensor Based on Surface Charge Modulated Ionic Conductance.* ACS Nano, 2009. **3**(4): p. 1004-1010.

52. Giakoumaki, E., et al., *Combination of amplification and post-amplification strategies to improve optical DNA sensing* Biosens. Bioelectron., 2003. **19**(4): p. 337-344.

53. Ge, H., *UPA, a universal protein array system for quantitative detection of protein–protein, protein–DNA, protein–RNA and protein–ligand interactions.* Nucl. Acids Res., 2000. **28**(2): p. e3(i–vii).

54. Haab, B.B., M.J. Dunham, and P.O. Brown, *Protein microarrays for highly parallel detection and quantitation of specific proteins and antibodies in complex solutions.* Genome Biol., 2001. **2**(2): p. 1-13.

55. Zhu, H. and M. Snyder, *Protein chip technology.* Curr Opin Chem Biol., 2003. **7**(1): p. 55-63.

56. Nuzzo, R.G. and D.L. Allara, *Adsorption of bifunctional organic disulfides on gold surfaces.* J. Am. Chem. Soc., 1983. **105**(13): p. 4481-4483.

57. Love, J.C., et al., *Self-Assembled Monolayers of Thiolates on Metals as a Form of Nanotechnology*. Chem. Rev., 2005. **105**(4): p. 1103-1170.

58. Labuda, J., et al., *Electrochemical nucleic acid-based biosensors: Concepts, terms, and methodology (IUPAC Technical Report).* Pure Appl. Chem., 2010. **82**(5): p. 1161-1187.

59. Nuzzo, R.G., B.R. Zegarski, and L.H. Dubois, *Fundamental Studies of the Chemisorption of Organosulfur Compounds on Au(111). Implications for Molecular Self-Assembly on Gold Surfaces.* J. Am. Chem. Soc., 1987. **109**(3): p. 733.

60. Fischer, D., A. Curioni, and W. Andreoni, *Decanethiols on Gold: The Structure of Self-Assembled Monolayers Unraveled with Computer Simulations.* Langmuir, 2003. **19**(9): p. 3567-3571.

61. Lavrich, D.J., et al., *Physisorption and Chemisorption of Alkanethiols and Alkyl Sulfides on Au(111).* J. Phys. Chem. B, 1998. **102**(18): p. 3456-3465.

62. Herne, T.M. and M.J. Tarlov, *Characterization of DNA Probes Immobilized on Gold Surfaces.* J. Am. Chem. Soc., 1997. **119**(38): p. 8916-8920.

63. Hodinka, R.L. and P.H. Gilligan, *Evaluation of the Campyslide agglutination test for confirmatory identification of selected Campylobacter species.* J. Clin. Microbiol., 1988. **26**: p. 47-49.

64. Miller, R.S., et al., *Evaluation of Three Commercial Latex Agglutination Tests for Identification of Campylobacter spp.* J. Clin. Microbiol., 2008. **46**(10): p. 3546-3547.

65. Elverdal, P., C.S. Jørgensen, and S.A. Uldum, *Comparison and evaluation of four commercial kits relative to an in-house immunofluorescence test for detection of antibodies against Legionella pneumophila.* Eur. J. Clin. Microbiol. Infect. Dis., 2008. **27**: p. 149–152.

66. Kuijf, M.L., et al., *TLR4-Mediated Sensing of Campylobacter jejuni by Dendritic Cells Is Determined by Sialylation.* J. Immunol., 2010. **185**: p. 748-755.

67. Wei, D., et al., *Development of a surface plasmon resonance biosensor for the identification of Campylobacter jejuni.* J. Microbiol. Methods, 2007. **69**(1): p. 78-85.

68. Hong, Y., et al., *Rapid Detection of Campylobacter coli, C. jejuni, and Salmonella enterica on Poultry Carcasses by Using PCR–Enzyme-Linked Immunosorbent Assay.* Appl. Environ. Microbiol., 2003. **69**(6): p. 3492-3499.

69. Endtz, H.P., et al., *Evaluation of a New Commercial Immunoassay for Rapid Detection of Campylobacter jejuni in Stool Samples.* Eur. J. Clin. Microbiol. Infect. Dis., 2000. **19**: p. 794-797.

70. Vo-Dinh, T., et al., *Phase-Resolved Fiber-Optics Fluoroimmunosensor.* Appl. Spectrosc., 1990. **44**(1): p. 128-132.

71. Vo-Dinh, T. and B. Cullum, *Biosensors and biochips: advances in biological and medical diagnostics.* Fresenius J. Anal. Chem., 2000. **366**: p. 540-551.

72. Plowman, T.E., et al., *Femtomolar sensitivity using a channel-etched thin film waveguide fluoroimmunosensor.* Biosens. Bioelectron., 1996. **11**(1-2): p. 149-160.

73. Balasubramanian, S., et al., *Lytic phage as a specific and selective probe for detection of Staphylococcus aureus—A surface plasmon resonance spectroscopic study.* Biosens. Bioelectron., 2007. **22**(6): p. 948-955.

74. Green, R.J., et al., *Surface plasmon resonance analysis of dynamic biological interactions with biomaterials* Biomaterials, 2000. **21**(18): p. 1823-1835.

75. Homola, J., *Surface Plasmon Resonance Sensors for Detection of Chemical and Biological Species.* Chem. Rev., 2008. 108(2): p. 462-493.

76. Myszka, D.G., SPR biosensors as biophysical research tools. FASEB J., 2000. 14: p. A1511.

77. Cleverley, S., I. Chen, and J. Houle, Label-free and amplified quantitation of proteins in complex mixtures using diffractive optics technology. J Chromatogr B Analyt Technol Biomed Life Sci., 2010. 878(2): p. 264-270.

3. Scanning Electrochemical Microscopy – Principle & Experimental Setup

3.1. Scanning Electrochemical Microscopy (SECM)

Measurement of an electric current through an ultra-microelectrode (UME) when moved in a solution in the vicinity of a substrate that instigates an electrochemical response from the tip. This perturbation then provides information about the nature and properties of the substrate. It has played a vital role in electrochemical sciences for the past two decades. As an electrochemical tool, it can be used to study the heterogeneous and homogeneous reactions and imaging the chemical reactivity and topography of a wide range of surfaces. Because of it sub-micron and nanometer-sized spatial resolution, SECM aids in monitoring local kinetics and interfacial phenomena. The most commonly used operational mode in the SECM is the tip generation-substrate collection (TG/SC) mode, where a reactant generated by the tip is detected at the substrate electrode. An alternate method is the substrate generation-tip collection (SG/TC) mode where the concentration profiles near the substrate can be studied without rastering or imaging the surface.

Although the SECM resembles a scanning tunneling microscope (STM), in the method used to raster the tip over the substrate, they differ from each other in the principle of operation and range of applications. Unlike the STM where the current between the tip and the substrate is non-faradaic, the current is defined by a redox process between the tip and substrate. This current is electron transfer controlled at the interface and mass transfer controlled across the bulk solution [1].

3.2. Ultramicroelectrodes (UME)

Ultramicroelectrodes give a quantitative analysis of the electrochemical measurements that can be performed using SECM. Fig. 3-1 shows a simplified setup of a SECM. The solution contains a species, O, whose concentration is *c*, and also contains a supporting electrolyte which reduces the solution resistance and ensures a diffusion controlled reaction between the electrolyte and the substrate.

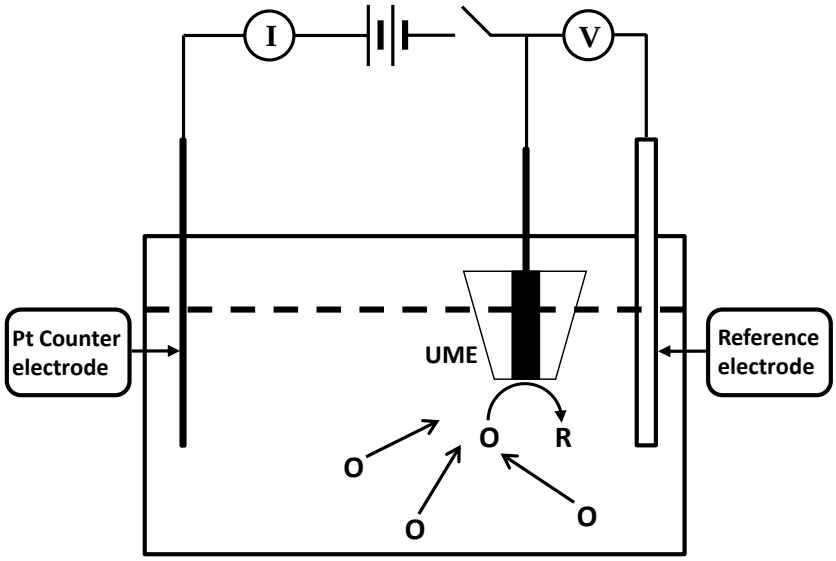

Figure 3-7 Schematic of a cell for ultramicroelectrode voltammetry

A platinum (Pt) auxiliary electrode completes the circuit. When the circuit is closed, a reduction reaction takes place at the tip,

$$O + ne \rightarrow R$$

resulting in a current flow and an oxidation reaction at the auxiliary electrode. Meanwhile the potential across the tip is monitored with respect to a standard silver/silver chloride (Ag/AgCl) reference electrode, which is represented by a standard voltammogram for an ultramicroelectrode (Fig. 3-2).

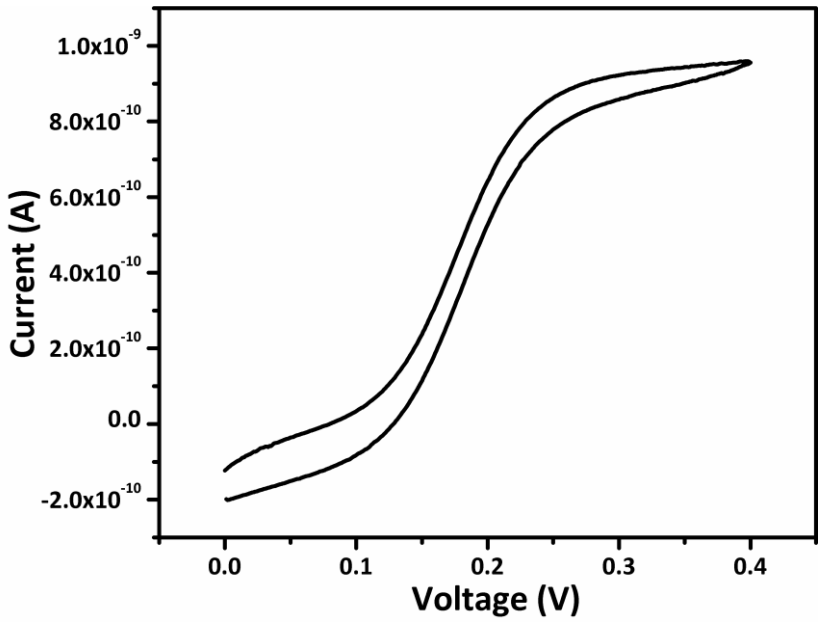

Figure 3-8 Typical voltammogram for a 10 μm ultramicroelectrode

The limiting current obtained as a result of diffusion of species, O, from the bulk to the electrode surface is completely mass-transfer controlled. For a conductive disk electrode of radius *a*, this steady state current when the tip is at an infinite distance from the substrate is give by:

$$i_{T,\infty} = 4nFDca \tag{3.1}$$

Although electrodes with other shapes, hemispheres and cones can be used, most of the SECM experiments are carried out with disk electrodes because of their high sensitivity. Besides, the current is independent of the radius of the insulating glass sheath, r_g, which is also represented as:

$$RG = \frac{r_g}{a} \tag{3.2}$$

Likewise, convection has little or no influence on the tip current because the diffusive flux of species O is relatively large compared to the size of the UME. Apparently, if the potential at the tip is sufficient enough to reduce species O to R, at a diffusion limited rate, then electrode

reaches a steady state at a relatively short time. Numerous applications list out when SECM is coupled with biological systems. These include imaging of biological structures, kinetics of enzymatic reactions to name a few. Measurements are usually carried out in buffered solutions, with the UME that does not interact with the immobilized substrate unlike most of the scanning probe techniques.

3.3. Feedback Mode

In the feedback mode, a steady-state diffusion controlled current $i_{T,\infty}$, is measured at the UME, where the ∞ implies the distance between the substrate and the tip. A hemispherical flux is used to actuate the current from the bulk to the electrode. If the tip electrode is far from the substrate, the infinite steady-state current is due to hemispherical diffusion (Fig. 3-3A). However, the diffusion layer will be hindered and the tip current decreases if the substrate is an insulator, and hence $i_T < i_{T,\infty}$. As a result, the value of i_T becomes smaller, as it gets closer to the substrate (Fig. 3-3B). At the limit when the distance between the tip and the substrate, *d*, approaches zero, i_T reduces to zero. This is termed as 'negative feedback'. On the contrary, if the substrate is a conductor, and maintained at a potential where R can be recycled back to species O, the tip current will increase. Although there is blockage of the diffusion of species O, it is regenerated by the oxidation of R at the substrate and diffuses to the tip, which in turn increases the current (Fig. 3-3C). Thus for a conductive substrate, where $i_T > i_{T,\infty}$, as *d* approaches zero, electron tunneling occurs at the tip and hence the current increases drastically, which is termed as 'positive feedback'. In order to completely understand and conceive the mechanism occurring at the tip and substrate, a quantitative explanation for entire feedback phenomena should be formulated.

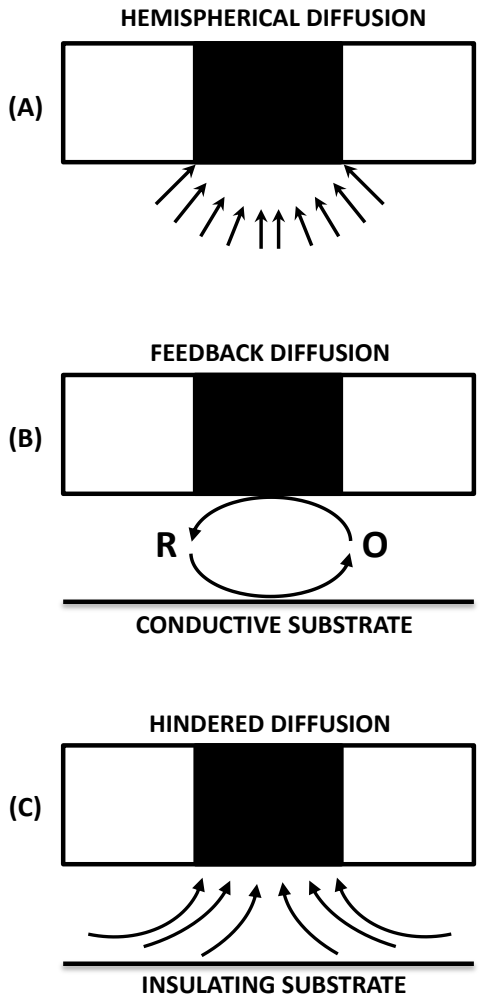

Figure 3-9 Basic principles of SECM: A) Far from the substrate [Hemispherical diffusion] B) Near the substrate [Feedback Diffusion-conductive] and C) Near the substrate [Hindered diffusion-insulating]

3.4. Theoretical Predictions

3.4.1. First-Order Heterogeneous Reaction for reaction between tip and substrate

In the feedback mode, the species O is reduced at the tip and can be reoxidized at the substrate. The process occurring between the tip and the substrate can be written as:

$$O + ne^{-} \rightarrow R \qquad \text{(UME)}$$

$$R - ne^- \rightarrow O \qquad \text{(Substrate)}$$

Theoretical predictions for the SECM include a combination of a cylindrical diffusion to the ultramicroelectrode (UME) and a thin-layer type diffusion space. As a result, this quasireversible prediction under non-steady state conditions can be given as:

$$\frac{\partial C_i}{\partial T} = \frac{\partial^2 C_i}{\partial z^2} + \frac{\partial^2 C_i}{\partial R^2} + \frac{1}{R}\frac{\partial C_i}{\partial R} \tag{3.3}$$

with boundary conditions: $0 < T$, $0 \leq R$, $0 < Z < L$

Other dimensionless variables are given as:

$$R = \frac{r}{a} \tag{3.4}$$

$$Z = \frac{z}{a} \tag{3.5}$$

$$C_i = \frac{c_i}{c_O^\circ} \tag{3.6}$$

$$T = \frac{tD_O}{a^2} \tag{3.7}$$

If the diffusion coefficients of both the species O and R are considered equal, then the problem can be described in terms of a single species. Then, the boundary conditions are given by:

$0 < T$, $0 \leq R < 1$, $Z = 0$ (UME surface)

$$\frac{\partial C_O}{\partial Z} = K_{f.T} C_O - K_{b,T}(1 - C_O) = J_T \tag{3.8}$$

$0 < T$, $1 \leq R \leq RG$, $Z=0$ (insulating sheath)

$$\frac{\partial C_O}{\partial Z} = 0 \tag{3.9}$$

$0 < T$, $0 \leq R \leq h$, $Z = L$ (substrate)

$$\frac{\partial C_O}{\partial Z} = K_{b,S} C_O - K_{f,S}(1 - C_O) = J_S \tag{3.10}$$

R > RG, 0 ≤ Z ≤ L:

$$C_O = 1 \tag{3.11}$$

where, J_T and J_s are the normalized fluxes of the species at the tip and substrate. Hence, it can be represented as:

$$K_{\frac{f}{b,S}} = k_{\frac{f}{b,S}} \frac{a}{D} \tag{3.12}$$

$$K_{\frac{f}{b,T}} = k_{\frac{f}{b,T}} \frac{a}{D} \tag{3.13}$$

$$RG = \frac{rg}{a} \tag{3.14}$$

$$h = \frac{a_s}{a} \tag{3.15}$$

where rg is the radius of the tip-insulating material and a_S is the substrate radius. Considering the definition of the problem, the initial condition is,

T = 0, 0 ≤ R, 0 ≤ Z ≤ L; $C_O = 1$ (3.16)

On the contrary, if the substrate is an insulator, then $J_S \equiv 0$. Also, the reactions occurring at the tip and the substrate are electrochemical in nature. Hence, the rate constants for reduction and oxidation are given by Butler-Volmer equations:

$$k_f = k^o \exp\left[-\alpha f\left(E - E^{o'}\right)\right] \tag{3.17}$$

$$k_b = k^o \exp\left[(1-\alpha) f\left(E - E^{o'}\right)\right] \tag{3.18}$$

Hence, the solution of the problem can be solved in terms of dimensionless currents $I_T(T)$ and $I_S(T)$ and can be given by,

$$I_T(T) = -\frac{\pi}{2}\int_0^1 J_T\,(T,R) R dR \tag{3.20}$$

$$I_S(T) = -\frac{\pi}{2}\int_0^h J_S\,(T,R)RdR \tag{3.21}$$

where I_T and I_S are the physical currents due to normalization of the tip current, $I = \frac{i}{i_{T,\infty}}$

This general formulation involves a mixed diffusion control for one of the electrodes and hence,

$0 < T, 0 \leq R \leq 1, Z = 0;$ $\qquad C_O = 0$ (3.22)

can be substituted with the boundary condition in Eq. 8, and Eq. 10 can be replaced with a much simpler boundary condition:

$0 < T, 0 \leq R \leq h, Z = L;$ $\qquad C_O = 1$ (3.23)

Hence the time dependent SECM problem was solved using a semi-analytical two dimensional equations as explained in [2] and [3]. For a conductive substrate, $i_T \geq i_{T,\infty}$, and it is always larger than the value calculated using the predicted 'thin-layer cell' theory (TLC). On the other hand, for an insulating substrate, $i_T \geq i_{T,\infty}$, and hence smaller the tip-substrate separation, the earlier the transients between SECM and the tip electrode occur.

3.4.2. Steady-State Conditions considered for reaction at SWNT nanocomposites

A steady state problem in SECM can be given by the following Laplace equation, with its respective boundary conditions, for oxidized or reduced form of the mediator [4].

$$\frac{\partial^2 C}{\partial R^2} + \frac{\partial^2 C}{\partial R^2} + \frac{1}{R}\frac{\partial C}{\partial R} = 0 \tag{3.24}$$

where, $C = \frac{c_{Red}}{c^b}$, $R = \frac{r}{a}$, $Z = \frac{z}{a}$, and a is the radius of the SECM tip (10 μm) (Fig. 3-4). The following boundary conditions generally apply:

$C(R,Z) = 0 \qquad R < 1;\ Z = 0$

$\frac{\partial C}{\partial R} = 0 \qquad R = 0\ ; 0 < Z < L$

$C(R,Z) = 1 \qquad R = R_{max};\ -Z_{max} < Z < L$

$C(R,Z) = 1 \qquad R > R_G;\ Z = -Z_{max}$

$\frac{\partial C}{\partial R} = 0 \qquad R = R_G;\ -Z_{max} < Z < 0$

$\frac{\partial C}{\partial Z} = 0 \qquad 1 < R < R_G; Z = 0$

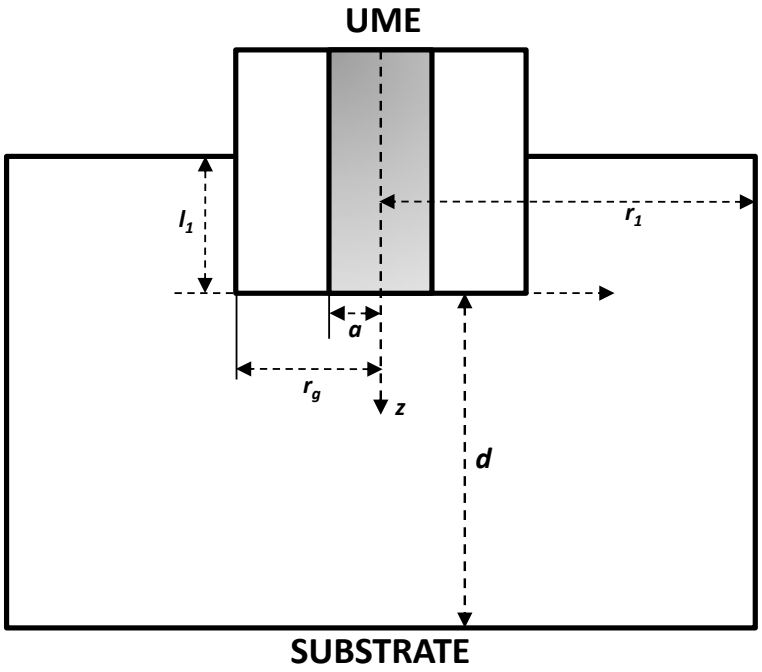

Figure 3-10 Geometry of the diffusion domain and the parameters defining the diffusion problem in SECM

where, L is the normalized tip-substrate distance and $L = \frac{d}{a}$. The boundary conditions for the electron transfer reaction between redox mediator and DNA-SWNT/Lysozyme-SWNT assembly is given by

$$D_{soln}\frac{\partial c}{\partial z}|_{z=d} = k_f c_{Ox}(r, z = d)\Gamma(r) - k_b c_{Red}(r, z = d)\big(\Gamma_{max} - \Gamma(r)\big) \qquad (3.25)$$

where, D_{soln} is the diffusion coefficient of the redox mediator and Γ is the surface concentration of the SWNTs, and Γ_{max} is the maximum surface concentration. But, if this equation is made dimensionless, then

$$\frac{\partial C}{\partial Z}|_{Z=L} = K_f(1-C)\theta - K_b C(1-\theta) \tag{3.26}$$

where, $K_f = k_f \Gamma_{\max} a/D_{soln}$, $K_b = k_b \Gamma_{max} a/D_{soln}$ and $\theta = \Gamma/\Gamma_{max}$. Lateral charge transport across the SWNT nanocomposites can be given by the following equation, assuming a thermally active mechanism

$$D_{surf}\left(\frac{\partial^2 \Gamma(r)}{\partial r^2} + \frac{1}{r}\frac{\partial \Gamma(r)}{\partial r}\right) - k_f c_{Ox}(r, z=d)\Gamma(r) + k_b c_{Red}(r, z=d)\big(\Gamma_{max} - \Gamma(r)\big) = 0$$

From the above equation, it is clear that D_{surf} is the parameter that characterizes lateral charge transport though the SWNT based material. The dimensionless form can be given as,

$$\frac{\partial^2 \theta}{\partial^2 R} + \frac{1}{R}\frac{\partial \theta}{\partial R} - \frac{1}{\gamma D_r}\Big(K_f(1-C)\theta - K_b C(1-\theta)\Big) = 0 \tag{3.27}$$

where $\gamma = \Gamma_{max}/(c^b a)$, the maximum surface concentration and $D_r = D_{surf}/D_{soln}$. During a steady-state SECM reaction, the response from the tip is sensitive to the ratio of the surface and solution diffusion coefficients and the maximum surface concentration of SWNTs. Therefore, the normalized tip current during feedback mode can be predicted as

$$\frac{I}{4nF D_{soln} c^b a} = \frac{\pi}{2}\int_0^1 R\frac{\partial C}{\partial Z} dR \tag{3.28}$$

As the amount of positive feedback is given by the dimensionless parameter γD_r, the diffusion coefficient characterizing the electron transport across the film can be correlated to the conductivity of the film as

$$\sigma = \frac{\Gamma_{max} F^2 D_{surf}}{RT\Delta z} = \frac{\gamma D_r F^2 a c^b D_{soln}}{RT\Delta z} \quad (3.29)$$

Hence this theoretical explanation gives the effect of lateral charge transfer across nanometer sized thin films including back diffusion across the plane of the microelectrode, and is related to the difference between the standard potentials of the SWNT nanomaterials and redox mediator.

3.4.3. Ohmic behavior at the substrate during charge injection

As discussed above, the SECM response observed at steady state is due to the combination of diffusion flux in the solution and the flux due to lateral charge transport in the nanotube film. As the diffusion flux is directly proportional to the concentration of the redox mediator, in order to observe a measurable effect due to lateral charge transfer, a sufficiently low concentration of the redox couple is to be used. Since, SWNTs have large coulomb gap, the nanotubes deposited on the surface can be considered as a multivalent redox species. Additionally, the transport mechanism of electrons through the layer is considered to be thermally activated tunneling. Besides, if the thickness of the nanocomposites film is extremely thin compared to the diameter of the tip, then it will not be polarized in the z-direction.

The layers of nanotubes are developed on an insulating substrate and hence hindered diffusion is observed at high redox mediator concentrations. At reduced concentrations, the relative contribution of mediator regeneration due to lateral electron transport in the film increases. Hence, the behavior changes from an insulator (negative feedback) to a conductor at a given concentration. As a result of this behavior change due to concentration dependence, the lateral charge transport model can be adopted. The model predicted, assumes that the monolayer exhibits ohmic behavior, i.e. the current at the tip electrode is directly proportional to the electrochemical potential gradient, which is valid in the absence of a coulomb blockade and low

potential gradients. Thus, the electrochemical potential of electrons in the nanotube monolayer μ is given as

$$\mu = \mu^0 - e(\phi(r) - \phi^0 \tag{3.30}$$

where $\mu^0$the standard is electrochemical potential, e is the charge, r is the radial coordinate and $\phi(r)$ is the local electrostatic potential in the film. Taking this in to consideration, the equilibrium electrochemical potential is given by

$$\mu_{eq} = \mu^0 + kT \ln(c^b_{red}/c^b_{Ox}) \tag{3.31}$$

where c^b_{Red} and c^b_{Ox} are the bulk concentrations of the reduced and oxidized species, k Boltzmann constant and T the absolute temperature. The conductivity due to electron transfer is adopted from Ohm's law,

$$i = -\sigma \frac{\partial \phi}{\partial r} \tag{3.32}$$

which can be expressed as the flux of the electrons, j as a function of the electrochemical potential gradient.

$$j = -\frac{\sigma}{N_A e^2} \frac{\partial(\mu - \mu^0)}{\partial r} \tag{3.33}$$

Introducing the following dimensionless quantities,

$$\tilde{\mu} = \frac{\mu - \mu^0}{kT} \tag{3.34}$$

$$C = \frac{c_{Red}}{c^b_{red} + c^b_{Ox}} = \frac{c_{Red}}{c^b} \tag{3.35}$$

$$R = r/r_e \tag{3.36}$$

$$K^0 = \frac{k^0 r_e}{D} \tag{3.37}$$

$$\Sigma = \frac{\sigma k T \Delta z}{e^2 r_e D c^b N_A} \tag{3.38}$$

Combining these dimensionless quantities, the electrochemical mass-transport on the substrate coupled with the diffusion equation can be given by

$$\frac{\partial^2 \tilde{\mu}}{\partial R^2} + \frac{1}{R}\frac{\partial \tilde{\mu}}{\partial R} - \frac{K^0}{\Sigma}\left((1-C)e^{\tilde{\mu}/2} - Ce^{\tilde{\mu}/2}\right) = 0 \tag{3.39}$$

Where, K^0 is the dimensionless standard rate constant of the electron-transfer reaction between the redox mediator and the nanotube layer, C is the dimensionless concentration of the redox mediator and Σ is the dimensionless conductivity of the film [5, 6].

3.5. Theoretical fitting of conducting and insulating approach curves

As discussed in the previous section, the equations representing a diffusion-controlled SECM process explains two limiting cases of the steady-state problem, i.e., 1) pure positive feedback produced by rapid generation of the reactant species, 2) pure negative feedback when no mediator regeneration occurs at the substrate. Hence, from the above theoretical considerations, for RG values from 1.1 to 10, we have

$$I(L) = \frac{1}{\left(0.292 + \frac{1.5151}{L} + 0.6553\exp\left(\frac{-2.4035}{L}\right)\right)} \tag{3.40}$$

for an insulating substrate with $i_T < i_{T,\infty}$ and thus a negative feedback. On the other hand, if $i_T > i_{T,\infty}$ for a positive feedback, we have

$$I(L) = 0.68 + \frac{0.78377}{L} + 0.3315\exp\left(\frac{-1.0672}{L}\right) \tag{3.41}$$

Where, $L = \frac{d}{a}$ and d being the tip-substrate distance and a the tip radius.

3.6. SECM setup

Introduced by Bard and coworkers in 1989 [7], the Scanning electrochemical microscope is an instrument that can analyze the chemistry at high resolution near interfaces. It is based on the reactions that occur between the small electrode and the close proximity of the substrate. SECM can be used to obtain reactivity images and quantitative measurements of reaction rates. Pointedly, a current flows through an ultramicroelectrode, near a conductive or an insulating substrate immersed in an electrolyte solution. In order to probe the diffusion layer, the UME can be perpendicular to the surface along the z-axis, and can be scanned at constant z-value across the surface (x and y-axes). The tip and sample are a part of the electrochemical cell, including the reference electrode (Ag/AgCl) and counter electrode (platinum electrode). The tip moves with a given resolution towards the substrate by means of piezoelectric elements or stepping motors driving differential springs. The instrument used in this research is a CHI900B Scanning Electrochemical Microscope consists of a digital function generator, a bipotentiastat, a high resolution data acquisition circuitry, a three dimensional nano-positioner with a combination of stepper motors and a XYZ piezo block, a stepper motor, piezo controller and a sample-cell holder. A 3D nano-positioner allows a spatial resolution of 1.6 nm and a maximum travelling distance of 2.5 cm. The instrument has a potential control range of ±10 V and a substrate potential of ± 10 V versus ± 3.276 V and a current range of ±10 mA, with a current measurability up to 1 pA (Fig. 3-5). The input impedance of the reference electrode is 10^{12} Ω and a compliance voltage of ± 12 V with the current measurement range from 1×10^{-12} – 0.001 A/V in 10 ranges. Speed of the ADC controller is 16-bits at 25 KHz and the dual high resolution ADCs have 20-bit

(1 kHz) and 24-bit (10 Hz) controllers. Other features include, an automatic *iR* compensation controller, with a RDE control giving a 0-10 voltage output.

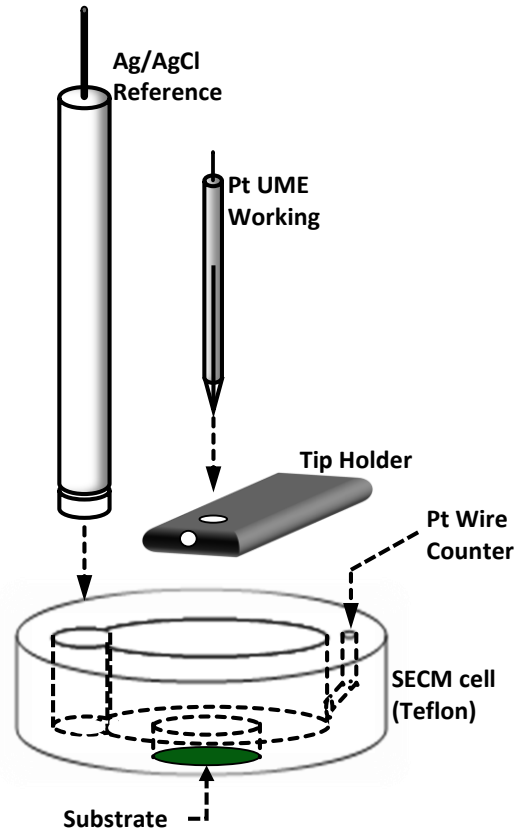

Figure 3-11 Schematic of an SECM electrochemical cell setup

3.6.1. Tip preparation and operation

Disk-in-Glass microelectrodes are the most conventionally used microelectrodes in SECM. A fine platinum wire 10 μm in diameter is placed in a 1 mm id Pyrex tube sealed at one end. The other end of the tube is heated in a nichrome wire helix in vacuum for an hour, followed by sealing the glass followed by inspecting the glass for any impurities and bubbles in the glass. The sealed end is then polished with sandpaper, until the cross section of the Pt wire is exposed. Electrical connections to the sealed end are made using silver paste. The glass wall

(insulating part) is conically sharpened with emery paper until the diameter of the flat glass section if 10 more than that of the Pt UME (R_G = 2.2) (Fig. 3-6).

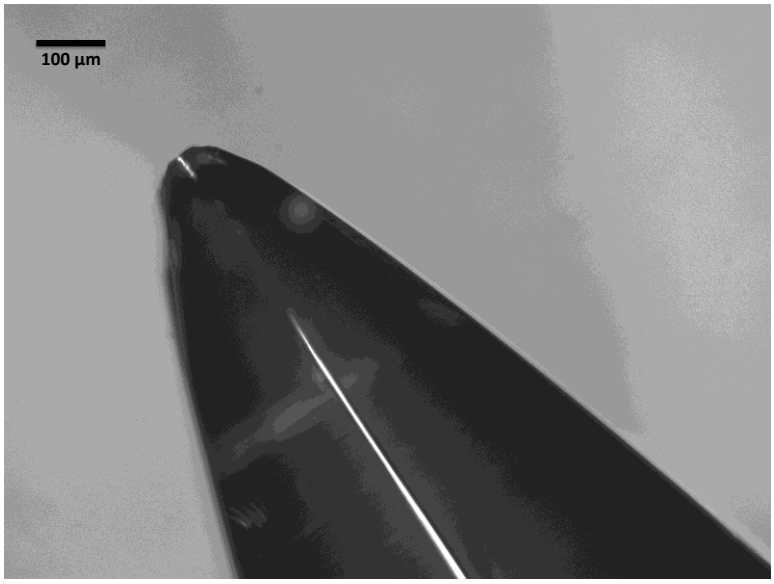

Figure 3-12 SEM image of the 10 µm Pt UME showing the insulating sheath and the tip (RG ≈ 2.2)

Before using the UME for SECM experiments, the electrode is polished with 3 µm, 0.03 µm and 0.05 µm alumina polishing liquid (Buehler, USA). The electrode is then washed with water and then washed in 0.5 M sulfuric acid (H_2SO_4) and 0.5 M nitric acid (HNO_3) for 5 minutes each. The UME is again washed with water and verified for impurities and imperfections at the surface. The next step is to fix the UME in the holder and connect the UME, reference and auxiliary electrode to their respective leads. A cyclic voltammogram is obtained between -0.2 to 0.5 V with a sensitivity of 1×10^{-9} and a scan rate of 0.01 V/s and a quiet time of 5 s.

At this point, the experiment parameter setup has been completed. The UME has to be positioned over the substrate electrode. A probe approach enables one to approach the tip quickly

to the substrate and based on the increase or decrease in tip current. The current variation implies as to how much the substrate is biased relative to the UME reaction. Before starting the probe approach, the potential values from the voltammogram are entered, with the sensitivity of the probe electrode set at 1×10^{-9} A. Probe stopping current is the value at which the tip electrode stops inching towards the substrate and should be set at 125 %. Maximum increment is the distance that the tip moves for each step and is set at 5 μm. Using the probe control, the tip is placed over the substrate. With a total travel distance of ~300 μm and a scan rate of 3 μm/s, the tip is scanned towards the surface in order to obtain a feedback curve.

3.6.2. Protocol for SECM setup

The following protocol is routinely used to analyze nanomaterials using SECM.

1. The UME is cleaned with 3 μm, 0.3 μm and 0.05 μm alumina particles for 30 s each
2. Wash with copious amount of DI Water
3. Rinse with 0.5 M sulfuric acid (H_2SO_4) and 0.5 M nitric acid (HNO_3) for 5 minutes each
4. Blot the surface with Kim wipe
5. Fix the UME to the holder and switch on the SECM controllers
6. Add 1 mM Ferrocenemethanol in the SECM electrochemical cell and position the tip in the solution such that it is partly immersed
7. Obtain a cyclic voltammogram in the range -0.4 to 0.4 V at 10 mV/s scan rate and in the presence of Ag/AgCl reference electrode
8. Switch to SECM technique and enter the peak potential values obtained from the voltammogram
9. Using the probe controller, position the tip close to the substrate and conduct a probe approach curve at a sensitivity of 1×10^{-9} A. Set the probe stopping current to 125 %

10. Once the tip reaches the substrate and shows a feedback response, retract the curve by ~300 μm and obtain a probe scan curve at a scan rate of 3 μm/s
11. After obtaining the feedback curves, record the data and report the results, using the equations discussed above, based on the type of feedback obtained

3.7. References

1. Bard, A.J., et al., *Scanning Electrochemical Microscopy. Introduction and Principles.* Anal. Chem, 1989. **61**(2): p. 132-138.
2. Mirkin, M.V. and A.J. Bard, *Multidimensional integral equations: a new approach to solving microelectrode diffusion problems: Part 2. Applications to microband electrodes and the scanning electrochemical microscope* J. Electroanal Chem, 1992. **323**(1-2): p. 29-51.
3. Bard, A.J., et al., *Scanning electrochemical microscopy. 12. Theory and experiment of the feedback mode with finite heterogeneous electron-transfer kinetics and arbitrary substrate size.* J. Phys. Chem., 1992. **96**(4): p. 1861-1868.
4. Ruiz, V., et al., *Probing Conductivity of Polyelectrolyte/Nanoparticle Composite Films by Scanning Electrochemical Microscopy.* Nano Lett., 2003. **3**(10): p. 1459-1462.
5. Liljeroth, P., et al., *Electron Transport in Two-Dimensional Arrays of Gold Nanocrystals Investigated by Scanning Electrochemical Microscopy.* J. Am. Chem. Soc., 2004. **126**(22): p. 7126–7132.
6. Ruiz, V., et al., *Molecular Ordering and 2D Conductivity in Ultrathin Poly(3-hexylthiophene)/Gold Nanoparticle Composite Films.* J. Phys. Chem. B, 2005. **109**(41): p. 19335–19344.

7. Bard, A.J., et al., *Scanning electrochemical microscopy. Introduction and principles.* Anal. Chem, 1989. **61** (2): p. 132–138.

4. Diffraction Optics Technology (DOTLAB)

4.1. Optical Transducers

Several years ago, optical sensing devices called ‘optrodes’ were introduced besides electrochemical platforms, originally to monitor pH and CO_2 concentrations. This kick started the novel field in optical sensors and a number of different optical transducers have been developed. Interactions between radiation and matter, dispersion, reflection, scattering, changing transmission or fluorescence are used to monitor probe and target interaction. Advantages include, high sensitivity, miniaturization of the sensor platform and cost efficient. Optical sensor platforms are capable of measuring surface concentration to about 25 ng/ml. Likewise advanced concepts such as total internal reflection and evanescent-field based light propagation have made a far-reaching improvement in optical sensor development. Two basic signal transduction are involved in optical sensor development, a) probing the surface for minute changes in refractive index by evanescent wave techniques such as surface plasmon resonance and b) fluorescence assays by labeling the sample [1].

4.2. Detection using diffraction based sensing

Diffraction based sensing can be used to observe biomolecular interactions between probe and target molecules. A diffraction pattern is obtained when a laser light impinges on a pattern of repeating parallel lines which could yield an image with equally spaced spots in a row. The addition of target molecules helps interact with the diffraction pattern, which in turn causes an increase in height or refractive index of the patterned substrate and apparently causes an increase in intensity of the diffraction image. Diffraction based sensing involves, grating-based

light diffraction and immobilized affinity surfaces for a sensitive platform without the use of chemi-luminescent and fluorescence labels [2].

4.2.1. Diffraction measurement and 'self-referencing'

Referencing plays an important role in developing label-free biosensors, which includes building a reference channel (RC) similar to the working channel (WC), and requires an extra set of electronic and fluidic system. Bailey *et al.*, [3] reported a micro-patterned technique to generate a surface grating that consist of functional and non-functional surfaces.

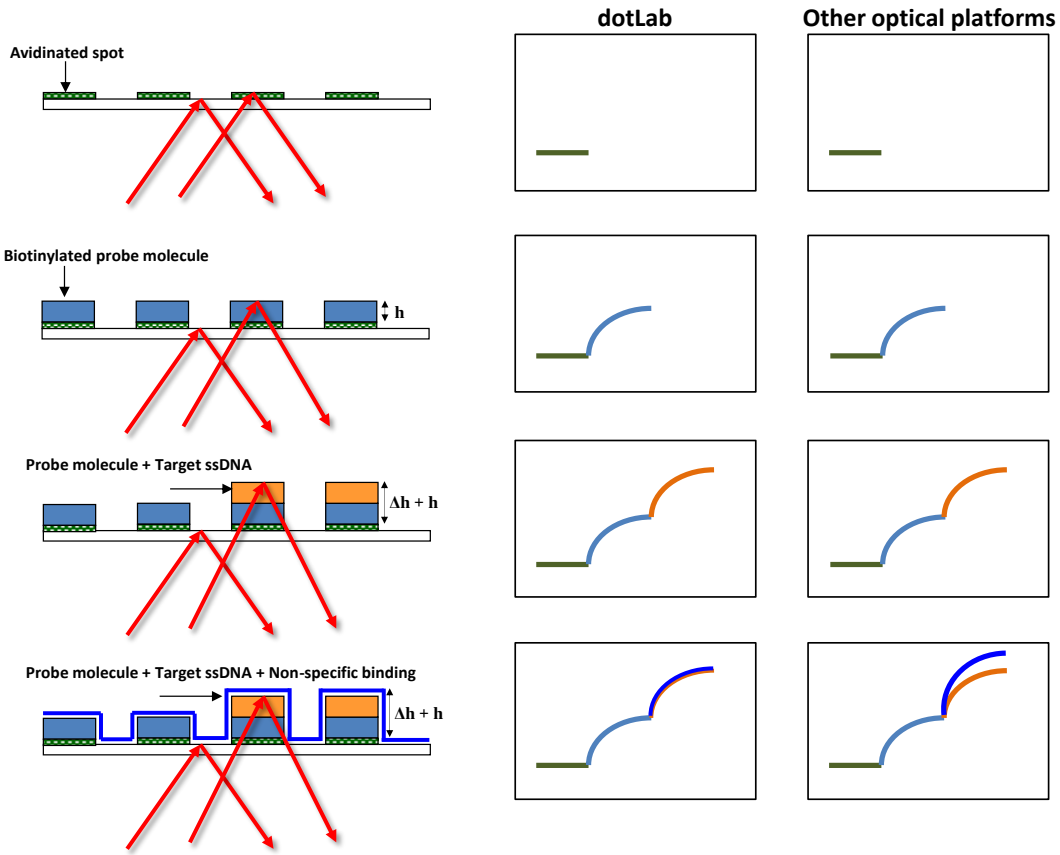

Figure 4-13 Schematic representation of the binding phenomena to patterned surface of polystyrene sensor. The illustration shows that diffraction based sensing is 'self-referencing'

The receptor molecules bind only to the functional surface and not to the passivated non-functional surface. Analyte association or dissociation modulates the amplitude of the recorded diffraction intensity. Meanwhile, the bulk effects that alter the refractive index across the functional and non-functional surfaces do not induce any change in diffraction intensity. Hence, the surface is said to be 'self-referencing' (Figure 4-1). Additionally, surface plasmon field enhancement can be used to boost the sensitivity of the diffraction based sensor platform [4].

4.2.2. Sensitivity

Nakajima *et al.*, [5] proposed a model to describe the intensity of diffracted beam through a transmission grating. As the sensor consists of two parts, a transparent portion and a semi-transparent region that partially absorbs light. During analyte adsorption, the transmitted beam is diffracted, as it passes through a grating and a change in intensity is observed. The intensity of the diffracted beam was given by

$$D = \Delta I = \frac{1}{2} I_0 - \frac{1}{2} I = \frac{1}{2} I_0 \left(1 - \frac{I}{I_0}\right) \tag{4.1}$$

Where, ΔI is the difference in intensities of the beams and I_0 and I are the beam intensities before and after transmission. But the intensity of transmitted light is given by Beer-Lambert's law

$$A = \log\left(\frac{I_0}{I}\right) \tag{4.2}$$

Substituting Eqn. 4.2 in Eqn. 4.1, we obtain the following relation

$$D = (1/2) I_0 (1 - 10^{-A}) \tag{4.3}$$

Although, diffraction based sensing can be related to fluorometry, both have different sensitivity levels and quantum yields. The efficiency of light collection in diffraction methods is of the order of 0.5; while most fluorescence based methods have an efficiency of 0.1-0.001. Hence,

these techniques are more universal, highly sensitive and show minimum fluorescence, which results in an infinitesimal signal loss.

4.3. dotLab system

dotLab system (DOT) was developed by Axela Biosensors Inc. (Toronto, Canada) and will be used for diffraction based experiments. In the DOT system, a coherent light strikes the regular pattern of capture molecules on the sensor surface creating interference patterns that produce a well defined image. When target molecules interact with the receptor surface, the height of the pattern increases which in turn increases the diffraction intensity. This change in intensity is monitored by a photo diode. As the process of diffraction across patterned surfaces is self-referencing, the transduction of binding events will occur exclusively for target binding to the probe surface, which minimizes non-specific binding. This is a characteristic advantage of DOT over other biosensing platforms. The DOT system is based on a near real-time and total internal reflection scheme which allows for 95% of the signal to be detected [6].

A 670 nm laser diode, class 3R with a maximum output of 4.0 mW and a beam divergence of 5.0 mRad was used as the light source, to produce a diffractive pattern. One end of the sensor was connected to a fluidic panel, which is responsible for circulating the buffer solutions and the other end is connected to a sensor manifold which aspirates the analyte from the well. The sensor chip was made of optically clear polystyrene with an interspersed prism situated below the flow channel. The linear flow channel which can hold a volume of 10.0 µl, consisted of eight, circular assay spots, each 2.0 mm in diameter, with 15.0 femto moles of avidin deposited on each spot (Figure 4-2) [7]. The sensor chip has an integrated prism which is responsible for the diffraction of the laser light (Fig. 4-3).

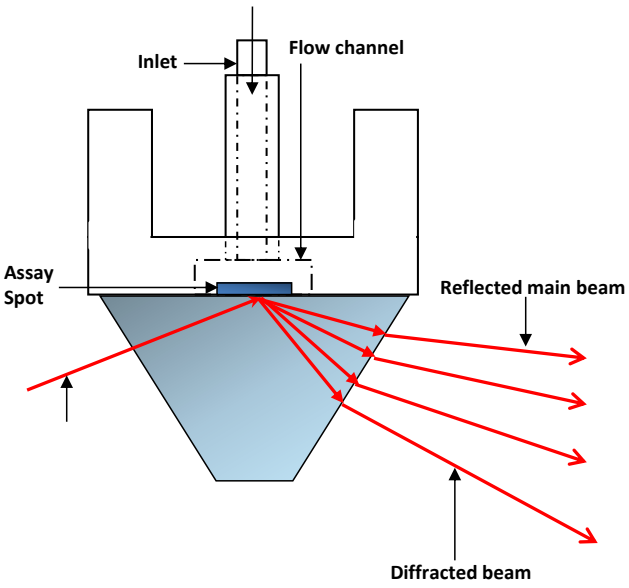

Figure 4-14 Cross section of a polystyrene dotLab sensor showing the microfluidic setup

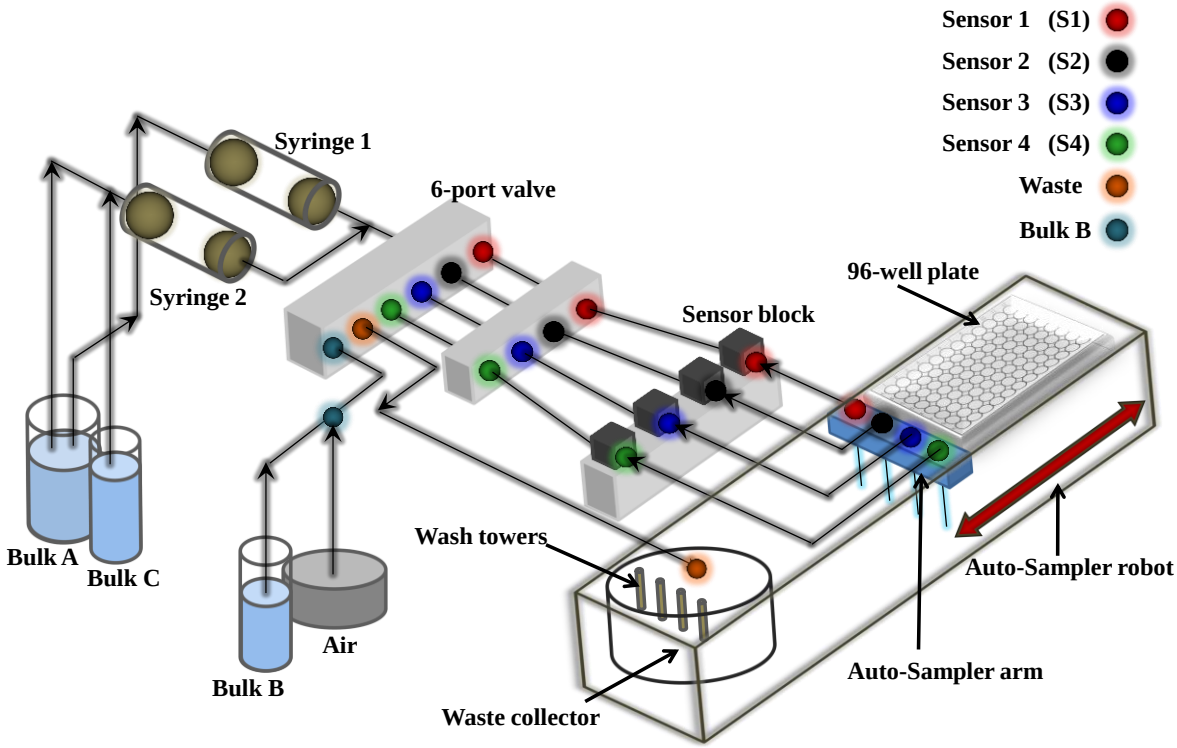

Figure 4-15 Schematic representation of a dotLab system

Every sensor is purchased from the manufacturer at a low cost (US$ 15 per chip) and has up to eight assay features along each linear flow channel. Each spot has a diameter of 2 mm and a depth of 0.25 mm. Neutravidin is immobilized on the diffraction pattern, in order for biotin labeled bio-probes to be attached as receptors for sensor development. The DOT system introduces the analyte sample through the channel using a high precision fluidic controller. Different reagents can be passed over the surface by introducing an air gap between each reagent, which in turn leads to a transient spike in the signal. dotLab software version 1.1.1 provided by Axela monitors the change in diffraction intensity near the sensing surface calculates the statistical noise in the signal and displays a self-referenced signal relative to biomolecular interactions in all the eight spots. The signal is generally displayed in diffraction intensity unit (DI) [8].

4.4. Protocol for sensor setup

The following protocol is routinely used to prepare the dotLab sensor for biosensor experiments.

1. Place the polystyrene sensors at room temperature and allow thawing for 2 hours.
2. Remove the sensor from its cladding and is dock it firmly in one of the four probe stations on the dotLab,
3. When fixed, a ‘click’ sound is heard from the sensor which indicates that the sensor in secured in place with optical platform
4. Open the dotLab software and start a new program. A schedule is designed according to the user’s requirements, which includes three priming steps and one tip wash step before the start of each experiment.
5. The analyte to be immobilized on the avidinated polystyrene surface and the one that has to be detected are added to the 96 well holder over the auto sampler.

6. Start monitoring the signal with the immobilization process (~45 minutes) and follow the change in DI vs. time with each analyte introduced.
7. Record the data in the data sheet and report the results

4.5. References

1. Brecht, A. and G. Gauglitz, *Recent developments in optical transducers for chemical or biochemical applications.* Sens. Actuators B: Chem., 1997. 38(1-3): p. 1-7.
2. Wolfbeis, O.S., *Analytical chemistry with optical sensors* Fresenius' J. Anal. Chem., 1986. 325(4): p. 387-392.
3. Bailey, R.C. and J.T. Hupp, *Large-scale resonance amplification of optical sensing of volatile compounds with chemoresponsive visible-region diffraction gratings.* J. Am. Chem. Soc., 2002. 124: p. 6767–6774.
4. Yu, F. and W. Knoll, *Immunosensor with Self-Referencing Based on Surface Plasmon Diffraction.* Anal. Chem., 2004. 76(7): p. 1971–1975.
5. Nakajima, F., et al., *Diffractive Optical Chemical Sensor Based on Light Absorption.* Anal. Chem., 1999. 71(13): p. 2262-2265.
6. Goh, J.B., et al., *A quantitative diffraction-based sandwich immunoassay.* Anal Biochem., 2003. 313(262-266).
7. Cleverley, S., I. Chen, and J. Houle, *Label-free and amplified quantitation of proteins in complex mixtures using diffractive optics technology.* J Chromatogr B Analyt Technol Biomed Life Sci., 2010. 878(2): p. 264-270.
8. Borisenko, V., et al., *Diffractive Optics Technology: A Novel Detection Technology for Immunoassays.* Clin. Chem., 2006. 52(11): p. 2168-2170.

5. Nanoelectronic Properties of Single-Walled Carbon Nanotubes based Antimicrobial Films

5.1. Introduction

Silicon semiconductor technology has exponentially increased in terms of production, with an increase in number of transistors per chip and thereby performance of the devices. Unfortunately, the limit of assembling transistors in the tera-scale may end due to the fundamental physical or economic limitations. Additionally silicon poses certain key material limitations with which it has to be replaced in the near future for tera-scale integration, including transit time, switching energy, thermal conductivity and dielectric constant of the interconnect material. Indeed, it has been predicted that even after four decades of advances in silicon semiconductor technology, a systematic analysis of the echelons of the limits of device manufacture; enormous potential lies in the tera-scale integration of multitrillion transistor chips.

Nanorods and nanotubes have been predicted to be a significant alternative in integrating nanostructured devices for efficient electron and exciton transport. Hierarchical assembly of these one dimensional nanomaterials paves way for the next generation of self-aligned devices. Theoretical predictions and experimental measurements show that carbon nanotubes form different forms and shapes; and that's their electrical or optoelectronic properties will exceed the performances of wide-band gap semiconductor materials. Although carbon nanotubes, more specifically single-walled carbon nanotubes (SWNTs) are considered to be highly anisotropic rigid rods, the major challenge lies in the assembly and processing of individually dispersed SWNTs in to usable devices, which has thwarted the development of suitable materials and interconnects for nanoelectronic devices [1-3]. Individual dispersion of carbon nanotubes can be

done using surfactants, polymers and biomolecules. More specifically, Smalley et al proposed a method to disperse SWNTs using various anionic and cationic surfactants. Kotov et al reported a novel method to disperse SWNTs using amphiphilic compounds. Dispersion using biomolecules has attracted mainly for its ease of preparation and versatility. The unique structure of DNA allows the sonication-assisted dispersion of SWNTs. As a result, it can be used to prepare fascinating nanoscale architectures based on layer-by-layer assembly.

Charge transport studies through DNA based nanomaterials paves way for a number of molecular electronic devices and insight in to the electrical properties of DNA. Various techniques were used to analyze the electron transport through DNA based surfaces and nanomaterials, including scanning tunneling microscopy, transient absorption spectroscopy and low-energy electron point source microscopy (LEEPS). We have used DNA as a biopolymer to individually disperse and wrap SWNTs, and have shown that the electrical and charge transport through nanocomposites can be verified using scanning electrochemical microscopy, where the conductivity through DNA wrapped SWNTs contributes to the change in steady state current and prevents insulation of consecutive layers, thereby enabling a response through a redox reaction [4].

5.2. Coupled self-assembly of SWNT based biopolymers

Controlled scalable bottom-up assembly of nanorods across the nano- to macro- length scales is one of the key obstacles to the fulfillment of their promising nanoscale properties. Both controlled placement and orientation are required for nanorod's anisotropic properties to be fully manifested in macro-scale materials. Carbon nanotube-based devices have been prepared using random deposition, electric field assisted assembly, flow alignment and chemical patterning [5-7]. However, none of these techniques can readily be extended to large scale manufacturing with controlled orientation and assembly. This prediction has motivated extensive efforts aimed at

developing new device concepts and fabrication approaches that may enable integration to go far beyond the limits of conventional microelectronics technology [8]. Similarly, dry deposition methods have been reported for micro-scale assembly of nanotubes using photolithographic techniques [9], but this process is complicated and requires a multitude of steps. Significant challenges remain for achieving large area assemblies; approaches to overcoming this challenge include patterned growth [10] and solid phase processing directly from the reactor [11] or from grown forests of materials [12, 13]. While these approaches are promising, particularly for smaller scale electronics, devices and sensors, fluid phase processes such as those developed for polymers are considered promising for their scalability and potential economic viability [14, 15]. Fluid phase processing requires unlocking the nanoscale promise of SWNT by dispersing them as individual nanotubes prior to reassembling them in a controlled manner. Because of SWNTs' ambiphobic nature and the large 500 eV/μm van der Waals attractions between them SWNTs tend to form large aggregates of entangled ropes. Superacids, dicholorobenzene, N-methyl pyrrolidone and surfactants are the most commonly used dispersants for SWNT. Stabilized dispersions of individual SWNT have also been developed using polymers and biomaterials [16-19]. Biopolymers such as DNA and Lysozyme provide attractive alternatives because of their greener chemistry and the ability to enable additional multi-functionality such as antimicrobial activity or sensing capability. Controlled self-assembly and proper integration of these high-performance building blocks is necessary to harnessing their diverse functional properties and allowing a wide range of applications from 3D integrated electronics to antimicrobial coatings [20, 21].

Here we report the results of extensive characterization of the electrochemical interfaces of DNA-SWNT-LSZ coatings made by the LBL assembly process on an insulating substrate.

Lateral charge transport measurements made by scanning electrochemical microscopy (SECM). SECM analysis showed that increasing the number of layers resulted in positive feedback and that biocoating assembled on an insulating substrate acted, as a conducting film. Lateral charge transport was due exclusively to the composite film alone. Whether the terminating layer of the coating was LSZ or DNA resulted in significant differences in lateral charge transport. CV and EIS confirmed the electrical conductivity of the films and the stability of their response. As expected the feedback current from SECM increases with number of layers and our findings indicate that there is no insulation between the interlaced layers of SWNT-DNA and SWNT-LSZ. These results demonstrate that the process used to form these mechanically robust antimicrobial coatings had the additional benefit of providing a conductive coating. This process can be extended to other SWNT-biological systems readily enabling the assembly of large area devices and sensors.

5.3. Experimental Section

5.3.1. Reagents

All aqueous solutions were prepared using Milli-Q reagent water (Millipore Corp., resistivity > 18 MΩ cm). Purified HiPCo SWNTs were purchased from Rice University (Houston, TX). Lysozyme from chicken egg whites and DNA from salmon testes were obtained from Sigma-Aldrich (St. Louis, MO). Clean glass microscopy slides (VWR International, West Chester, PA) were used as substrates. SWNT-LSZ and SWNT-DNA dispersions were prepared using the method of Nepal *et al* [22]. All chemicals were used as received. First, glass slides were cleaned using a piranha solution composed of 3:1 96% H_2SO_4/30% H_2O_2. Slides were then subsequently alternately immersed for 15 min each in an aqueous dispersion of SWNT-LSZ and SWNT-DNA.

5.3.2. Apparatus

SECM (CH-900, CH Instruments Inc., Austin, TX) was used to evaluate charge injection kinetics and lateral charge transfer through multilayer $(SWNT\text{-}LSZ/SWNT\text{-}DNA)_n$ films. A three electrode system was employed with a platinum wire serving as the counter electrode, Ag/AgCl as a reference electrode and a 10 μm platinum ultra-micro electrode (UME) as the working electrode. Optical micrographs indicated a 2.2 ratio of SECM tip radius to platinum disk electrode (R_G) radius. The solutions were de-aerated with nitrogen prior to use. The UME was held at a potential of +0.25 V vs. Ag/AgCl and approach curves were obtained at a scan rate of 30 μms^{-1}. The current at the UME was recorded as a function of distance as the SECM tip approached the glass substrate.

Impedance spectroscopy measurements were taken using a Solartron 1260 frequency response analyzer (Farnborough, UK) with a frequency range of 0.001–10 Hz and signal amplitude of 5 mV. Measurements were carried out under open-circuit voltage with a two-probe configuration in which a separate reference electrode was not used. All impedance spectra were fitted to equivalent electrical circuits using ZView software (Huntington Beach, CA). Cyclic voltammetric and EIS were performed using a BAS CV-100W potentiostat/galvanostat. A one-compartment 2 mL glass cell with a working volume, Ag/AgCl reference electrode, and a platinum wire auxiliary electrode was used for the measurements.

5.3.3. Layer-by-Layer assembly

DNA-SWNT and LSZ-SWNT were prepared according to protocol [22], and zeta potential measurements of both the solutions indicated that the cationic and anionic nature of LSZ-SWNT (+22 mV) and DNA-SWNT dispersions (-30 mV) provided an excellent platform for the formation of the nanocomposites $[(LSZ\text{-}SWNT)\text{-}(DNA\text{-}SWNT)]_n$.

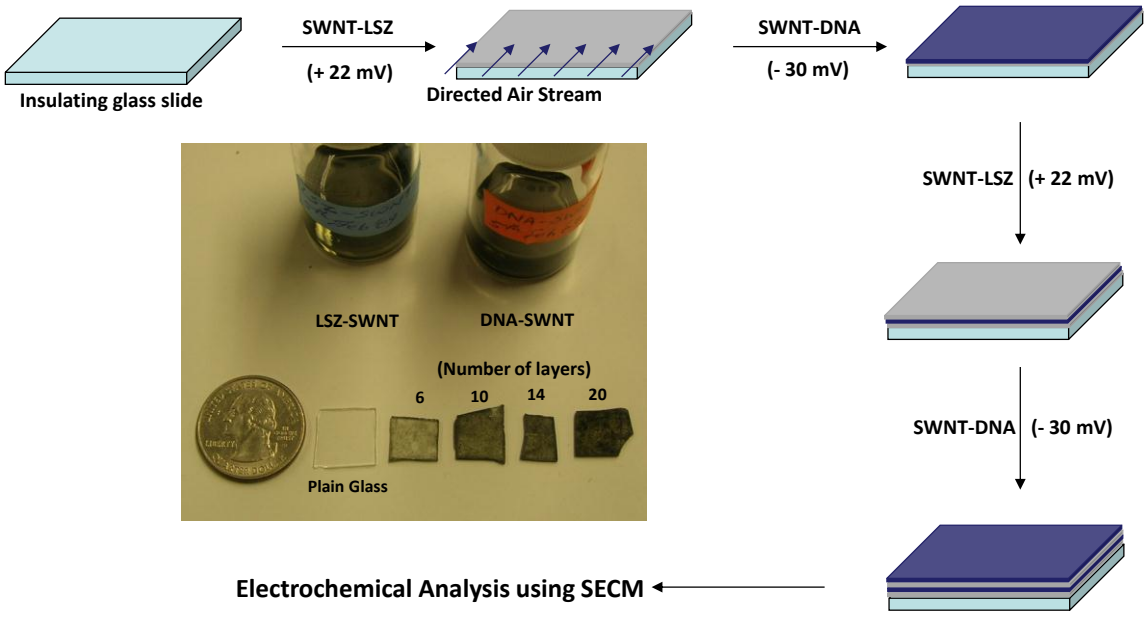

Figure 5-16 Schematic showing the Layer-by-Layer assembly of SWNT nano-coating

The orientation of the nanotubes was controlled in each layer by applying a directed air stream between each deposition step (Figure 5-1). Additionally, the air stream enabled shear alignment of SWNTs within each individual layer, and hence each individual layer had a distinct orientation.

5.4. Results and Discussion

5.4.1. Charge injection through the nano-film

We investigated the lateral conductivity of different layers using SECM steady-state feedback mode approach curves. Most previous work on SWNT SECM characterization has focused on SWNTs' potential use as a probe but here we have used it as a coating. The mechanism of charge injection is as shown in Figure 5-2. The UME is set at approached towards the substrate at a constant scan rate. Since, we expect the film to be conductive; there is a lateral (in-plane) and cross-film electron transport in the multilayer polymer/nanoparticle film.

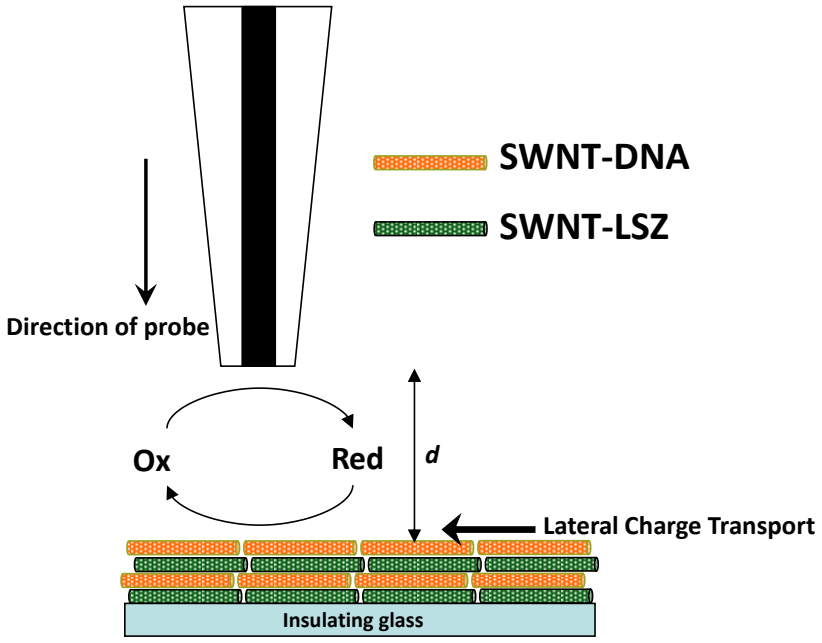

Figure 5-17 Schematic of the proposed mechanism of charge transfer through the nano-coating

One of the principle advantages of using SECM for investigating conductivity of nanotube assemblies is that, the method is non-invasive, highly localized and does not require the film to be externally biased. Besides, the film substrate is an insulating glass slide, and hence the response obtained is solely due to the charge injection across the film. Figure 5-3 shows typical UME experimental approach curves (microelectrode tip current versus distance from the film surface) as a function of SWNT-LSZ and SWNT-DNA layer numbers as coating using the same concentration of redox mediator (1 mM FcMeOH + 0.1 M KCl) was used. A clear increase of the steady-state current is observed as the tip approaches the film [23, 24]. The regeneration of the electro-active species is driven by the lateral conductivity within the film and the kinetics of the redox process. An increase in tip current is therefore attributed to the lateral conductivity across the SWNT-LSZ and SWNT-DNA. Positive feedback increases with the number of layers and therefore layers are not insulated from another.

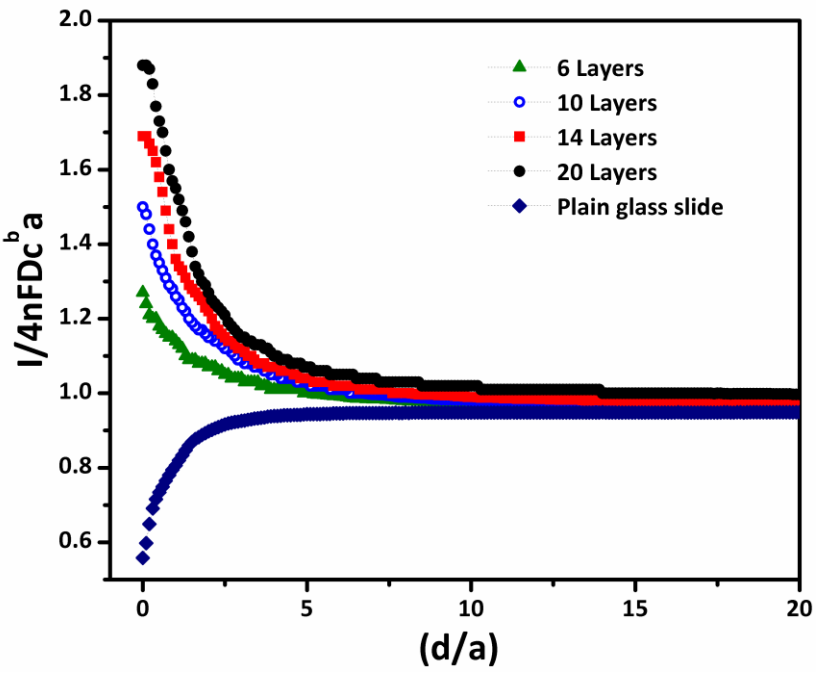

Figure 5-18 Approach curves at identical concentrations of redox mediator to nano-composite films composed of different number of SWNT-LSZ/SWNT-DNA layers

Increased current is a result of fine carbon nanotube assembly control, indicating that transport along the layer is dominated by single-electron transport along a localized area in the nanotube or a whole lot of bundles [19, 25]. Clearly, the tip-generated oxidized mediator FcMeOH is capable of oxidizing the multilayer and thereby regenerating $FcMeOH^+$, which diffuses back to the tip. Figure 5-4 shows approach curves for a substrate with ten alternating layers of SWNT-LSZ/SWNT-DNA at different bulk concentrations of FcMeOH. Positive feedback becomes more pronounced as a result of lateral charge transfer within the film when the concentration of the redox mediator is decreased. The observed tip current increase is due solely to lateral charge transfer and not background charge accumulation. Positive feedback with FcMeOH is a clear effect of the coatings present on top of the glass slide, confirming that regeneration of the mediator comes from the multilayer.

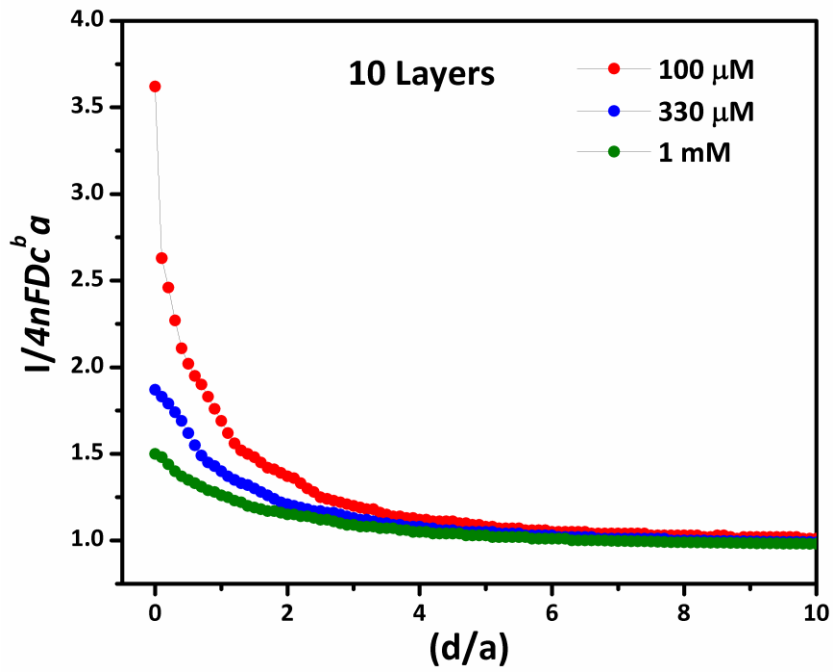

Figure 5-19 Approach curves for 10 layers of SWNT-LSZ/SWNT-DNA at different concentrations of redox mediator. The concentration of the solution redox mediator from top to bottom is 100 μM, 330 μM and 1 mM

A similar result has been obtained using a two-dimensional network of SWNT [26, 27]. Approach curves were also recorded for plain glass slides acting as controls. Control slides gave negative feedback at all times. Background measurements were performed by swapping the mediator with the supporting electrolyte alone to allow observations of current intensity variation. The approach curve exhibits negative feedback in the absence of multilayers, verifying a insulate surface. The biocoating proved to be very robust, giving consistent electrochemical results over periods of up to six continuous hours.

5.4.2. Nanoelectronic properties of alternate layers

Investigation of the effects of the number of layers and whether the top layer was SWNT-LSZ or SWNT-DNA showed that the magnitude of positive feedback depends on the uppermost deposited layer (Figure 5-5). A slightly higher current was observed for 10 layers terminating in

SWNT-DNA than 11 layers terminating in SWNT-LSZ. Lysozyme has a high dielectric response when dissolved in water and may not transfer electrons at neutral pH. At neutral pH, LSZ has a net charge of +8 if charge distribution in the side chains is considered [28]. The positive nature of LSZ results in minimal diffusion to the SWNT backbone due to electrostatic repulsion. Thus, electron transfer from FcMeOH is blocked with respect to the redox couple. Alternatively, DNA can facilitate electron transfer to dissolve the mediator [4]. We conclude that the regeneration of mediator is accentuated as SWNT-DNA is deposited. SECM analysis on non-SWNT coupled DNA and LSZ layers assembled on glass slides was also conducted to verify lateral charge transfer. This is in agreement with Lie *et al* [29] who observed negative current in the approach curves for DNA monolayers immobilized on silicon substrates.

To further investigate the effect of the outermost layer composition, impedance spectroscopy was used to determine the impedance associated with the electrode reactions rather than the inherent electrical resistance of the material. Fig. 3 shows that the resistance increased from 6 to 18 kΩ cm^2 with decreasing numbers of layers demonstrating higher resistance, which is consistent with the evidence obtained by SECM. However, it was observed that when the last layer deposited was SWNT-LSZ there was slightly increased resistance, which was contrary to observations for SWNT-DNA. The SWNT-DNA appeared to provide additional sites for the electrochemical reaction and effectively enhance electronic transfer it has been proposed by different authors that DNA can facilitate electron tunneling [4]. In contrast, our observations suggest that LSZ block the active sites and increase electrode resistance. EIS measurements were performed in the presence of FcMeOH as redox couple ions. Figure 4 shows the electrochemical impedance spectra (Nyquist plots, Z″ vs. Z′) for the layers. The diameter of the semicircle represents the charge-transfer resistance (R_{ct}) at the electrode surface.

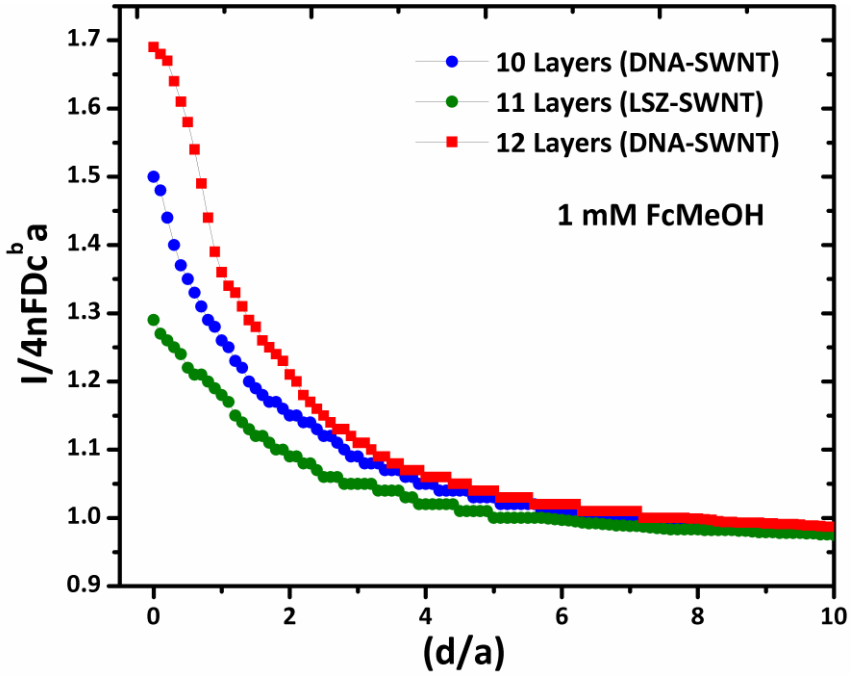

Figure 5-20 Approach curves for alternating layers of SWNT-LSZ/SWNT-DNA assembly

As shown in Figure 4, the diameter of the semicircle, indicating the corresponding R_{ct}, decreases as the number of layer is increased. This change can be attributed to increased repulsion between the redox marker ions and the electrode surface; the repulsion impedes the charge-transfer through the interface. The calculated values of charge transfer resistance increased in the range of 600 and 1700 Ω cm^2 with the number of layers, resulting in an increased electrostatic repulsion of the charged probe and hence the inhibition of the electron transfer.

5.4.3. Nano-bioelectrode

Electrochemical characterization of the coating was carried out by cyclic voltammetry of the 20 layers at different scan rates in 0.1 M of KCl in the presence of 1 mM FcMeOH is shown in Figure 5-6. The electrode exhibits a couple of redox peaks (V vs. Ag/AgCl) and the peak current increases linearly with scan rate. The small peak-to-peak potential separation and the peak potential dependence on the scan rate indicate a reversible electrochemical process. The

inset in Figure 5-6 shows the effect of the scan rate on the anodic peak currents. Scan rate was varied between 10 mV/s (1) and 250 mV/s (2). The response is linear with slopes of 0.7 indicating an anodic surface electrochemical reaction with a diffusion component for the anodic process; a diffusion controlled reaction. The cyclic voltammogram further indicated that films are conducive and have a stable response. The biocoatings are capable of working in a wide potential range, from −1 V to +1 V, in aqueous solution using both reductive and oxidative mediators. Further detailed studies on these effects, and other details of the electrochemical response, are under investigation for future reporting. Electrochemical Impedance Spectroscopy was carried out in the same redox mediator, in the frequency interval 50 KHz to 30 mHz with respect to Ag/AgCl electrode (0.57 V). As shown in Figure 5-7, the Nyquist plots indicated that as the number of layers increases, the charge transfer resistance (R_{ct}) decreases, from 1700 Ωcm^2 to 600 Ωcm^2.

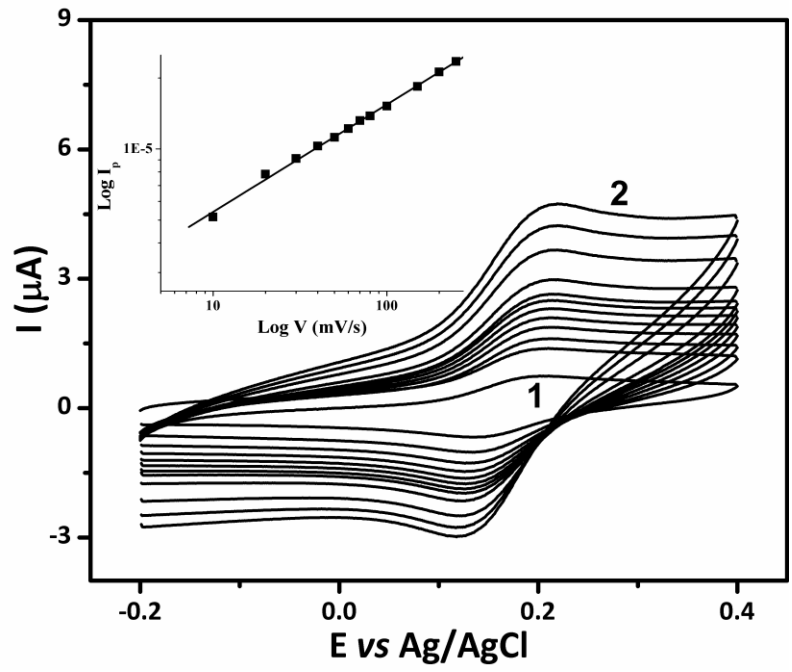

Figure 5-21 Cyclic coltammogram at different scan rates shows that the coating behaves as a bio-electrode

5.4.4. Impedance Analysis

To further investigate the effect of the outermost layer composition, impedance spectroscopy was used to determine the impedance associated with the electrode reactions rather than the inherent electrical resistance of the material. Figure 5-8 shows that the resistance increased from 6 to 18 $k\Omega\,cm^2$ with decreasing numbers of layers demonstrating higher resistance, which is consistent with the evidence obtained by SECM. However, it was observed that when the last layer deposited was SWNT-LSZ there was slightly increased resistance, which was contrary to observations for SWNT-DNA. The platform which houses the substrate was custom built using conductive soldering metal and copper connects. Both ends of the holder were sputter coated with gold for increased conductivity (Figure 5-9). The SWNT-DNA appeared to provide additional sites for the electrochemical reaction and effectively enhance electronic transfer it has been proposed by different authors that DNA can facilitate electron tunneling. In contrast, our observations suggest that LSZ block the active sites and increase electrode resistance.

5.5. Conclusion

In conclusion, we have applied a simple and reliable technique for the biocoating fabrication using layer-by-layer technique, and we have used a complementary suite of methods to provide the first electrochemical characterization of this system. The positive feedback response obtained with SECM shows that the presence of the SWNT-biological coating causes conducting surfaces to behave with finite electrode kinetics. In addition to enhanced electron flow, impedance spectroscopy demonstrated the decrease of charge-transfer resistance measurements at number of layer. These results show that the combination of Nature's toolbox and single-walled carbon nanotubes enable multifunctional conductive coatings where the charge transport can be tailored based on the number of layers and the composition and polarity of the outermost layer.

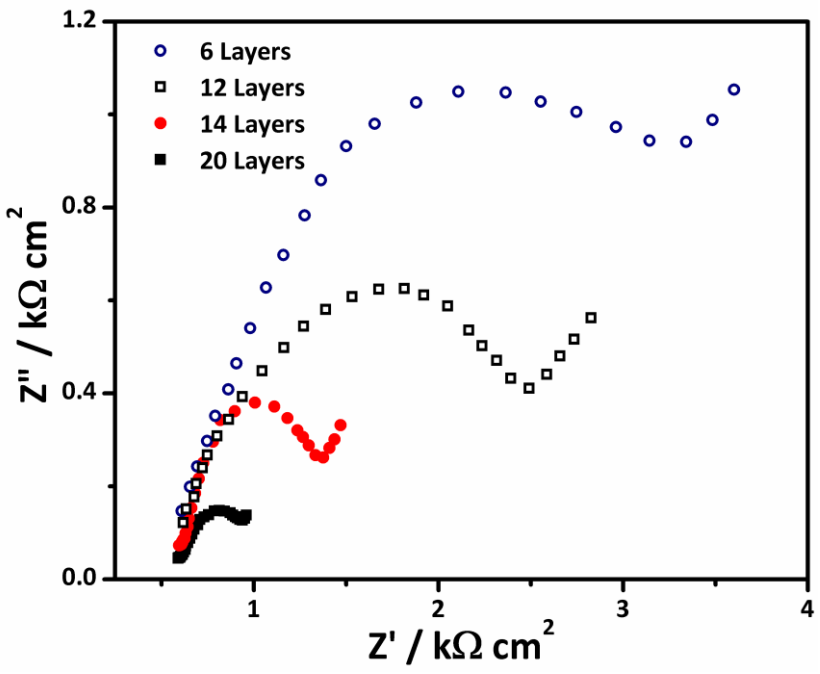

Figure 5-22 EIS spectra for different layers of assembly

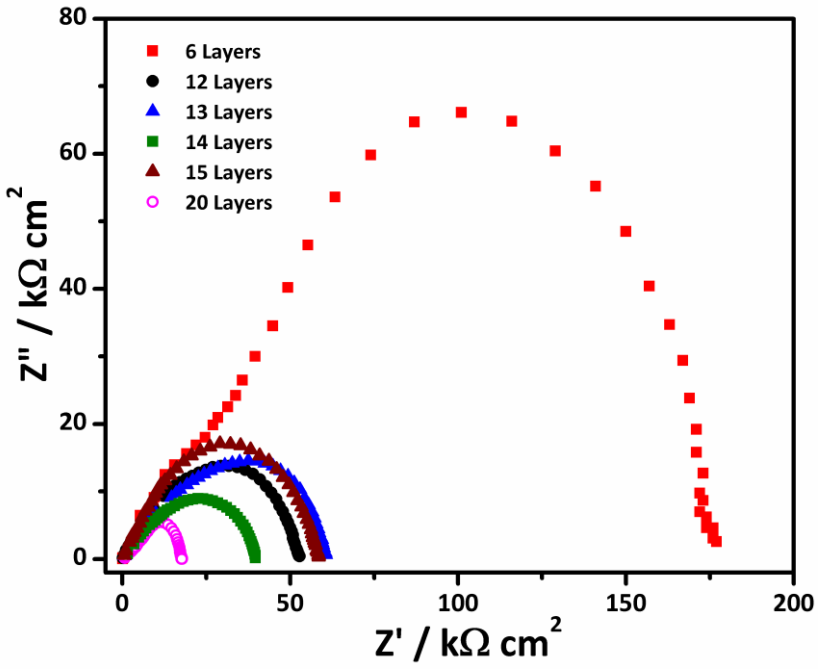

Figure 5-23 Representative impedance responses of the different number of layers at open circuit

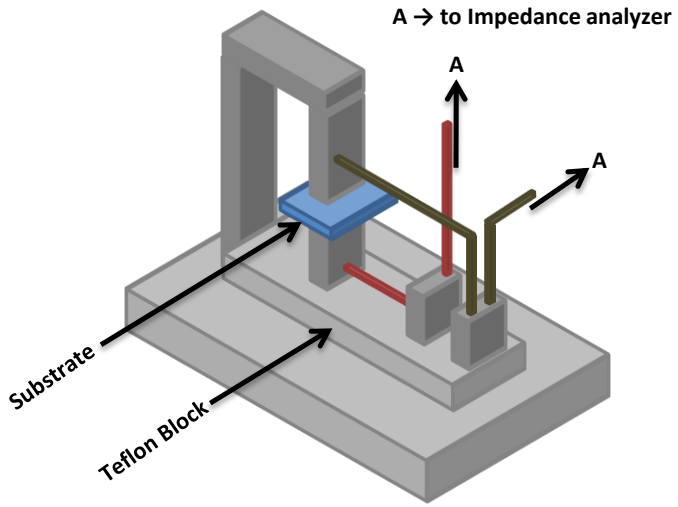

Figure 5-24 Schematic of the custom built platform to hold the glass substrates for impedance analysis

Expected advancements in the separation of metallic and semiconducting SWNTs will further increase flexibility and performance. This research indicates that combination of SWNTs with biopolymers offer great promise for creating new, sustainable bio-interfaces with controllable electrical and mechanical parameters. We believe that these approaches can be extended to the creation of new SWNT-biological coatings for a variety of electrochemical processes, and applications in electronics and sensing.

5.6. References

1. Huang, Y., et al., *Directed Assembly of One-Dimensional Nanostructures into Functional Networks.* Science, 2001. 291(5504): p. 630-633

2. Vigolo, B., et al., *Macroscopic Fibers and Ribbons of Oriented Carbon Nanotubes.* Science, 2000. 290(5495): p. 1331-1334

3. Rao, S.G., et al., *Large-scale assembly of carbon nanotubes.* Nature, 2003. 425: p. 36-37.

4. Lie, L.H., et al., *Electrochemical detection of lateral charge transport in metal complex-DNA monolayers synthesized on Si(111) electrodes.* J. Electroanal. Chem., 2007. 603: p. 67-80.

5. Shim, B.S. and N.A. Kotov, *Single-Walled Carbon Nanotube Combing during Layer-by-Layer Assembly: From Random Adsorption to Aligned Composites.* Langmuir, 2005. 21: p. 9381-9385.

6. Wang, H., et al., *Shear-SANS study of single-walled carbon nanotube suspensions.* Chem. Phys. Lett., 2005. 416: p. 182-186.

7. Reches, M. and E. Gazit, *Controlled patterning of aligned self-assembled peptide nanotubes.* Nat. Nanotechnol., 2006. 1: p. 195-200.

8. Duan, X., Y. Huang, and C.M. Lieber, *Nonvolatile Memory and Programmable Logic from Molecule-Gated Nanowires.* Nano Lett., 2002. 2: p. 487-490.

9. Huang, S., L. Dai, and A.W.H. Mau, *Controlled Fabrication of Large-Scale Aligned Carbon Nanofiber/Nanotube Patterns by Photolithography.* Adv. Mater., 2002. 14(16): p. 1140-1143.

10. Shao, M., et al., *Karman vortex street assisted patterning in the growth of silicon nanowires.* Chem. Commun., 2007. 8: p. 793-794.

11. Li, Y., I.A. Kinloch, and A.H. Windle, *Direct Spinning of Carbon Nanotube Fibers from Chemical Vapor Deposition Synthesis.* Science, 2004. 304: p. 276 - 278.

12. Zhang, M., et al., *Strong, Transparent, Multifunctional, Carbon Nanotube Sheets* Science, 2005. 309: p. 1215 - 1219.

13. Zhang, M., K.R. Atkinson, and R.H. Baughman, *Multifunctional Carbon Nanotube Yarns by Downsizing an Ancient Technology* Science, 2004. 306(5700): p. 1358-1361.

14. Tang, Z., et al., *Biomedical Applications of Layer-by-Layer Assembly: From Biomimetics to Tissue Engineering.* Adv. Mater., 2006. 18(24): p. 3203–3224.

15. Glotzer, S.C., et al., *Self-assembly of anisotropic tethered nanoparticle shape amphiphiles.* Curr. Opin. Colloid Interface Sci., 2005. 10: p. 287-295.

16. Niyogi, S., et al., *Selective Aggregation of Single-Walled Carbon Nanotubes via Salt Addition.* J. Am. Chem. Soc., 2007. 129(7): p. 1898–1899.

17. Ginic-Markovic, M., et al., *Synthesis of New Polyaniline/Nanotube Composites Using Ultrasonically Initiated Emulsion Polymerization.* Chem. Mater., 2006. 18(26): p. 6258–6265.

18. Park, C., et al., *Actuating Single Wall Carbon Nanotube–Polymer Composites: Intrinsic Unimorphs.* Adv. Mater., 2008. 20(11): p. 2074-2079.

19. Li, Z., et al., *Comparative Study on Different Carbon Nanotube Materials in Terms of Transparent Conductive Coatings.* Langmuir, 2008. 24(6): p. 2655–2662.

20. Nepal, D., et al., *Strong Antimicrobial Coatings: Single-Walled Carbon Nanotubes Armored with Biopolymers.* Nano Lett., 2008. 8(7): p. 1896–1901.

21. Kaul, A.B.M., K. G., P. von Allmen, and R.L. Baron *Single, aligned carbon nanotubes in 3D nanoscale architectures enabled by top-down and bottom-up manufacturable processes* Nanotechnology, 2009. 20(7): p. 75303.

22. Nepal, D., et al., *Supramolecular Conjugates of Carbon Nanotubes and DNA by a Solid-State Reaction.* Biomacromolecules, 2005. 6(6): p. 2919–2922.

23. Zhang, J., et al., *Combined scanning electrochemical microscopy–Langmuir trough technique for investigating phase transfer kinetics across liquid/liquid interfaces modified by a molecular monolayer.* Electrochem. Commun., 2003. 5: p. 407.

24. Mandler, D. and P.R. Unwin, *Measurement of Lateral Charge Propagation in Polyaniline Layers with the Scanning Electrochemical Microscope.* J. Phys. Chem. B, 2003. 107(2): p. 407-410.

25. Strano, M.S., et al., *Electronic Structure Control of Single-Walled Carbon Nanotube Functionalization* Science, 2003. 301(5639): p. 1519 - 1522.

26. Wilson, N.L., et al., *Assessment of the Electrochemical Behavior of Two-Dimensional Networks of Single-Walled Carbon Nanotubes.* Anal. Chem., 2006. 78(19): p. 7006–7015.

27. Gardner, C.E., P.R. Unwin, and J.V. Macpherson, *Correlation of membrane structure and transport activity using combined scanning electrochemical–atomic force microscopy.* Electrochem. Commun., 2005. 7: p. 612-618.

28. Cheng, A.K.H., B. Ge, and H. Yu, *Aptamer-Based Biosensors for Label-Free Voltammetric Detection of Lysozyme.* Anal. Chem., 2007. 79(14): p. 5158–5164.

29. Lie, L.H., et al., *Immobilisation and synthesis of DNA on Si(111), nanocrystalline porous silicon and silicon nanoparticles.* Faraday Discuss., 2004. 125: p. 235.

6. Affinity Based DNA Optical Sensors for the Detection of *hipO* Gene from *Campylobacter jejuni*

6.1. Introduction

Campylobacter jejuni is a significant cause of human bacterial gastroenteritis [1-3] and can be acquired from contact with farm animals or ingestion of contaminated poultry products, raw milk or impure water. This pathogen has been implicated in 80 outbreaks in the US alone [4], and the Centers for Disease Control and Prevention estimate that campylobacteriosis affects over 2.4 million people annually in the US. In 2008, 5,825 cases of campylobacteriosis were reported through FoodNet, with 12.68 cases per 100,000 people [5]. Campylobacteriosis has also been associated with the development of illnesses such as Guillian-Barre syndrome, reactive arthritis, Reiter syndrome, diarrheal infections, intestinal malignancy and dehydration [6, 7].

Traditional laboratory procedures are used for *Campylobacter* detection, which include plate culturing or extracting the bacteria from samples followed by serotype or genotype based diagnostic assays [8, 9]. Although these methods are sensitive, they can take up to 96 hours for the analysis to be done. Therefore, development of sensors capable of offering a rapid and inexpensive alternative, coupled with real-time monitoring and specific detection of low concentrations of *C. jejuni* in food products, is needed to ensure public safety.

Numerous biosensor platforms have been developed for the detection of food-borne pathogens [10]. Nucleic acid-based sensing platforms have been widely described, including piezoelectric sensors that measure frequency changes resulting from the hybridization of immobilized probes with a corresponding target [11, 12], chemi-luminescence based systems where fluorescently labeled probes are immobilized onto transducer surfaces [13], aptamer-based

sensing using DNAzymes to design functional chimera structure-like probes [14]. However, these methods are rigorous, time-consuming and possess low sensitivity in comparison to other detection platforms [15, 16].

Recently, there have been reports of detection of pathogenic food-borne bacteria using disease causing genes as probe molecules [17, 18]. Detection using Polymerase Chain Reaction (PCR) is very selective but may lack the required sensitivity for the rapid screening of samples [19]. Electrochemical DNA microarrays are advantageous over PCR-based assays for their high sensitivity, portability and also better performance without labeling the probes. They can also be used for multiple target preparation. This method is quite sensitive but produces high background signals that are difficult to separate, and the sensing platform is destroyed after every measurement. This is problematic for the reusability, reliability and robustness of the surface structures that are developed over the electrodes [20]. An alternative to these methods is DNA-based biosensors, which can be selective, specific and robust. For example, self-assembled monolayers of ssDNA probes specific to targeted ssDNA can be immobilized on sensor surfaces, allowing indirect detection of a bacterium of interest [21].

Hybridization-based sensing platforms were developed using DNA probes labeled with fluorophores. Although these methods are specific and sensitive, they may suffer from photo-bleaching and have limited differentiation between hybridized and non-hybridized sequences in the mixture. Moreover, signals that arise from non-specific adsorption and diffusion across the colloid are difficult to analyze. While, DNA sequences can be labeled with nano-particles for effective signal enhancement, a disadvantage is the attachment of nano-particles by thiol linkage that which can form dense layers of DNA on each particle [22]. Covalent bond formation on

gold is employed to develop anti-fouling biosensor surface, often via thiol-gold linkages or avidin-biotin chemistries [11, 23].

The basis for the difference between *C. jejuni* and any other bacteria is the expression of the *N*-benzoylglycine amidohydrolase (*hippuricase*) gene. The hallmark of the hippuricase activity is the conversion of hippuric acid into benzoic acid and glycine. This gene is the key feature in discriminating *C. jejuni* from other similar *Campylobacter* species, such as *C. coli*. Diffraction Optics (DOT) sensors are widely used for label-free detection and real-time monitoring of bio-molecular interactions. This technique has been widely employed for the detection of proteins and small molecules [24], and live cells [25, 26]. A variety of biotin labeled ligands including proteins, antibodies and DNA can be immobilized on the DOT sensor chip.

Our present work accounts the development of hybridization-based Diffraction Optics Technology (DOT) and Surface Plasmon Resonance (SPREETA) sensing platforms. False positive responses due to analyte concentration and bulk refractive index are eliminated in the DOT and only the diffraction phenomena across the grating is recorded, which are precisely advantageous over other label-free optical biosensor technologies. Accordingly, a low limit of detection of 5 nM was obtained. A range of surface chemistries and the extensive possibilities in label-free and amplified modes, coupled with low cost disposable sensor chips makes it an attractive optical sensing device. The application of this coupling strategy to two devices was conducted with the aim of exploiting its applicability in different instrumentations using the same sensor formats.

6.2. Experimental

6.2.1. Reagents

Potassium phosphate monobasic, Phosphate buffered saline (pH 7.4) containing 0.138M NaCl and 0.0027M KCl (PBS) and 6-Mercapto-1-hexanol were obtained from Sigma-Aldrich

(St. Louis, MO). Tween-20, EDTA, sodium phosphate dibasic and sodium chloride were used as received from Fisher-Scientific (Pittsburgh, PA). Reductactryl™ (Cleland's reagent) was obtained from Calbiochem (San Diego, CA).

6.2.2. Sensor Platforms

DOT sensors chips (Axela Inc., Toronto, Canada) were used for diffraction experiments (Fig. 1). A 670 nm laser diode, class 3R with a maximum output of 4.0 mW and a beam divergence of 5.0 mRad was used as the light source, to produce a diffractive pattern. One end of the sensor was connected to a fluidic panel, which is responsible for circulating the buffer solutions and the other end is connected to a sensor manifold which aspirates the analyte from the well. The sensor chip was made of optically clear polystyrene with an interspersed prism situated below the flow channel. The linear flow channel which can hold a volume of 10.0 µl, consisted of eight, circular assay spots, each 2.0 mm in diameter, with 15.0 femto moles of avidin deposited on each spot [27]. These spots constituted the grating where light is diffracted in a predictable manner.

The SPREETA (Texas Instruments, Dallas, TX) is a robust, two-channeled SPR system comprised of a multi-channel SPR sensor, flow cell, and 12-bit three-channel DSP electronic control box (ECB). The sensing region is coated with a semi-transparent gold film (~50 nm) with a Cr-adhesion layer (1-2 nm). A two-channel polypropylene flow cell coupled with a silicone gasket was used to establish a flow system along with a peristaltic pump (Ismatec, Cole-Parmer Instrument Co., Chicago, IL) at a flow rate of 25.0 µl/min at 25^{o}C. Multi-channel SPREETA software version 10.83 (Texas Instruments) monitored the changes in RI near the sensing surface, calculated the statistical noise in the signal and displays the results. The signal is generally displayed in response unit (RU) (1 response unit = 10^{-6} refractive index unit) [28].

6.2.3. DNA Probes

Primers and probes were designed from the hippuricase gene (*hipO*) of *C. jejuni* (accession number Z36940.1). The forward (5'- GAC TTC GTG CAG ATA TGG ATG CTT-3') and reverse (5'-CGA TAT TGA TAG GCT TCT TCG GTA GTA-3') primers amplified a 344 bp segment. The short (SP, 5'- GGT GGT GCT AAG GCA ATG ATA G-3') and long (LP, 5'-GGT GGT GCT AAG GCA ATG ATA GAA GAT GGA TTG TTT GAA AAA TTT GAT AG-3') probes attached to the 344 bp segment. Primers and probes were synthesized by Integrated DNA Technologies (Coralville, IA). Reverse and complementary ssDNA (IDT) corresponding to the amplified segment were diluted in TE Buffer (10 mM Tris, 0.1 mM EDTA, pH 8.0). The disulfide bonds of thiolated DNA probes were cleaved by resuspending in TE buffer along with Reductactryl™ 1:50, allowing formation of self-assembled monolayers (SAM) with higher surface density and better reproducibility [29]. This mixture was then agitated at room temperature (RT) for 15 min followed by syringe filtration (0.2 μm).

Experiments were also conducted using a scaffold of LP (5'-GGT GGT GCT AAG GCA ATG ATA GAA GAT GGA TTG TTT GAA AAA TTT GAT AG-3') and short target (5'-CTA TCA TTG CCT TAG CAC CAC C -3'). Equimolar mixture of the probe and target were mixed together and annealed in up to 95^{o}C. A DNA probe with a 22-mer double strand and 28-mer single strands was formed. This was followed by slow cooling of the mixture [DNA scaffold colloids paper]. Reduction of the DNA was done using Reductactryl™ in order to cleave the disulfide bonds present in the long probe. This mixture was then agitated at room temperature (RT) for 15 min followed by syringe filtration (0.2 μm). Experiments were also conducted by attaching a long probe (LP) (5'-GGT GGT GCT AAG GCA ATG ATA GAA GAT GGA TTG TTT GAA AAA TTT GAT AG-3') and a second 22-mer (5'-CTA TCA TTG CCT TAG CAC CAC C -3') ssDNA.

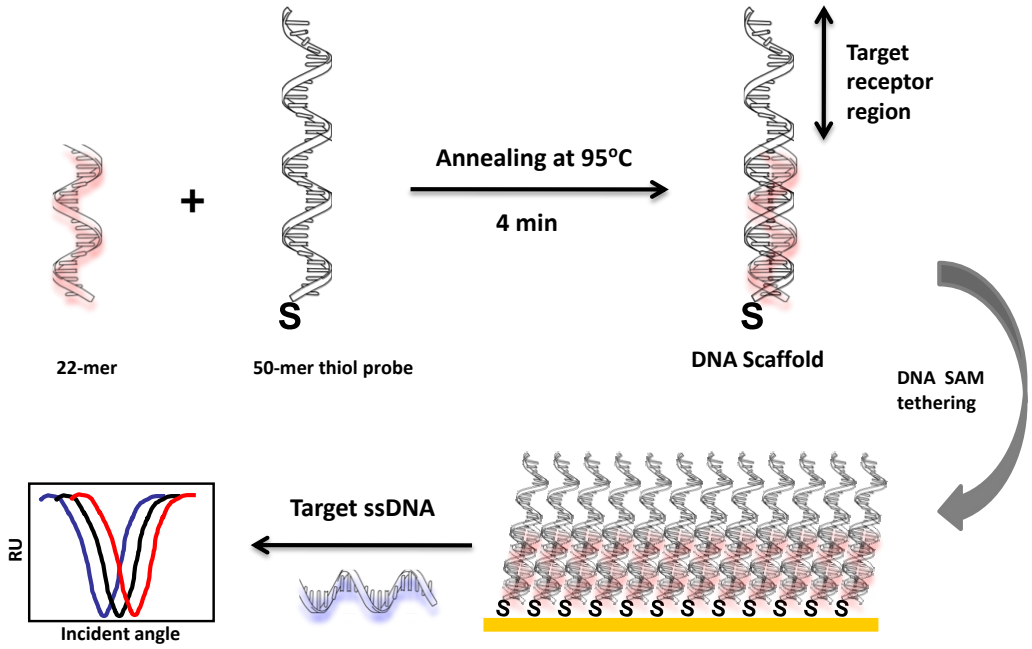

Figure 6-1 Illustration of the formation of DNA scaffolds using a 50-mer long probe and 22-mer short probe by annealing the complimentary regions in both the strands

Equimolar mixture of the probe and target were mixed together and annealed up to 95^{o}C. A DNA probe with a 22-mer double strand and 28-mer single strand was formed (Figure 6-1). This was followed by slow cooling of the mixture [30]. Disulfide bonds in the long probe were cleaved with Reductactryl™.

6.3. Immobilization of DNA probes

6.3.1. dotLab

Analyte is passed at a standard flow rate of 500.0 µl / min is maintained all throughout the experiment in the mixer mode. Flow of reagents was controlled by the method that was programmed before the start of the analysis (Table 6-1). 500 µL of a mixture of 1X PBS and 0.0025% Tween (PBST) was primed over the neutravidin modified polystyrene surface. The non-specific area across the flow channel was blocked with BSA (5.0 mg/ml) for 3 minutes. Subsequently, biotinylated DNA probes (1.0 µM) were injected for 45 minutes followed by

washing with buffer. Changes in diffraction intensity were monitored using dotLab™ software. After a sequence of washing steps, the target was injected sequentially in graded concentrations through a precise fluidic system and pre-defined incubation time.

6.3.2. SPREETA

Gold surface of SPREETA™ sensors were carefully cleaned with piranha solution followed by argon plasma cleaning. The uniqueness of SPREETA allows real-time monitoring of the specific interactions between the probe and target using sensing and reference channels. Thiolated probes (1.0 µM) suspended in the immobilization buffer were passed over the gold surface for 3 hours.

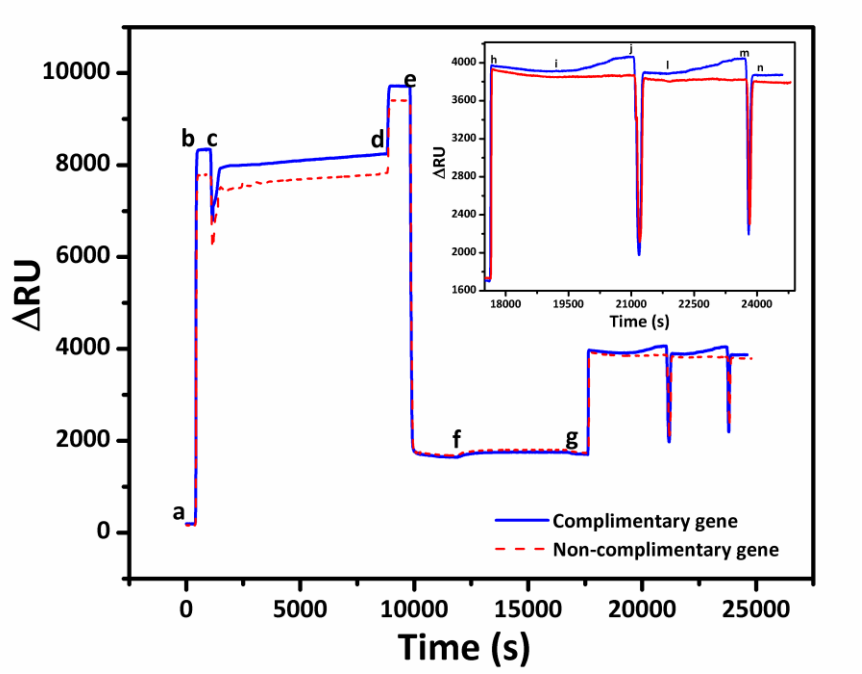

Figure 6-2 Response curve for DNA immobilization and hybridization using SPREETA sensor

Short immobilization time ensured no degradation of DNA occured during assembly on the surface [31]. Apparently, a low pH was required to form a self-assembled monolayer [32]. After DNA immobilization, the surface was thoroughly washed and 1 mM 6-Mercapto-1-hexanol (MCH) was injected. Long DNA probes (1.0 µM) were resuspended in immobilization

buffer and injected over freshly cleaned surface for 3 hours. MCH was not immobilized on the surface because the DNA scaffolds presumably formed a tightly packed monolayer which prevents non-specific binding [33]. The surface was washed after immobilization in order to remove loosely bound probes. This short time was selected because DNA is present in a low pH buffer which rapidly degrades ssDNA in solution [34]. Apparently, a low pH is required to develop the self-assembled monolayer. Hence the assembly of thiolated DNA probes should be done within a short period of time. Binding of the probes (1 µM) to the gold surface is facilitated by passing the ssDNA at a flow rate of 25 µl / min in recycling mode. The thiolated probes are injected for 3 hrs, and the change in RU after washing the surface was found to be 1380 ± 15 (Figure 6-2). The SPR response is as follows, (a) priming the surface with water, (b) establishing a baseline with immobilization buffer, (c) modification of surface by passing 1 µM thiol-labeled ssDNA probes (d) washing the surface with buffer to remove unbound ssDNA probes. Surface is then washed with water at (e), because of the 1 mM aqueous MCH that is passed in order to minimize non-specific binding (f). (g) washing the surface with water to remove unbound MCH, (h) establishing baseline with hybridization buffer, (i) injection of target ssDNA from 2.5 nM to 1280 nM, (j) regenerating the surface using 1 mM HCl, (k) establishing a baseline again and also removing any HCl present, (l) target injection after regeneration of surface, (m) denaturation of dsDNA, (n) washing the surface with hybridization buffer for 3rd injection. Loosely bound DNA is removed by a 30 second wash after passing the DNA. It is also speculated that the 22 bp ssDNA forms a densely packed crystalline or semi-crystalline monolayer, due to Van der Waals forces between the ssDNA.

Step Number	Reagent Name	Reagent Volume (uL)	Reagent FlowRate (uL/min)	Air Gap (uL)	Incubation Type	Incubation Volume (uL)	Incubation Duration	Incubation Flowrate (uL/min)
1: Wash/Condition	PBS (0.0025% Tween)	500	2000	–	Mix	25	00:02:00	500
2: Wash/Condition	PBS (0.0025% Tween)	500	2000	–	Mix	25	00:02:00	500
3: Wash/Condition	PBS (0.0025% Tween)	500	2000	–	Mix	25	00:02:00	500
4: Tip Wash	PBS (0.0025% Tween)	500	2000	–	–	–	–	–
5: Load	BSA (5mg/ml)	50	500	5	Mix	10	00:03:00	500
6: Wash/Condition	PBS (0.0025% Tween)	500	2000	–	Mix	25	00:02:00	500
7: Tip Wash	PBS (0.0025% Tween)	500	2000	–	–	–	–	–
8: Load	Biotinylated probe ssDNA (1 uM)	50	500	5	Mix	10	00:45:00	500
9: Wash/Condition	PBS (0.0025% Tween)	500	2000	–	Mix	25	00:02:00	500
10: Tip Wash	PBS (0.0025% Tween)	500	2000	–	–	–	–	–
11: Load	BSA (5mg/ml)	50	500	5	Mix	10	00:03:00	500
12: Wash/Condition	PBS (0.0025% Tween)	500	2000	–	Mix	25	00:02:00	500
13: Tip Wash	PBS (0.0025% Tween)	500	2000	–	–	–	–	–
14: Load	Target ssDNA 5 nM	50	500	5	Mix	10	00:05:00	500
15: Wash/Condition	PBS (0.0025% Tween)	500	2000	–	Mix	25	00:02:00	500
16: Tip Wash	PBS (0.0025% Tween)	500	2000	–	–	–	–	–
17: Load	Target ssDNA 10 nM	50	500	5	Mix	10	00:05:00	500
18: Wash/Condition	PBS (0.0025% Tween)	500	2000	–	Mix	25	00:02:00	500
19: Tip Wash	PBS (0.0025% Tween)	500	2000	–	–	–	–	–
20: Load	Target ssDNA 20 nM	50	500	5	Mix	10	00:05:00	500
21: Wash/Condition	PBS (0.0025% Tween)	500	2000	–	Mix	25	00:02:00	500
22: Tip Wash	PBS (0.0025% Tween)	500	2000	–	–	–	–	–
23: Load	Target ssDNA 40 nM	50	500	5	Mix	10	00:05:00	500
24: Wash/Condition	PBS (0.0025% Tween)	500	2000	–	Mix	25	00:02:00	500
25: Tip Wash	PBS (0.0025% Tween)	500	2000	–	–	–	–	–
26: Load	Target ssDNA 80 nM	50	500	5	Mix	10	00:05:00	500
27: Wash/Condition	PBS (0.0025% Tween)	500	2000	–	Mix	25	00:02:00	500
28: Tip Wash	PBS (0.0025% Tween)	500	2000	–	–	–	–	–
29: Load	Target ssDNA 160 nM	50	500	5	Mix	10	00:05:00	500
30: Wash/Condition	PBS (0.0025% Tween)	500	2000	–	Mix	25	00:02:00	500
31: Tip Wash	PBS (0.0025% Tween)	500	2000	–	–	–	–	–
32: Load	Target ssDNA 320 nM	50	500	5	Mix	10	00:05:00	500
33: Wash/Condition	PBS (0.0025% Tween)	500	2000	–	Mix	25	00:02:00	500
34: Tip Wash	PBS (0.0025% Tween)	500	2000	–	–	–	–	–
35: Load	Target ssDNA 640 nM	50	500	5	Mix	10	00:05:00	500
36: Wash/Condition	PBS (0.0025% Tween)	500	2000	–	Mix	25	00:02:00	500
37: Tip Wash	PBS (0.0025% Tween)	500	2000	–	–	–	–	–
38: Load	Target ssDNA 1280 nM	50	500	5	Mix	10	00:05:00	500
39: Wash/Condition	PBS (0.0025% Tween)	500	2000	–	Mix	25	00:02:00	500
40: Tip Wash	PBS (0.0025% Tween)	500	2000	–	–	–	–	–

Table 6-1 Summary of method for the detection of *hipO* gene programmed using dotLab software

6.4. Detection of target DNA

6.4.1. dotLab

All solutions were prepared in PBST buffer. In order to determine the limit of detection, target DNA was serially diluted from 0.005 µM to 1.28 µM and introduced sequentially, starting

with the lowest concentration. Complementary target DNA had the sequence, 5’ – CTA TCA TTG CCT TAG CAC CAC C - 3’ and the non-complimentary DNA is 5’ – CCG TCG TAG ACA TAC TAC ATC G - 3’. Each dilution was passed for 5 minutes until saturation of target binding. Between injections of each aliquot, the surface was washed thoroughly with PBST. The difference in signal between the PBST baseline and respective intensity was determined for each concentration. Biotinylated DNA probes diluted in PBST is introduced at a flow rate of 500 µl/min. Auto sampler aspirates the analyte from the tray, which is controlled by the two syringe pumps. Volume and flow rate is defined in the method and analyte location is assigned in the schedule. Loosely bound DNA was removed by priming the surface with PBST, which showed a decrease in signal. Before the molecules bind to the surface, a weak intensity image is produced upon illumination. However, when the probe molecules are immobilized on to the surface, an increase in height of the diffraction pattern is produced, which in turn corresponds to the increase in intensity. Probes are immobilized without fluorescent and chemi-luminescent labels, over a highly sensitive and accessible platform for the detection of biomolecular interactions. Each 10 µl flow channel is connected to the fluidic system and the analyte is passed at a standard flow rate of 500 µl / min is maintained all throughout the experiment in the mixer mode for 5 minutes, with a data acquisition rate of 1 Hz. Detection of the binding phenomena can be monitored by inquiring with the laser light in a total internal reflection mode, without the laser passing through the flow channel, so that 95 % of the signal can be measured. The signal is generally displayed in diffraction intensity (DI). The protocol was established as recommended by the manufacturer. Non-specific binding spots were covered using 5 mg/ml BSA in PBST buffer. Buffers and the analyte are injected through the automated fluidic system.

6.4.2. SPREETA

Hybridization experiments were conducted in hybridization buffer (150 mM NaCl, 20 mM Na_2HPO_4, 0.1 mM EDTA, 0.005 % Tween 20, pH – 7.4). Target DNA was serially injected from lowest (2.5 nM) to highest (1280 nM) concentrations for 5 minutes. Sensors were washed after every injection to remove any loosely bound DNA. Origin Pro 8 (OriginLab Corporation, MA) software was used to calculate the net response by subtracting the working channel signal (baseline) from the control channel. The loosely bound DNA is washed with buffer for 30 seconds. Net response was calculated by deducting the control signal from sensing signal. This allows the elimination of the signal generated due to non-specific adsorption of cells to the sensor surface, as well as change in RI due to bulk refractive index of the solution. Specificity of the system was tested using a non-complimentary target ssDNA which was injected from 5 nM to 1280 nM. Similarly, a non-complimentary nucleotide was also passed through to check for specificity and there was no detectable signal from the control channel. As in the case of the dotLab system, a dose-response curve was plotted with different concentrations of the target ssDNA from 2.5 nM to 1280 nM.

In the case of longer probes, the target DNA is serially passed over the surface starting from the lowest concentration (10 nM to 640 nM) for 5 minutes. A non-complimentary target is also passed over the surface to verify specificity.

6.4.3. Electrochemical Impedance Spectroscopy (EIS)

AC electrochemical impedance spectroscopy was carried out using an FRA2 - µAUTOLAB – TYPE III electrochemical impedance analyzer (Metrohm USA Inc., Westbury, NY). A one-compartment 2.0 mL glass cell with a working volume, Ag/AgCl reference electrode and a platinum wire auxiliary electrode was used for the measurements. The sensing surface was characterized over a wide range of frequency (10 Hz to 100 MHz; $E^{0'}$ = 180 mV versus Ag/AgCl)

in the presence of 5 mM $K_3Fe(CN)_6 + K_4Fe(CN)_6$ in 0.1 M KCl. A linear region for the bare gold electrode implies at low frequency shows that the reaction across the electrode is diffusion controlled [35].

6.5. Results and Discussion

6.5.1. Immobilization of Biotinylated DNA probes (dotLab)

The response curve for probe binding at different concentrations is shown in Figure 6-2. A net response (Figure 6-3) was determined by deducting the control signal from the sensing signal. Probe optimization was done by passing a wide range of concentrations over the surface. The working range lies between 0.5 μM and 1 μM. Hence this was chosen as the probe concentration as there is very minimum difference in intensity across these concentrations. This confirmed the high specificity of the system using biotinylated ssDNA probes. Using the same concentration (1 μM)) for 20 cycles of hybridization/regeneration on the same chip in 7 days, the average value was $4.7 \times 10^{-2} \pm 1.16 \times 10^{-2}$ DI units (96% relative standard deviation, $R^2 = 0.995$) (data not shown). This is comparable with diffraction-based assays or surface plasmon resonance platforms [36, 37]. The ability of cross-linking biotinylated ssDNA was examined using the dotLab system. The dotLab system is a relatively new optical biosensor based on diffractive optics technology. This system uses a sensor chip with an integrated prism situated below the flow channel, which monitors biomolecular interactions in real time within a complex media. Because diffraction is inherently self-referencing, nonspecific binding to both the patterned and unpatterned regions will not affect the signal. Such characteristic offers an important advantage over other optical biosensor systems in which any surface binding event will cause non-specific binding. Besides, the dotLab biosensor is a cost-effective platform that has the format flexibility to provide a quick and simple solution to both assay development and routine analysis.

6.5.2. Immobilization of Thiolated DNA probes (SPREETA)

Using previously established methods [28, 38]; the surface coverage of DNA probes was determined to be 3.64 x 10^{12} ± 0.15 molecules/cm^2, with a surface coverage density of 0.44 ± 0.12 ng/mm^2 [32]. Change in RU after washing the surface was found to be 1380 ± 15. The charge transfer resistance (R_{ct}), after immobilization of DNA on gold electrode was 8.0 kΩ. It is speculated that 22 bp ssDNA probes form a densely packed semi-crystalline monolayer, due to Van der Waals forces between the ssDNA [39, 40].

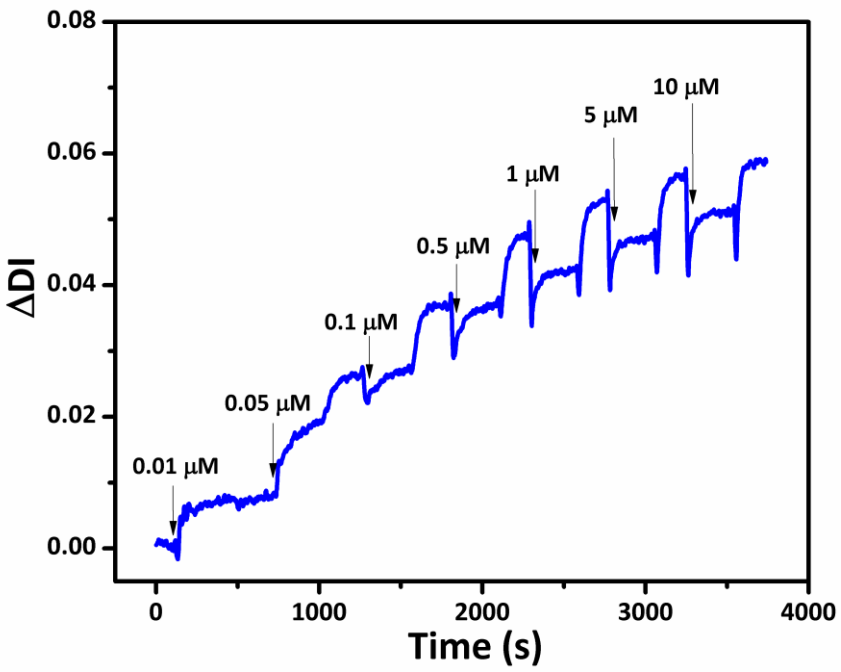

Figure 6-3 Sensor response to probe immobilization. There was a continuous increase in net change, which was calculated by subtracting the subsequent PBST baseline

EIS was performed for each step of DNA immobilization and hybridization to better understand the immobilization of thiolated probes on the surface and to characterize the electrical properties of the interfacial interaction between DNA probes before and after incubation with target DNA (Figure 6-4).

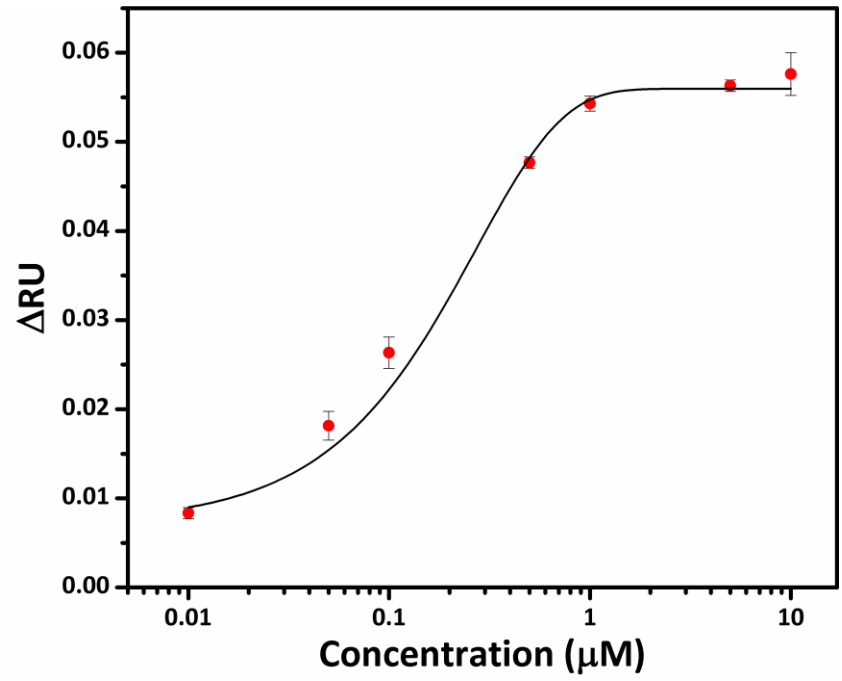

Figure 6-4 Dose-Response curve for probe binding. The net response curves were plotted by subtracting the response signal from the base line.

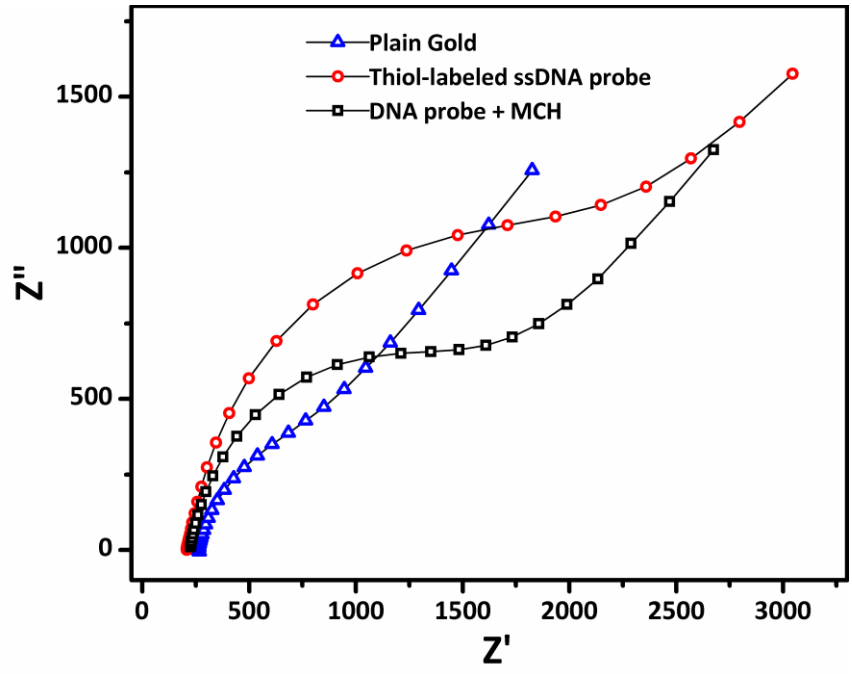

Figure 6-5 Faradaic response for immobilization of thiolated ssDNA on SPREETA. Frequency intervals: 10 mHz to 100 KHz and measurements carried out at 0.32 V vs. Ag/AgCl.

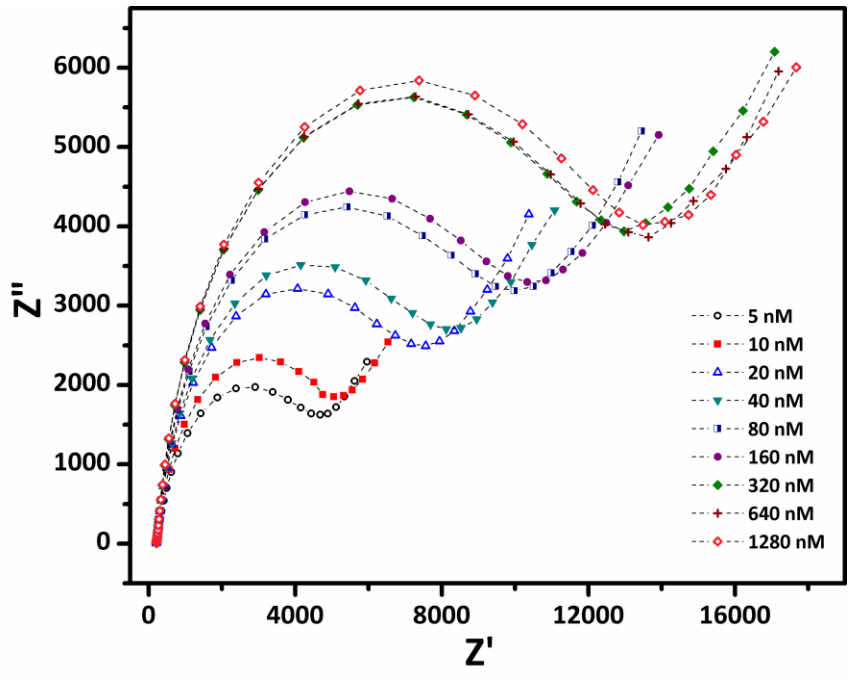

Figure 6-6 Nyquist plots for the electrode in a 5.0×10^{-3} mol L^{-1} $[Fe(CN)_6]^{3-/4-}$+ 0.1 mol L^{-1} KCl aqueous solution. Faradaic response for detection of target ssDNA

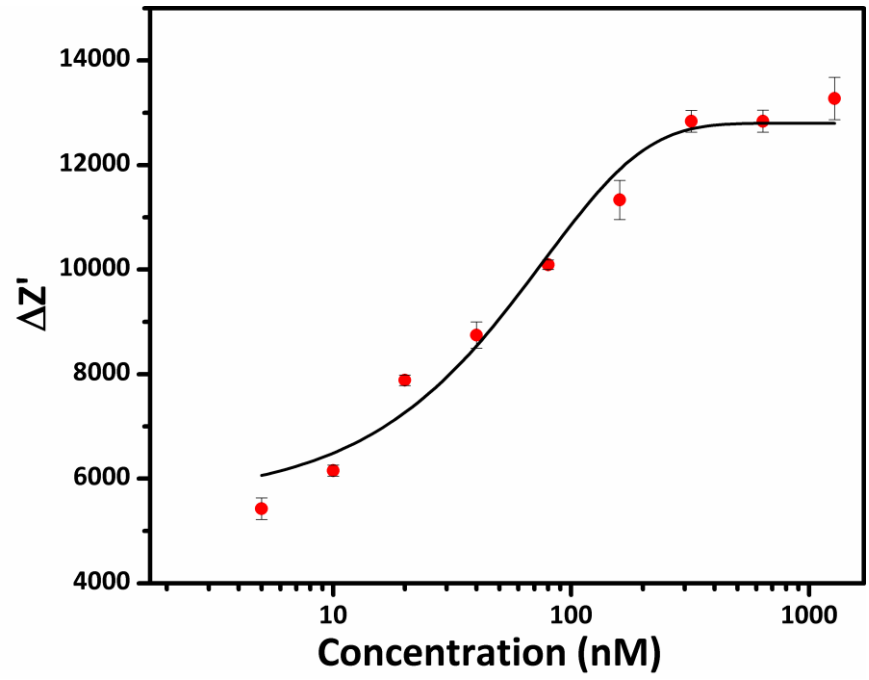

Figure 6-7 Dose-Response curve for impedance spectrum obtained during target binding

Incubation of MCH resulted in a decrease in R_{ct} (4 kΩ), indicating that the inclusion of MCH spacer thiol allows redox molecules to freely reach the electrode, thereby reducing tunneling distance where no redox process occurs. Figure 6-5 shows the EIS of the DNA hybridization using complimentary target. Clearly, R_{ct} increases with target concentration. This is attributed to the increase in repulsive electrostatic interactions along the backbone of the SH-ssDNA which later doubles with double-stranded DNA [41, 42]. Additionally, the limit of detection using EIS was verified to be 5 nM (Figure 6-6) from a curve which is a sigmoidal fit with a regression coefficient of 0.94.

6.5.3. DNA detection - dotLab

Here, we show the application of dotLab as a biosensor by using ssDNA specific to the *hippuricase* gene of *C. jejuni*. An interaction between immobilized probe and target causes a shift in intensity and a gradual increase in signal (Figure 6-7). DNA hybridization occurs through concentrations 5 nM and 1280 nM. When injecting the *hippuricase* target gene at different concentrations, a shift resulting from DNA hybridization was detected. The net response for each concentration was calculated by subtracting the non-detectable response ($\Delta DI \sim 2.94 \times 10^{-3}$) from specific signal. Non-detectable hybridization signals were obtained from this target. It can be seen that DNA has hybridized (concentrations 0.005 µM to 1.28 µM), indicated by the rise in signal. On analyzing the binding profile, the base line from where binding starts is approximately 4.26×10^{-3} DI units and the amount of binding in each step is taken as a reference from this point The limit of detection, determined as the lowest concentration of target DNA that produced a distinguishable net response (signal/noise>3), was 5.0 nM (Figure 6-8) and demonstrates the high specificity of the dotLab. Spurious signals due to non-specific binding are eliminated, as the diffraction efficiency depends on the difference in height between the patterned and non-patterned areas [43]. Since diffraction phenomena on the dotLab are inherently self-referencing,

nonspecific binding to both the patterned and unpatterned regions will not affect the signal. Such characteristic offers an important advantage over other optical biosensor systems in which any surface binding event will cause non-specific binding. Besides, the dotLab biosensor is a cost-effective platform that has the format flexibility to provide a quick and simple solution to both assay development and routine analysis [44, 45].

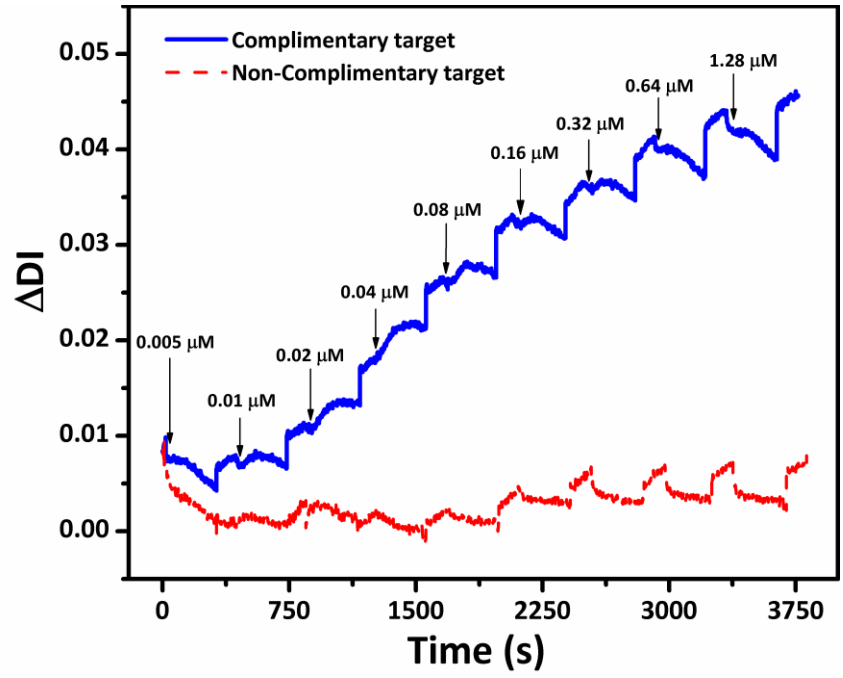

Figure 6-8 Representative response curves for the detection of the hippuricase gene. The target was serially diluted and introduced over the sensing surface, starting with the lowest concentration.

6.5.4. DNA Detection - SPREETA

In order to evaluate the performance of the device, a calibration curve has been obtained with different concentrations of target ssDNA injected serially from 2.5 nM to 1280 nM (Figure 6-9). The limit of detection was estimated to be 2.5 nM (Figure 6-10). The introduction of target

resulted in an initial drop in RU, which is attributed to the bulk refractive index change as the amount of drop is similar in both channels.

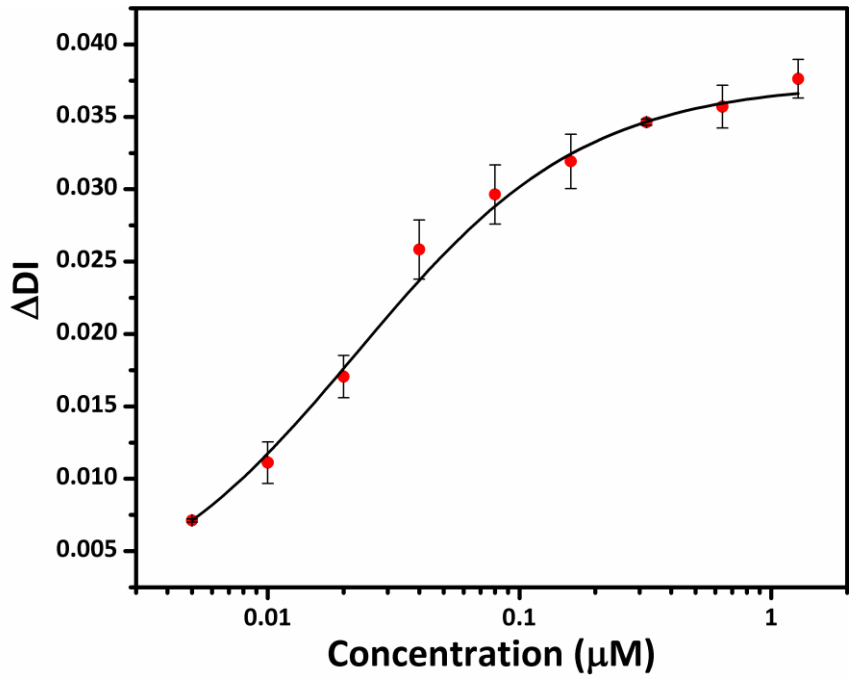

Figure 6-9 Dose-Response curve for hippuricase gene target binding.

This is attributed to the bulk refractive index change as the amount of drop is similar in both channels. Following the initial drop, the RU signal in the sensing channel increased with DNA binding, while the reference channel remained constant. For instance, when the target solution was injected, the change in RU at a concentration of 320.0 nM was found to be 101.45 ± 10 (n = 10), with a non-detectable signal of $\Delta DI < 2$ from the non-complimentary target ssDNA. The same surface can be regenerated using 2.5 mM HCl and reused more than 20 times over one week with only a small change in CV (11%). The sensor surface was regenerated by a 2 minute treatment with 2.5 mM HCl followed by a buffer wash. Regeneration efficiency was found to be between 89-95 % across the concentration range from 2.5 nM to 1280 nM. In the case of longer probes, the target DNA was serially passed over the surface from the lowest to highest

concentrations (10.0 nM to 80.0 nM) with a complimentary nucleotide on the reference channel (Figure 6-11).

Finally, as observed from the range of concentration and analytical curves, the sensitivity of the SPREETA and dotlab in the detection of the *hipO* gene of *C. jejuni* is higher than that of the BIAcore or amperometric detection platforms. The calculated lower limit of detection was 2.5 nM for SPR and 5.0 nM for dotlab.

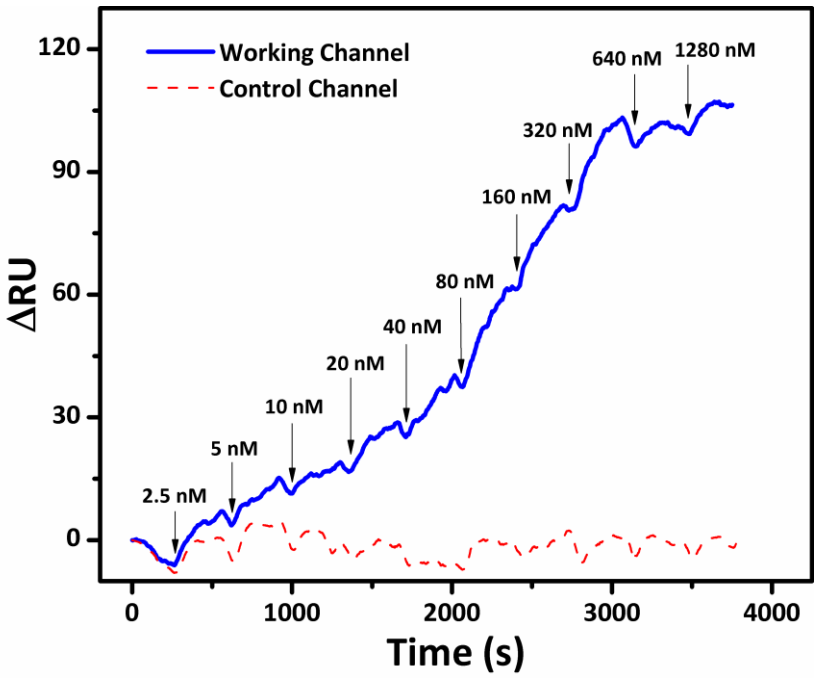

Figure 6-10 Representative response curves for the detection of the hippuricase gene. Graded concentrations of ssDNA were introduced to both, sensing channel and control channel (both blocked with spacer thiol).

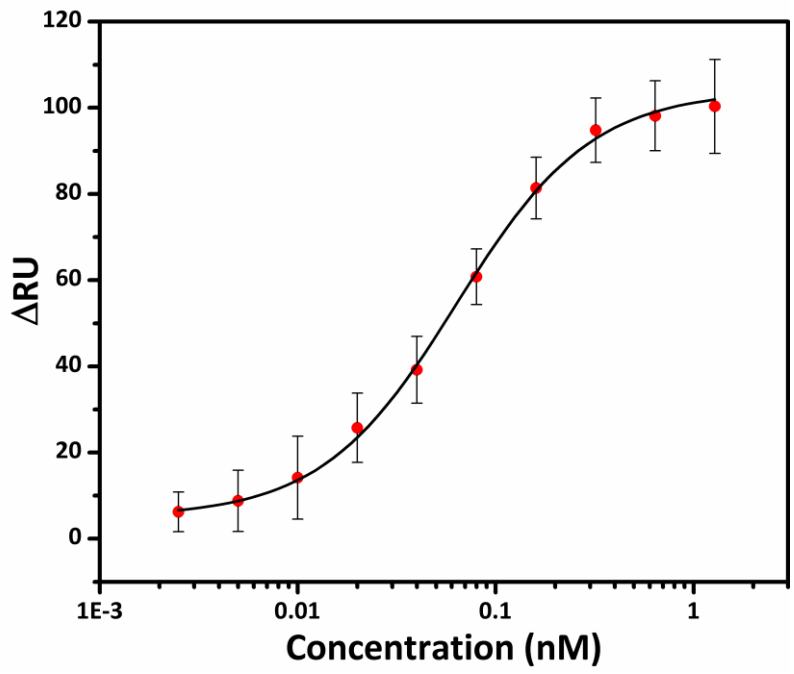

Figure 6-11 Dose-Response curve for hippuricase gene target binding

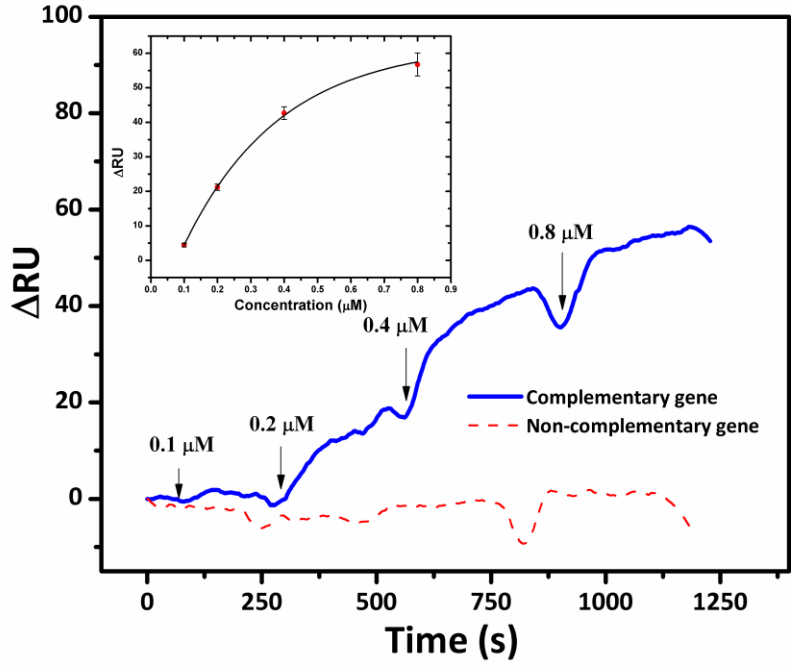

Figure 6-12 A representative response curve for long DNA probes immobilized on gold surface. The concentration of probes used was 1 μM. Inset shows calibration curve for the same.

6.6. Conclusion

We have reported a comparative study of immobilization techniques based on direct coupling of thiolated probes and covalent binding of biotinylated DNA to a patterned avidinated surface. Detection of DNA segments from the *hippuricase* gene of *C. jejuni* using diffraction optics technology (dotLab) and surface plasmon resonance was achieved. Development of self-assembled monolayers was used as the primary sensing mechanism, using by covalent immobilization of thiolated and biotinylated probes. Probes were not labeled and were immobilized using simple physical adsorption on to the surface of polystyrene or a gold sensor thereby avoiding complex and expensive surface chemistries for fast, responsive DNA sensors. Further experiments are underway to improve sensitivity and reusability of these optical sensing platforms using ssDNA from asymmetric PCR and real samples.

6.7. References

1. Stewart-Tull, D.E.S., et al., *Virulence spectra of typed strains of Campylobacter jejuni from different sources: a blinded in vivo study.* J. Med. Microbiol., 2009. **58**: p. 546-553.
2. Suzuki, H. and S. Yamamoto, *Campylobacter Contamination in Retail Poultry Meats and By-Products in the World: A Literature Survey.* J Vet Med Sci., 2009. **71**(3): p. 255-261.
3. Engberg, J., et al., *Quinolone and Macrolide Resistance in Campylobacter jejuni and C. coli: Resistance Mechanisms and Trends in Human Isolates.* Emerg. Infect. Dis, 2001. **7**(1): p. 24-34.
4. Altekruse, S.F., et al., *Campylobacter jejuni—An Emerging Foodborne Pathogen.* Emerg. Infect. Dis, 1999. **5**(1): p. 28-35.

5. Vugia, D., et al., *Preliminary FoodNet Data on the Incidence of Infection with Pathogens Transmitted Commonly Through Food --- 10 States, 2008.* MMWR, 2009. **58**(13): p. 333-337.

6. Galanis, E., *Campylobacter and bacterial gastroenteritis.* CMAJ, 2007. **177**(6): p. 570-571.

7. Tauxe, R.V., *Campylobacter jejuni: current status and future trends*, ed. I. Nachamkin, M.J. Blaser, and L.S. Tompkins. 1992, Washington, D.C.: Eds. ASM Press.

8. Perera, V.N., et al., *Molecular mimicry in Campylobacter jejuni: role of the lipo-oligosaccharide core oligosaccharide in inducing anti-ganglioside antibodies.* FEMS Immunol Med Microbiol., 2007. **50**(1): p. 27-36.

9. Bradbury, W.C., et al., *Investigation of a Campylobacter jejuni Outbreak by Serotyping and Chromosomal Restriction Endonuclease Analysis.* J. Clin. Microbiol., 1984. **19**(3): p. 342-346.

10. Ivnitski, D., et al., *Biosensors for detection of pathogenic bacteria.* Biosens. Bioelectron., 1999. **14**(7): p. 599-624.

11. Passamano, M. and M. Pighini, *QCM DNA-sensor for GMOs detection.* Sens. Actuators B, 2006. **118**(1-2): p. 177-181.

12. Chen, Q., et al., *Real-time monitoring of the strand displacement amplification (SDA) of human cytomegalovirus by a new SDA-piezoelectric DNA sensor system.* Biosens. Bioelectron., 2009. **24**(12): p. 3412-3418.

13. Ding, C., H. Zhong, and S. Zhang, *Ultrasensitive flow injection chemiluminescence detection of DNA hybridization using nanoCuS tags.* Biosens. Bioelectron., 2008. **23**(8): p. 1314-1318.

14. Lu, N., C. Shao, and Z. Deng, *Rational design of an optical adenosine sensor by conjugating a DNA aptamer with split DNAzyme halves.* Chem. Commun., 2008: p. 6161-6163.

15. Leung, A., P.M. Shankar, and R. Mutharasan, *Label-free detection of DNA hybridization using gold-coated tapered fiber optic biosensors (TFOBS) in a flow cell at 1310 nm and 1550 nm.* Sens. Actuators B, 2007. **131**(2): p. 640-645.

16. Yang, X., et al., *Nucleic acids detection using cationic fluorescent polymer based on one-dimensional microfluidic beads array.* Talanta, 2009. **77**(3): p. 1027-1031.

17. Ikebukuro, K., Y. Kohiki, and K. Sode, *Amperometric DNA sensor using the pyrroquinoline quinone glucose dehydrogenase–avidin conjugate.* Biosens. Bioelectron., 2002. **17**(11-12): p. 1075-1080.

18. Wang, J. and M. Jiang, *Dendritic Nucleic Acid Probes for DNA Biosensors.* J. Am. Chem. Soc., 1998. **120**(32): p. 8281-8282.

19. Mikkelsen, S.R., *Electrochemical biosensors for DNA sequence detection.* Electroanalysis, 2005. **8**(1): p. 15-19.

20. Drummond, T.G., M.G. Hill, and J.K. Barton, *Electrochemical DNA sensors.* Nat. Biotechnol., 2003. **21**(10): p. 1192-1199.

21. Love, J.C., et al., *Self-Assembled Monolayers of Thiolates on Metals as a Form of Nanotechnology.* Chem. Rev., 2005. **105**(4): p. 1103-1170.

22. Hering, K.K., et al., *Microarray-Based Detection of Dye-Labeled DNA by SERRS Using Particles Formed by Enzymatic Silver Deposition.* ChemPhysChem, 2008. **9**(6): p. 867-872.

23. Fang, X., et al., *Designing a Novel Molecular Beacon for Surface-Immobilized DNA Hybridization Studies.* J. Am. Chem. Soc., 1999. **121**(12): p. 2921-2922.

24. Mines, G.A., et al., *Microporous Supramolecular Coordination Compounds as Chemosensory Photonic Lattices.* Angew. Chem., Int. Ed., 2002. **41**(1): p. 154-157.

25. Morhard, F., et al., *Immobilization of antibodies in micropatterns for cell detection by optical diffraction.* Sens. Actuators B, 2000. **70**(1-3): p. 232-242.

26. St.John, P.M., et al., *Diffraction-Based Cell Detection Using a Microcontact Printed Antibody Grating.* Anal. Chem., 1998. **70**(6): p. 1108-1111.

27. *http://www.axela.com/docs/literatures/*. 2007.

28. Balasubramanian, S., et al., *Lytic phage as a specific and selective probe for detection of Staphylococcus aureus—A surface plasmon resonance spectroscopic study.* Biosens. Bioelectron., 2007. **22**(6): p. 948-955.

29. Huang, E., et al., *Surface Structure and Coverage of an Oligonucleotide Probe Tethered onto a Gold Substrate and Its Hybridization Efficiency for a Polynucleotide Target.* Langmuir, 2001. **17**(4): p. 1215-1224.

30. Sakao, Y., et al., *Hybridization of oligonucleotide by using DNA self-assembled monolayer.* Colloids Surf B Biointerfaces., 2005. **40**(3-4): p. 149-152.

31. Williams, M.C., et al., *Effect of pH on the Overstretching Transition of Double-Stranded DNA: Evidence of Force-Induced DNA Melting.* Biophys J., 2001. **80**(2): p. 874-881.

32. Herne, T.M. and M.J. Tarlov, *Characterization of DNA Probes Immobilized on Gold Surfaces.* J. Am. Chem. Soc., 1997. **119**(38): p. 8916-8920.

33. Nakamura, F., et al., *Preparation of a Branched DNA Self-Assembled Monolayer toward Sensitive DNA Biosensors.* Nano Lett., 2003. **3**(8): p. 1083-1086.

34. Williams, M.C., et al., *Effect of pH on the Overstretching Transition of Double-Stranded DNA: Evidence of Force-Induced DNA Melting.* Biophys. J., 2001. **80**: p. 874-881.

35. McEwen, G.D., F. Chen, and A. Zhou, *Immobilization, hybridization, and oxidation of synthetic DNA on gold surface: Electron transfer investigated by electrochemistry and scanning tunneling microscopy.* Anal. Chim. Acta., 2009. **643**(1-2): p. 26-37.

36. Goh, J.B., et al., *A quantitative diffraction-based sandwich immunoassay.* Anal. Biochem., 2003. **313**(2): p. 262-266.

37. Wang, R., et al., *Immobilisation of DNA probes for the development of SPR-based sensing.* Biosens. Bioelectron., 2004. **20**(5): p. 967-974.

38. Naimushin, A.N., et al., *Detection of Staphylococcus aureus enterotoxin B at femtomolar levels with a miniature integrated two-channel surface plasmon resonance (SPR) sensor.* Biosens. Bioelectron., 2002. **17**(6-7): p. 573-584.

39. Nuzzo, R.G. and D.L. Allara, *Adsorption of bifunctional organic disulfides on gold surfaces.* J. Am. Chem. Soc., 1983. **105**(13): p. 4481-4483.

40. Dubois, L.H. and R.G. Nuzzo, *Synthesis, Structure, and Properties of Model Organic Surfaces.* Annu. Rev. Phys. Chem., 1992. **43**: p. 437-463.

41. Li, D., et al., *Kinetic study of DNA/DNA hybridization with electrochemical impedance spectroscopy.* Electrochem. Commun., 2007. **9**(2): p. 191-196.

42. Li, C.-Z., Y. Liu, and J.H.T. Luong, *Impedance Sensing of DNA Binding Drugs Using Gold Substrates Modified with Gold Nanoparticles.* Anal. Chem., 2005. **77**(2): p. 478-485.

43. Bailey, R.C. and J.T. Hupp, *Large-Scale Resonance Amplification of Optical Sensing of Volatile Compounds with Chemoresponsive Visible-Region Diffraction Gratings.* J. Am. Chem. Soc., 2002. **124**(23): p. 6767-6774.

44. Jiang, X., S. Liu, and R. Narain, *Degradable Thermoresponsive Core Cross-Linked Micelles: Fabrication, Surface Functionalization, and Biorecognition.* Langmuir, 2009. **25**(23): p. 13344-13350.

45. Deng, Z., et al., *Well-Defined Galactose-Containing Multi-Functional Copolymers and Glyconanoparticles for Biomolecular Recognition Processes.* Macromolecules, 2009. **42**(17): p. 6393-6405.

7. Overall Conclusion

Surface science coupled with nanotechnology has the potential to bring about the next revolution in nanoelectronics and medical research. Nevertheless, development of 3D nanoarchitectures and macromolecular devices still remains a challenge. 'Bottom-up' nanofabrication techniques appear to be an inexpensive and efficient alternative to 'top-down' approaches that escalate costs for precision manufacturing. Biological templates such as aptamers, DNA and proteins provide a more sophisticated means to develop organized self-assembled nanomaterials templates for 'bottom-up' nanofabricated macromolecular devices. Extensive ruggedness and the apt chemical functionalities make DNA a suitable tool to develop DNA-templated nanomaterials. Single-walled carbon nanotubes have turned out be a promising candidate for the development of efficient electronic and sensing devices due to their high conductivity and efficient charge transfer. Moreover, being the central icon in modern biology, and having extensive applications in genomics and gene sensing; it can also be used as a nanomaterial template to building macromolecular electronic devices and in medical diagnostics.

This research mainly focuses on the 'bottom-up' surface engineering of DNA in developing molecular scaffolds and templates for nanoelectronics and biosensing. We have investigated the application of DNA as a dispersant and nanomaterial template for single-walled carbon nanotubes in developing 3D superstructures for macromolecular electronics and analyzing their electrochemical and charge transfer kinetics. Scanning electrochemical microscopy (SECM) was used to analyze the electrical and charge transfer kinetics across these nanomaterials. The steady state positive feedback obtained from the ultramicroelectrode clearly

indicates that the presence of DNA aids in electron hopping across two adducts, and these layers are not insulated from one another. Besides, the response curves at varying concentrations of the redox mediator indicate that the current response is solely due the charge injection through multiple layers and that these layers are not insulated from one another.

Finally, a portable and reliable optical DNA biosensor platform has been developed for the detection of the *hippuricase* gene from pathogenic bacteria with high sensitivity and specificity. Our main aim in this part of the research was to develop a prototype biosensor for the detection of the disease causing gene from this bacteria at low levels, which is of great importance due to the economic and health concerns that rises from *C.jejuni* outbreaks. Although, antibody and enzymatic sensors serve as a versatile biosensing platform, they are not desired because most of the systems remain expensive, require a high level of purity and cumbersome procedures to prepare and may in some cases give a false positive response. Here, we have shown the versatility of tethered DNA molecular structures and scaffolds for responsive and 'real-time' detection of the highly specific *hipO* gene from *C. jejuni*. Single-stranded DNA was immobilized on to gold surface on the SPREETA platform and an avidinated polystyrene surface in the DOT via chemisorption with minimal time in developing the biosensor surface. The detection limit was found to be 2.5 nM and 5 nM respectively. A competitive inhibition assay using non-complimentary gene demonstrates that the detection was highly specific and selective. In conclusion, a unique blend of DNA with nanomaterials combined with its superior attributes can be used in developing futuristic macroscale electronic devices and clinical diagnostic systems.

8. Future Recommendation

8.1. Localized Surface Plasmon Resonance (LSPR) based biosensors

As discussed in this research, three dimensional nanostructures have a significant contribution in the growth of novel technologies for biosensing and medical diagnostics. The elementary steps for charge transfer, molecular rearrangement and chemical reactions take place at the nano-scale. Manifestations of these mechanisms require a controlled fabrication of nanomaterials to harness their properties to the fullest. Such designs are popular in the development of optical communication devices and light routers. Essentially, it also has widespread applications in the fabrication of biosensor platforms based on the type of biomolecular interactions that take place at any interface [1].

When an electromagnetic radiation impinges on the conduction electrons of any nanoparticle, then coherent surface oscillations occur, which is termed as surface plasmon resonance (Figure 8-1).

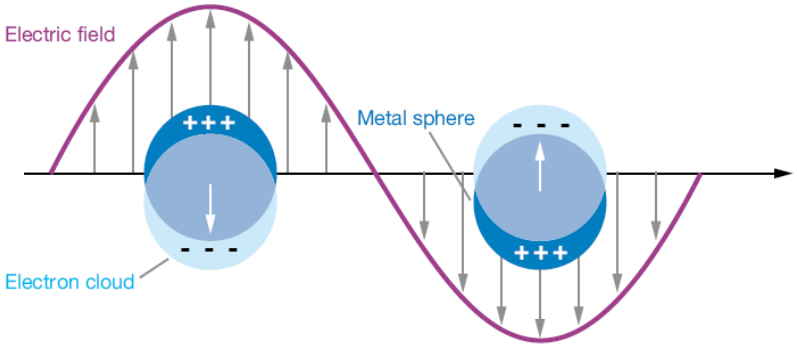

Figure 8-13 Schematic representation of localized surface plasmon resonance across a metallic nanoparticle

By definition, any nanoparticle capable of a negative real and positive imaginary dielectric constant is capable of exhibiting the phenomena of surface plasmon resonance. Consequently, when an electromagnetic wave interacts with nanoparticles which are much smaller than its own wavelength, then the particles resonate with a frequency known as localized surface plasmon resonance. Further analysis of the properties of LSPR led to the development of surface-enhanced Raman scattering (SERS). SERS is a powerful tool in identifying specific bio-molecules using their unique vibrational spectrum. Gold nanoparticles (AuNPs) have a distinct spectral signature and this signature depends on the size, shape and orientation of these particles.

The main aim of developing 3D nanostructures for LSPR sensing is to provide the maximum surface area for biomolecular immobilization. Carbon nanotubes prove to be better templates for attaching AuNP and also act as a binding scaffold for better assembly. There have been a few major strategies for 3D assembly of LSPR platforms. AuNPs were assembled using alternate deposition of bi-functional cross-linkers.

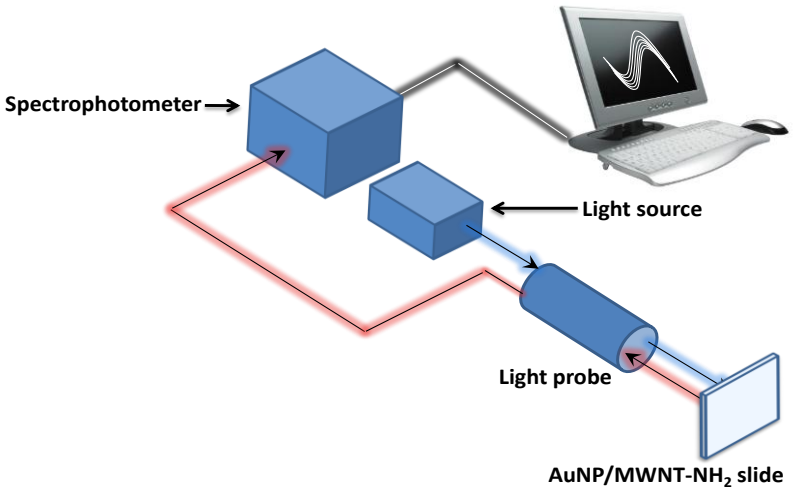

Figure 8-14 Schematic of the setup for LSPR sensing using a transmission mode UV-Vis Spectrophotometer

Although, they claim that this technique provides better sensitivity, it may hinder target molecules to penetrate through the tiny crevices and reach the probe receptors immobilized on the AuNP surface [2]. We report the layer-by-layer assembly of a novel carbon nanotube/gold nanoparticle (CNT/AuNP) based sensing platform for label free DNA sensing and enzymatic biosensors [3-5]. Ionic nature of gold nano-particles and poly-cationic nanomaterials facilitates in the layer-by-layer assembly of 3D nanoarchitectures [6]. This 3D structure provides a highly accessible AuNP structure, with high composite density and sufficient path for the diffusion of target molecules to their respective receptors. Besides, LSPR phenomena can be observed on a conventional UV-Vis spectrophotometer in transmission mode [7]. Work is still in progress in order to optimize the size and shape of nanoparticles and also in selecting the right template that would increase the aspect ratio for biomolecular immobilization and better communication between the probe and target.

8.2. References

1. Willets, K.A. and R.P. Van Duyne, *Localized surface plasmon resonance spectroscopy and sensing.* Annu. Rev. Phys. Chem., 2007: p. 267-297.
2. Ye, J., et al., *Enhanced localized surface plasmon resonance sensing on three-dimensional gold nanoparticles assemblies* Colloids Surf. A: Physicochem. Eng. Aspects, 2008. 321(1-3): p. 313-317.
3. Pan, B., et al., *Growth of multi-amine terminated poly(amidoamine) dendrimers on the surface of carbon nanotubes* Nanotechnology, 2006. 17(10): p. 2483.
4. Jia, N., et al., *Decorating multi-walled carbon nanotubes with quantum dots for construction of multi-color fluorescent nanoprobes.* Nanotechnology, 2010. 21: p. 45606.

5. Goyanes, S., et al., *Carboxylation treatment of multiwalled carbon nanotubes monitored by infrared and ultraviolet spectroscopies and scanning probe microscopy* Diamond Relat. Mater., 2007. 16(2): p. 412-417.

6. Guo, L., G. Chen, and D. Kim, *Three-Dimensionally Assembled Gold Nanostructures for Plasmonic Biosensors.* Anal. Chem. , 2010. 82(12): p. 5147-5153.

7. Endo, T., et al., *Localized surface plasmon resonance based optical biosensor using surface modified nanoparticle layer for label-free monitoring of antigen- antibody interaction.* Sci. Technol. Adv. Mater., 2005. 6: p. 491-500.